*The dysfunction and therapeutic potential of the endocannabinoid system in Huntington's disease.*

Alipi Naydenov

A dissertation submitted in partial fulfillment of the requirements for the degree of

Doctor of Philosophy

University of Washington
2014

Reading Committee:
Nephi Stella, *chair*
Thomas Bird, *member*
Gwenn Garden, *member*

Program Authorized to Offer Degree:

Neurobiology and Behavior

University of Washington

## Abstract

The dysfunction and therapeutic potential of the endocannabinoid system in Huntington's disease.

Alipi Naydenov

Chair of the Supervisory Committee:

Nephi Stella, Professor
Department of Pharmacology

Huntington's Disease is an autosomal dominant progressive neurodegenerative disease, which features profound disturbance of the basal ganglia, and in particular medium spiny neurons of the caudate/putamen. Of the many molecular changes that accompany this disease, impaired endocannabinoid signaling is among the earliest and most well-described. The purpose of this thesis is to describe the contribution of impaired endocannabinoid signaling to the progressive Huntington's phenotype, and to test the potential for leveraging the protective nature of endocannabinoid signaling to control some features of the disease, including seizures. We report that genetic rescue of endocannabinoid signaling in a mouse model of Huntington's disease prevents synaptic loss in the striatum, but does not block the development of a motor phenotype, suggesting an unexpected uncoupling of these pathogenic mechanisms. Additionally, we describe a pharmacologic approach to augment endocannabinoid signaling in order to control both chemically-induced convulsions and spontaneous seizures in a mouse model of Huntington's disease, and conclude that this approach might represent a novel antiepileptic strategy.

# ACKNOWLEDGEMENT

I would like to thank my advisor, Dr. Nephi Stella, for his guidance and for his commitment to mentoring. Nephi has set an example of genteel conduct in science which will stick with me for the duration of my career, and I am grateful for his patience and generosity, particularly in challenging moments. I would like to thank the members of my committee, Dr. Gwenn Garden, Dr. Nigel Bamford, Dr. Tom Bird, Dr. John Clark, and Dr. John Neumaier, all of whom have taken time out of their busy schedules to guide me and who were an integral part of my graduate journey.

I feel lucky to have a strong support system which was instrumental in helping me through my graduate years. I would like to thank my mother and father, for the many times when they helped me think through the challenges ahead of me and for their unfailing support. I am grateful to Jackie and Rosie for being there and for their patience with me during this endeavor. I am also grateful to Misho, Rosa, Alipi, and Dora, for their support and opening an opportunity for me and for our family. I am especially grateful to Caleb, who was always available to listen, to talk, and to support me, and without whom my graduate experience would not have been as rewarding. Finally, I would like to thank Henry, for his many contributions.

# I. Introduction

*This chapter may be used as a template for a future review article.*

## 1.1 **Thesis Overview.**

The research described in this thesis can be generalized as a study of the endocannabinoid (eCB) system in Huntington's disease (HD), including both the eCB dysfunction inherent to HD pathology, and also the therapeutic potential of augmenting eCB signaling. This chapter (I) outlines the rationale for the research and begins with background information on eCB signaling, including the different arms of the eCB signaling system. The second part reviews HD, beginning with a description of the clinical features of the disease, and then covering pathophysiology, mouse models, and culminating in a more specific discussion regarding the state of eCB signaling in HD, and the potential utility of targeting the eCB system in juvenile-onset HD for control of epileptic seizures.

Chapter 2 (**II**) describes genetic rescue of a subpopulation of $CB_1$ receptors expressed on medium spiny neurons (MSNs), which are lost in HD and in mouse models. The goal of this study was to test the hypothesis that the early and specific loss of MSN-expressed $CB_1$ receptors ($CB_{1(MSN)}$) is a key pathogenic event in HD. This study demonstrated that genetic rescue of $CB_{1(MSN)}$ blocks the loss of striatal presynaptic markers which have been widely used as a marker of striatal pathology, but does not rescue motor impairment in R6/2 mice, a model of HD.

In Chapter 3 (**III**), R6/2 mice are used to study the ability of eCB signaling to control spontaneous seizures, which are also observed in a subset of HD patients with an aggravated and accelerated disease course. The goal of these studies was to determine the extent to which augmenting the availability of the major eCB in the brain at presynaptic $CB_1$ receptors as well as possibly at other receptors can control the incidence of seizures.

## 1.2 Background

### 1.2.1 The eCB signaling family.

The endocannabinoid (eCB) system allows for quick communication between nearby cells using molecules which are synthesized from existing cellular structures (plasma membrane), in a manner that is cost-efficient for the cell, requiring few enzymatic steps. At least some elements of the eCB signaling system seem to be

evolutionarily ancient (eCB synthesis enzymes), whereas others are found only in vertebrates and invertebrate chordates (cannabinoid receptors). However, even early life forms which lack cannabinoid receptors possess eCB-mediated signaling with features similar to eCB signaling in higher life forms. For example, the leech lacks $CB_1$ or $CB_2$, but features eCB-mediated long-term depression (LTD), through a TRPV-like receptor (Elphick, 2012). Indeed, eCB synthesis enzymes are widely distributed in the animal kingdom, although their molecular targets have not been clearly studied. The cannabinoid receptors share 44% homology, and seem to have derived from a single GPCR found in an ancestor common to all chordates, possibly the sea squirt, and later diverged as a result of a gene duplication (Elphick, 2012). Among mammals, members of the eCB signaling family are highly conserved, and the expression of eCB receptors is highly similar across mammalian species, with high expression in cerebral cortex, hippocampus, and basal ganglia. In this introduction, the members of the eCB signaling system will be introduced with an emphasis on 2-AG signaling through $CB_1$ in the CNS.

#### 1.2.1.1 The Receptors

The prevailing conception of the eCB system begins with the 2+2: the two cloned receptors, $CB_1$ and $CB_2$, and the two major eCBs, 2-arachydonylglycerol (2-AG), and arachydonlyethanolamine (AEA), which has acquired the colloquial name "anandamide." $CB_1$, the first molecularly identified member of the endocannabinoid family, is a $G_i$-coupled GPCR, belonging to the Class A "rhodopsin-like" family of GPCRs (Matsuda et al., 1990). Although $CB_1$ is routinely referred to as primarily a neuronal receptor, this ignores a widespread distribution which, in addition to neurons, includes the digestive tract, in the pituitary, thyroid, and adrenal glands, endothelial cells, Kupffer and stellate cells of the liver, adipocytes, Leydig cells and spermatogonia, among others. However, because it was quickly discovered that $CB_1$ is the primary target for $^{\Delta 9}$THC, there arose strong interest in studying the signaling

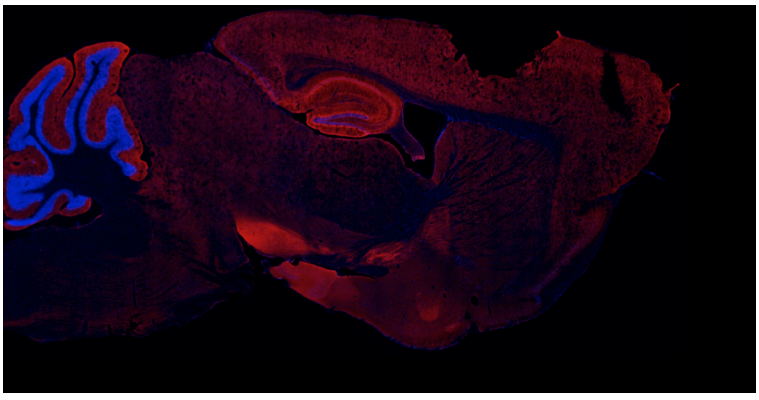

**Figure 1.1:** $CB_1$ expression in mouse brain.

of this receptor in the CNS. $CB_1$ expression in the brain varies strongly by cell type, and is generally expressed at high levels in GABAergic cells, and at lower levels in glutamatergic cells (Steindel et al., 2013). A major advance was the subcellular localization of $CB_1$ receptors to presynaptic terminals, where they were found to regulate GABA release in hippocampal interneurons (Katona et al., 1999). This lead to the blockbuster finding that endocannabinoid signaling originates postsynpatically and terminates presynaptically, and was the first known example of "retrograde signaling" at the GABAergic synapse (Wilson and Nicoll, 2001). Retrograde signaling has been found to be a motif of endocannabinoid signaling through $CB_1$ in many types of synapses including glutamatergic (Kreitzer and Malenka, 2007), GABAergic (Wilson and Nicoll, 2001), and cholinergic (Lawrence, 2008), among others. Retrograde signaling is further classified by effect duration as either short term depolarization-induced suppression of inhibition/excitation (DSI/DSE), or long term depression (LTD or eCB-LTD) (Gerdeman and al, 2002; Regehr et al., 2009).

The popular description of $CB_2$ as being expressed on immune cells is somewhat more accurate - $CB_2$ is expressed in monocytes, B cells, T cells, neutrophils, eosinophils, and NK cells (Miller and Stella, 2008). Interestingly this receptor can also be found on osteoclasts, where recent work suggests it may regulate bone density (Idris et al., 2005; Karsak, 2005) - accordingly, the only known phenotype of *cnr2*$^{-/-}$ mice is osteoporosis (Ofek et al., 2006). In healthy brain, the presence of $CB_2$ expression remains a controversial topic, largely due to the absence of a reliable antibody which does not label other proteins in *cnr2*$^{-/-}$ brain. Thus, despite several immunohistochemical reports describing $CB_2$ in Purkinje cells and in hippocampus, these findings need to be repeated with a specific antibody or complemented by in-situ hybridization studies, for confirmation. The current prevailing consensus, until proven otherwise, is that $CB_2$ receptors are not expressed in a healthy brain, but in cases of injury or chronic disease such as multiple sclerosis and amyotrophic lateral sclerosis, microglia become activated and begin express $CB_2$ in their activated state (Miller and Stella, 2008). $CB_2$ signaling controls microglial migration in response to activation by 2-AG, but this effect may also be dependent on the abnormal cannabidiol (abn-CBD) receptor, a putative cannabinoid

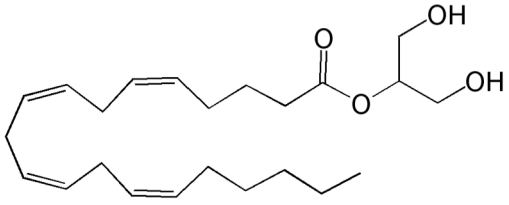


**Figure 1.2:** Molecular structure of 2-AG.

receptor, as it can be blocked by both SR144528 and the abn-CBD antagonist, O-1918 (Offertáler et al., 2003; Walter et al., 2003a).

In addition to $CB_1$ and $CB_2$, there are a number of putative members of the endocannabinoid family which have been characterized in systems lacking $CB_1$ or $CB_2$ receptors. The most frequently mentioned putative cannabinoid receptor is GPR55, which has very low sequence homology to $CB_1$ and $CB_2$ receptors, but is a target for several cannabinoid agonists including AM251, HU210, d9THC, and possibly anandamide, and is antagonized by SR141716 (Ross, 2009). Although lysophosphatidylinositol is generally agreed on as an endogenous GPR55 agonist, whether any actual eCBs bind to GPR55 is a hotly contested question (Ross, 2009). Another putative cannabinoid receptor is thought to exist in the vasculature, where vasodilation occurs in response to abn-CBD, an analog of cannabidiol which does not bind to $CB_1$ or $CB_2$ receptors (Franklin and Stella, 2003). Finally, TRPV1 is an endovallinoid receptor which is a close cousin of the endocannabinoid receptors because its major ligand is AEA. While AEA is a partial agonist at $CB_1$ receptors, it is a full agonist at TRPV1, raising the question whether AEA is most appropriately labeled and eCB or an endovallinoid. The distinction may be arbitrary, as AEA has been shown to regulate the level of 2-AG signaling at $CB_1$ through a TRPV1 dependent mechanism, demonstrating that the two signaling systems are highly interlinked (Maccarrone et al., 2008).

**1.2.1.2 Endocannabinoids:**

AEA was the first *bona fide* eCB to be discovered, when it was isolated from porcine brain (Devane et al., 1992). It was found to cause cannabinomimetic behavioral effects, including hypothermia and hypolocomotion (Crawley et al., 1993), and to displace synthetic cannabinoid receptors in binding assays (Mackie et al., 1993). AEA synthesis remains somewhat disputed, but is generally thought to be a two-step process catalyzed by NAPE-PLD, and possibly by other, uncloned enzymes (Di Marzo, 2011; Di Marzo et al., 1994). AEA is a partial agonist at $CB_1$ and $CB_2$ receptors with comparable affinity at both receptors, but is a full agonist at TRPV1 receptors.

Although AEA was discovered first, the second eCB, 2-AG, has become recognized as the principal brain eCB, due to its greater efficacy at $CB_1$ receptors (where it is a full agonist) and higher brain concentration (Stella et al., 1997). Like AEA, 2-AG is made on-demand from larger lipid substrates found in the plasma membrane. 2-AG is synthesized by sn-1 specific diacyclglycerol lipase alpha (DAGLα), which catalyzes the cleavage of 2-AG from arachidonic acid (AA) containing DAG. There are three mechanisms which can initiate 2-AG production. (1) Postsynaptic depolarization induces calcium- and DGLα-dependent 2-AG production in a setting of robust calcium increase (Kreitzer, 2002; Wilson and Nicoll, 2001). (2) Concurrent activation of $G_{q/11}$-coupled group 1 metabotropic glutamate receptors (mGluRs) and less robust intracellular calcium release triggers calcium-assisted receptor-driven 2-AG release (Hashimotodani et al., 2005; Ohno-Shosaku et al., 2001). (3) Robust activation of mGluRs triggers calcium-independent receptor-driven 2-AG release (Maejima et al., 2001). Additionally, there is a recently described mechanism by which CaMKIIα can inhibit DGLα by phosphorylating Ser782 and Ser808, and this is notably the only known mechanism for *repression* of 2-AG production (Shonesy et al., 2013). Unlike AEA, 2-AG is a full agonist at $CB_1$ and $CB_2$ receptors, has a higher affinity for both receptors compared to AEA, and does not act at TRPV1. In addition to 2-AG and AEA, other endocannabinoids have been described which bind to cannabinoid receptors, including oleamide, virodhamine, N-Dihomo-$_\gamma$-linolenoyl ethanolamine, and others. However, the roles played by these endocannabinoids are not as well understood, and they will not be discussed here.

**1.2.1.3 Endocannabinoid Hydrolysis Enzymes**

The principal AEA hydrolysis enzyme, fatty acid amide hydrolase (FAAH), was purified from rat liver in 1996 (Cravatt et al., 1996), and a knockout mouse was generated shortly thereafter (Cravatt et al., 2001). $FAAH^{-/-}$ mice show a 50-100-fold reduction in anandamide hydrolysis and over a 10-fold increase in AEA levels, therefore FAAH is considered to be effectively the only AEA hydrolysis enzyme (REF). These mice also

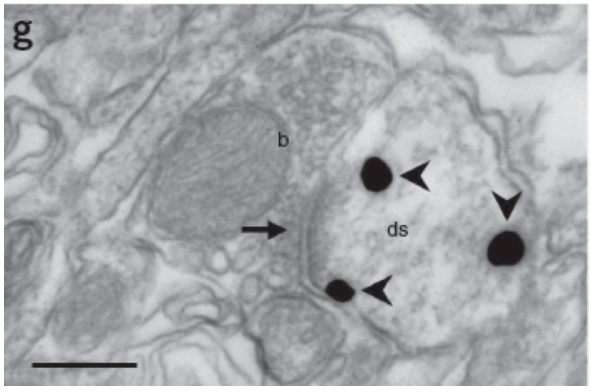


**Figure 1.3:** ABHD6 (arrowheads) is expressed postsynpatically, by EM. Reproduced from (Marrs et al., 2010) with permission.

display decreased pain sensitivity, increased basal eCB signaling, and enhanced $CB_1$-dependent behavioral response to FAAH administration, which can be blocked by a $CB_1$ antagonist (REF). In contrast to AEA, the bulk of 2-AG hydrolysis is mediated by at least 3 enzymes. In cell homogenates, monoacylglycerol lipase (MGL) is responsible for 80-85% of 2-AG hydrolysis, while ABHD12 is responsible for approximately 10%, and ABHD6 is responsible for approximately 5% (Blankman et al., 2007). However, these figures do accurately represent the contribution of these enzymes in vivo. In particular, ABHD6 is distinct in that it is located post-synaptically, at the site of 2-AG synthesis, and exerts equal control over the availability of 2-AG at local $CB_1$ receptors compared with MGL (Marrs et al., 2010). Nevertheless, whereas global deletion of MGL results in increased 2-AG concentration and resulting partial desensitization of $CB_1$ receptors (Pan et al., 2011), deletion of ABHD6 does not. Therefore, the unique post-synaptic localization of ABHD6 coupled with its low intrinsic activity together endow this enzyme with the ability to exert strong control over local $CB_1$ receptors, while having negligible effects on distant $CB_1$ receptors. Furthermore, because all hydrolysis enzymes rely on endogenous mechanisms of 2-AG production (see above), ABHD6 achieves spatiotemporal selectivity, in that at any given moment, it augments signaling only at $CB_1$ receptors where signaling is already taking place.

### 1.2.2 The eCB system in Huntington's Disease

#### 1.2.2.1 Huntington's chorea

George Huntington famously described the disease which would later bear his name at the age of 22, in the first of only two papers he would ever write, succinctly entitled "On Chorea." Sir William Osler would later deliver famous praise of this paper, "In the history of medicine, there are few instances in which a disease has been more accurately, more graphically or more briefly described." The young physician relied on observations from his father and grandfather, both also physicians who had cared for the same afflicted Long Island family for over 70 years. He described, in two pages, the autosomal dominant nature of the disease "it never skips a generation to manifest itself in another," as well as the progressive motor findings which culminate in death, and even noted the accompanying psychiatric involvement (Huntington, 1967). Huntington's disease begins with the gradual onset of a labile mood, affective changes, disinhibition, and general personality change (Duff

et al., 2007). Diagnosis usually follows the development of motor symptoms, and frequently occurs in the fourth decade of life. Motor symptoms include the classic finding of chorea, an uncontrollable dance-like writhing, as well as twitching, grimacing, dystonia, ataxia, dysphasia, and in late disease, rigidity, bradykinesia, weight loss, and difficulty swallowing. Motor symptoms are progressive and culminate in death, most frequently from sequelae related to aspiration. The average time from diagnosis to death is approximately 20 years (Foroud et al., 1999), and prevalence has been estimated at 4-10 cases per 100,000 persons of European descent (Zuccato et al., 2010). Approximately 5-10% of HD cases involve repeat expansions > 60 CAG repeats, which present before age 21 (Foroud et al., 1999). This is termed juvenile HD (JHD) and represents an accelerated and aggravated form of HD, which also features a unique array of findings not observed in adult-onset HD patients. Specifically, 38% of JHD patients feature severe myoclonic epilepsy (Cloud et al., 2012), which is frequently a presenting symptom (Gambardella et al., 2001), and the proportion of JHD patients with epilepsy increases further in patients who carry higher numbers of repeats and present at an earlier age (Cloud et al., 2012). Indeed, another group found that 57% of patients presenting before age 10 featured seizures, and many of these patients did not develop chorea until later in disease (Gonzalez-Alegre and Afifi, 2006). The most common epileptiform finding in these patients is polyspike waves, however this is based on a review of HD patients which included some individuals over age 20 (Landau and Cannard, 2003).

**1.2.2.2 Pathophysiology of Huntington's disease**

Huntington's disease is an autosomal dominant neurodegenerative disorder caused by a triplet expansion repeat in exon 1 of the IT15 gene (also: *HTT*) on chromosome 4, which codes for huntingtin, a 348kDA protein expressed highly in neurons (MacDonald et al., 1993; Sharp et al., 1995). The most obvious neuropathology associated with the disease is the loss of the majority of medium spiny neurons (MSNs) in the caudate/putamen of HD patients (Reiner et al., 1988), although there is also more widespread degeneration involving cortial structures (Rosas et al., 2005; 2006). This degeneration is thought to be caused by a loss of BDNF delivery through the corticostriatal synapse (Zuccato et al., 2001), however this cannot be the full explanation because expression of mutant huntingtin (mt-htt) in only MSNs is sufficient to result in neurodegeneration and motor phenotype (Brown et al., 2008). It is known that mt-*Htt* is capable of binding to DNA and controlling gene

expression (Zhai et al., 2005), and that soluble mt-*Htt* can interfere with transcription factors or disrupt the function of gene promoters (Benn et al., 2008). In fact, there is widespread dysregulation of gene expression in HD mice (Luthi-Carter et al., 2002) and patients (Hodges, 2006), which is most profound in the striatum and can be recapitulated in expression profiles derived only from MSNs collected by laser capture microscopy (Zucker, 2004). Therefore, one can conclude that HD pathology, particularly in the striatum, arises from a combination of both network pathologies and cell-autonomous events.

**1.2.2.3 eCB signaling in HD**

HD patients exhibit an early and profound loss of $CB_1$ receptor expression on MSN terminals, first in indirect pathway neurons as early as Grade 0, and later in the direct pathway (Glass et al., 2000). Furthermore, the loss of CB1 receptors precedes all other synaptic markers which are eventually lost from MSN terminals. Similarly, $CB_1$ downregulation is reliably measured in most mouse models of HD pathogenesis, including R6/2 (Horne et al., 2012; Luthi-Carter et al., 2002; Mccaw et al., 2004), R6/1 (Dowie et al., 2009; Naver et al., 2003), YAC128 (Pouladi et al., 2012) and HdhQ150 (Woodman et al., 2007). Like human patients, mouse models also feature loss of MSN-expressed $CB_1$ ($CB_{1\ (MSN)}$) prior to the loss of other synaptic markers, including dopamine D2 and D1 receptors (Glass et al., 2000), and striatal synaptophysin (Cepeda et al., 2003; Goto and Hirano, 1990). Overall, these findings have contributed to the notion that $CB_{1(MSN)}$ loss is an early pathological event which may control downstream pathology in HD.

It should be noted that the loss of $CB_1$ in HD is generally considered to be limited to specific neuronal populations. In the striatum, $CB_1$ receptors are lost in MSN axon terminals (Dowie et al., 2009; Horne et al., 2012), but preserved on corticostriatal terminals (Chiodi et al., 2012). In striatal interneurons, $CB_1$ signaling is selectively lost from NPY interneurons, but not from cholinergic, parvalbumin, or somatostatin interneurons (Horne et al., 2012). Additionally, there seems to be a discrepancy between transcript and protein levels of $CB_1$. For example, cortical and hippocampal $CB_1$ transcription is decreased in R6/2 mice (Denovan-Wright and Robertson, 2000; Horne et al., 2012), but protein expression is unchanged in both cortex (Horne et al., 2012)and hippocampus (unpublished data). There is also a discrepancy between binding and immunohistochemical studies and *in vivo* studies using a newly developed PET ligand for $CB_1$.

The significance of the loss of $CB_{1(MSN)}$ remains hotly disputed. Genetic deletion of $CB_1$ receptors was found to exacerbate and accelerate the motor phenotype of R6/2 mice by two independent groups (Blázquez et al., 2010; Mievis et al., 2011), suggesting that $CB_{1(MSN)}$ loss is a pathogenic event. However, attempts to pharmacologically augment $CB_1$ signaling have yielded mixed results. The Glass laboratory tested a full $CB_1$ agonist (HU210), a partial $CB_1$ agonist (THC), and an inhibitor (URB597) of fatty acid amide hydrolase, and found no improvement in the motor phenotype of R6/1 mice with any of the treatments. In contrast, the Guzman laboratory reported a full rescue of both motor and pathological phenotypes in R6/2 mice after chronic treatment with THC. The discrepancy between the two studies is puzzling, especially with regard to THC which was tested by both laboratories, but may be related to the fact that the Glass laboratory used a higher dose (10 mg/kg) than the Guzman laboratory (2 mg/kg). It is well-known that $CB_1$ receptors, like many GPCRs, are highly vulnerable to desensitization and tolerance with strong chronic activation. However, it could also be argued that a pharmacological approach is not well suited to a genetic model which features selective loss of $CB_1$ from some neuronal populations but not others, especially considering that the loss in MSNs is nearly complete. Essentially, a cannabinoid agonist administered to HD mice could be conceptualized as acting at the receptor populations which have been spared, rather than those that have been lost, rendering interpretation of the result fairly difficult. Additionally, agonists like THC are also active at $CB_2$ receptors, which may also be involved in HD pathophysiology.

In a healthy striatum, $CB_2$ receptor expression should be minimal, if at all present. However, Huntington's disease, like other neurodegenerative disease, is associated with gliosis, and increased CB2 expression, presumably by activated microglia (Palazuelos et al., 2009). Indeed, CB2 expression colocalizes with both Iba1 and CD68, suggesting expression on microglia which have switched from resting to an M1 phenotype (Palazuelos et al., 2009). Genetic deletion of *cnr2* in R6/2 mice results in an accelerated and aggravated phenotype, suggesting that induced $CB_2$ expression is protective in these mice. One possible mechanism to explain this effect is the observation that deletion of CB2 receptors results in increased lesion size in response to malonate, and conversely that $CB_2$ activation results in a decreased local expression of TNFα, an inflammatory mediator (Palazuelos et al., 2009; Sagredo et al., 2009). Thus, $CB_2$ receptors might be protective in

excitotoxicity conditions, which are widely believed to exist in HD and R6/2 mice (Milnerwood et al., 2010; Okamoto et al., 2009). Conversely, another study demonstrated a protective effect of selective activation of peripheral $CB_2$ receptors, mediated by changes in IL6 levels that were driven by CB2 activity (Bouchard et al., 2012). IL-6 is elevated in HD mouse models (Bjorkqvist et al., 2008), and it has been shown that $CB_2$ activity can modulate IL-6 levels, suggesting that the beneficial effect of $CB_2$ receptors might actually be derived from a peripherally-mediated renormalization of cytokine levels.

Thus, the purpose of the first part of this doctoral work is to dissect the contribution of the loss of $CB_{1(MSN)}$ to HD pathology, by genetically rescuing this loss using a cell-type specific knock-in system. GPR88 is an orphan GPCR which was recently described by the Palmiter lab as being highly expressed in striatal MSNs, with some expression in the inferior olive and otherwise only sporadic expression in other brain areas (Quintana et al., 2012). This expression pattern was leveraged to selectively target MSNs using a *Gpr88*$^{+/Cre}$ mouse developed by the Palmiter lab, in combination with a conditional $CB_1$ knock-in mouse, in an R6/2 background (see *Section II*).

**1.2.3 The eCB signaling system and seizure control**

The endocannabinoid system is a logical target for control of epilepsy, based on the retrograde inhibition of presynaptic release mediated by the activity of 2-AG at $CB_1$ receptors. Indeed, one of the first major findings to result from the generation of the $CB_1$ knockout ($CB_1$-KO) was the observation that $CB_1$-KO mice experience spontaneous seizures (Zimmer et al., 1999), which result in the death of approximately 20% of animals in the first six months of age (unpublished observations). Soon afterwards, the Lutz laboratory described an increased susceptibility to kainate-induced seizures in $CB_1$-KO mice, and this effect was localized to $CB_1$ expressed on glutamatergic terminals by conditional knockout studies (Lutz, 2004; Marsicano, 2003). Indeed, genetic overexpression of $CB_1$ receptors on hippocampal pyramidal neurons is sufficient to improve seizure severity and mortality after kainate injection (Guggenhuber et al.).The interplay between seizures and $CB_1$ receptors seems to be bidirectional, as a single febrile seizure induced in early life is sufficient to cause long-lasting increased expression in specific hippocampal synapses (Chen et al., 2003). This long-term plasticity results in the development of limbic hyperexcitability, but it can be prevented by application of $CB_1$ antagonist during

febrile seizure induction (Chen et al., 2007). Intriguingly, similar protective effects can be observed after head injury, as treatment with a $CB_1$ antagonist quickly following injury improved long term changes in seizure susceptibility (Echegoyen et al., 2009).

The use of cannabinoid agonists (or antagonists) to control seizures suffers from a number of pitfalls including cannabinomimetic side effects, receptor desensitization, and differential effect on seizure susceptibility based on cell-type. These pitfalls have resulted in a mixed literature on the cannabinoid system in epilepsy. Whereas endocannabinoids generally seem to be antiepileptic and $CB_1$ antagonists are proepileptic (Katona and Freund, 2008; Wallace et al., 2002), endocannabinoids can become proepileptic in high doses – for example, fatty acid amide hydrolase (FAAH) knockout mice demonstrate increased susceptibility to seizures (Clement et al., 2003). Additionally, low doses of $CB_1$ antagonists can be paradoxically antiepileptic. However, cannabinoid agonists have generally been found to be antiepileptic in several models of induced epilepsy (Citraro et al., 2013; Naderi et al., 2008), and elevated endocannabinoid during seizures, leading to the hypothesis that endocannabinoid signaling tone is protective in epilepsy (Wallace, 2003).

**II. Genetic rescue of $CB_1$ receptors on medium spiny neurons prevents loss of excitatory striatal striatal markers but not motor phenotype in R6/2 mice.**

This section is adapted from a manuscript in preparation for submission.

**2.1 Overview and Rationale**

The early down-regulation of $CB_1$ receptor expression on medium spiny neuron (MSN) terminals was first observed in post-mortem tissue of HD patients (Glass et al., 2000), and this down-regulation is reliably measured in most mouse models of HD pathogenesis, including R6/2 (Horne et al., 2012; Luthi-Carter et al., 2002; Mccaw et al., 2004), R6/1 (Dowie et al., 2009; Naver et al., 2003), YAC128 (Pouladi et al., 2012) and HdhQ150 (Woodman et al., 2007). Indeed, it was recently reported that mutant huntingtin directly acts at the *cnr1* promoter to inhibit expression (Blasquez et al). Loss of MSN-expressed $CB_1$ ($CB_{1\ (MSN)}$) precedes the loss of other synaptic markers, including dopamine D2 and D1 receptors (Glass et al., 2000), and striatal synaptophysin (Cepeda et al., 2003; Goto and Hirano, 1990). This pattern of loss lead to the hypothesis that $CB_{1(MSN)}$ loss is an early pathological event which may control downstream pathology in HD and mouse models. Indeed, knockout of $CB_1$ receptors in R6/2 mice both exacerbates and accelerates the motor phenotype (Blázquez et al., 2010; Mievis et al., 2011), and aggravates pathological findings (Blázquez et al., 2010), suggesting that $CB_1$ receptor signaling participates through an unknown mechanism in the development of HD.

In addition to cannabinoid signaling, $CB_1$ receptors participate in several arms of dopaminergic signaling in MSNs. $CB_1$ and D2 receptors form functional heteromers, which flip ligand-directed $CB_1$ signaling from $G_{i/o}$ to $G_s$ (Kearn, 2005), and stimulation of $CB_1$/D2 heteromers results in twice as much Erk1/2 phosphorylation as is achieved by stimulating $CB_1$ alone (Kearn, 2005). Additionally, mice lacking $CB_1$ receptors ($cnr^{-/-}$ mice) show impaired pErk1/2, pDARPP32, and Fos signaling in MSNs after a single administration of amphetamine. This effect is also observed in mice lacking $CB_1$ in either GABAergic or CamKIIα-expressing neurons, suggesting that the $CB_{1(MSN)}$ may be required for proper signaling (Corbillé et al., 2007). The consequences of $CB_1$ loss are generally detrimental, as $CB_1$ signaling is thought control pro-survival signaling in healthy cells. For example, $cnr^{-/-}$ mice have decreased levels of BDNF (Aso et al., 2008; Steiner et al., 2007), and agonist-mediated $CB_1$ signaling results in Akt (Gómez del Pulgar et al., 2000) and Erk1/2 phosphorylation (Marsicano,

2003). However, there is a growing appreciation of the diversity of $CB_1$ function at different synapses, driven by conditional knockout studies. Therefore, it is difficult generalize about all $CB_1$ receptors; we need instead to study specific populations of $CB_1$ receptors.

Several attempts to increase $CB_1$ signaling in HD mouse models have resulted in divergent conclusions. One study treated R6/1 mice with either a full $CB_1$ agonist (HU210), a partial $CB_1$ agonist (THC), or an inhibitor (URB597) of fatty acid amide hydrolase, a serine hydrolase that inactivates the prototypical endocannabinoid (eCB) anandamide. The motor phenotype was not improved by any of these three treatment paradigms (Dowie et al., 2010). Conversely, another study treated R6/2 mice with a lower concentration of THC (2 mg/kg, compared with 10 mg/kg), and found improvement in several motor and neuropathological measures. A caveat to pharmacologically manipulation of $CB_1$ in HD mice is that the loss of this receptor's function is restricted to select neuronal types, whereas agonists activate large populations of $CB_1$ receptors irrespective of cell type. This is not desirable in a setting of receptor loss in restricted populations; for example in R6/2 mice, presynaptic $CB_1$ signaling is down-regulated in MSN axon terminals (Dowie et al., 2009; Horne et al., 2012), while it is preserved on corticostriatal terminals (Chiodi et al., 2012). Furthermore, in striatal interneurons, $CB_1$ signaling is selectively lost from NPY interneurons, but not from cholinergic, parvalbumin, or somatostatin interneurons (Horne et al., 2012). Therefore, the effects of delivering cannabinoid agonists systemically are difficult to interpret. Adding to this difficulty, the selectivity of cannabinoid drugs is limited by clear off-target responses, including through $CB_2$ receptors (Walter et al., 2003b), TRPV1 and GPR55 (Pertwee et al., 2010), and several additional GPCRs and ion channels. To circumvent these issues and directly test the pathophysiological relevance of the down-regulation of $CB_1$ signaling in MSNs in HD, we generated a conditional flox-stop $CB_1$ knock-in mouse line and backcrossed it to both the *Gpr88*$^{+/Cre}$ mouse line and to R6/2 mice, generating a new R6/2 mouse line in which an extra copy of *cnr1* is selectively expressed in all MSNs. Using this new genetic tool, we studied whether this cell selective genetic rescue of $CB_1$ signaling in MSNs affects classic motor behaviors and histopathological hallmarks in R6/2 mice.

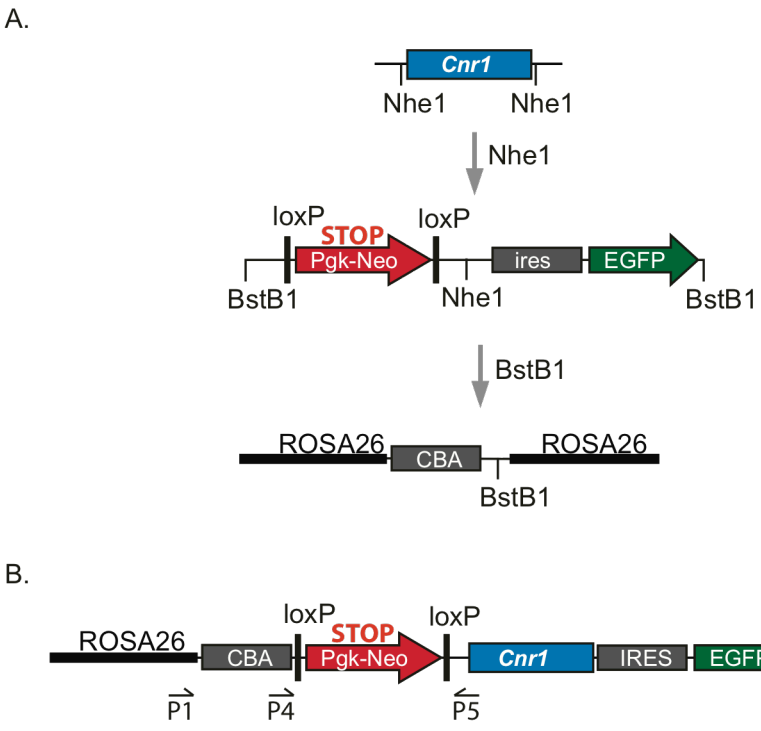


**Figure 2.1: Generation of fsCB$_1$ mice.**(A) Mouse *cnr1* was inserted at an Nhe1 site in a vector containing a floxed pgk-neo flanked by ires-EGFP, and then the construct was inserted into *Rosa26* at a BstB1 site, to produce the final targeting vector (B).

## 2.2 Results

### 2.2.1 Generation of R6/2 mice with genetic rescue of $CB_{1\ (MSN)}$.

We inserted a mouse *cnr1* open reading frame between a loxP-flanked *Pgk-Neo* resistance gene and ires EGFP and then move that cassette into a *Gt*(*Rosa26)Sor* targeting vector with the CBA promoter (CMV-chicken b-actin) at the transcription start (Figures 2.1A, 2.2). We refer to this modified *Gt*(*Rosa26)Sor* locus as $R26^{fsCB1}$; females with this gene were bred with $Gpr88^{+/Cre}$ males that express Cre recombinase predominantly in MSNs to activate $CB_1$ expression in MSNs (Quintana et al., 2012). Because low levels of GPR88 expression have been reported in other brain areas including the cortex, we performed PCR to test for the excision of Pgk-Neo, and thus activation of the $fsCB_1$ insert, in other brain regions. Whereas DNA from dissected striatum showed a band indicating Pgk-Neo excision, DNA from tail, cortex, and thalamus did not (Figure 2.1B).

$CB_1$ receptor loss occurs first in the indirect pathway, and later in the direct pathway in HD patients and mouse models (Dowie et al., 2009; Glass et al., 2000; Horne et al., 2012). To measure whether we were able to genetically restore $CB_1$ receptors in R6/2 mice, we performed semi-quantitative IHC staining in the GP (Figure 2.1C) and SNr (Figure 2.1D), the respective targets of indirect- and direct-pathway MSNs. By co-staining for either Leu-Enkephalin (Enk) or Substance P (SP), we identified regions of interest, and measured $CB_1$ receptor expression (Figure 2.1C-D). In the GP of R6/2 animals $CB_1$ protein was reduced to 64% ± 12% of wild-type (WT) levels ($p=0.003$) and this loss was restored ($F_{(2,30)}=7.2$, $p=.003$) to 91% ± 10% of WT levels in R6/2-$CB_{1(MSN)}$ mice. In the SNr, there was a trend towards loss of $CB_1$ receptors in R6/2 mice compared with WT or R6/2-$CB_{1(MSN)}$ mice ($F_{(2,28)}=1.9$, $p=.16$). Because the indirect pathway shows $CB_1$ loss before the direct pathway, it is possible that the mice die before the full expression of the molecular phenotype.

### 2.2.2 Knock-In $CB_1$ receptors are functional.

To examine the functionality of the $R26^{fsCB1}$ allele, we bred it and $Gpr88^{+/Cre}$ into a $cnr1^{-/-}$ background. By using $Gpr88^{+/Cre}$ females, which express Cre recombinase in the ova, expression of $R26^{fsCB1}$ allele is expressed globally. Global expression was verified for all animals by PCR reaction from tail DNA (Figure 2.3A).

To test the ability of $fsCB_1$-derived $CB_1$ receptors to couple to G-proteins, we performed a GTPγS-binding assay. First, a dose-response curve was established for CP55,940-mediated induction of GTPγS binding to $CB_1$

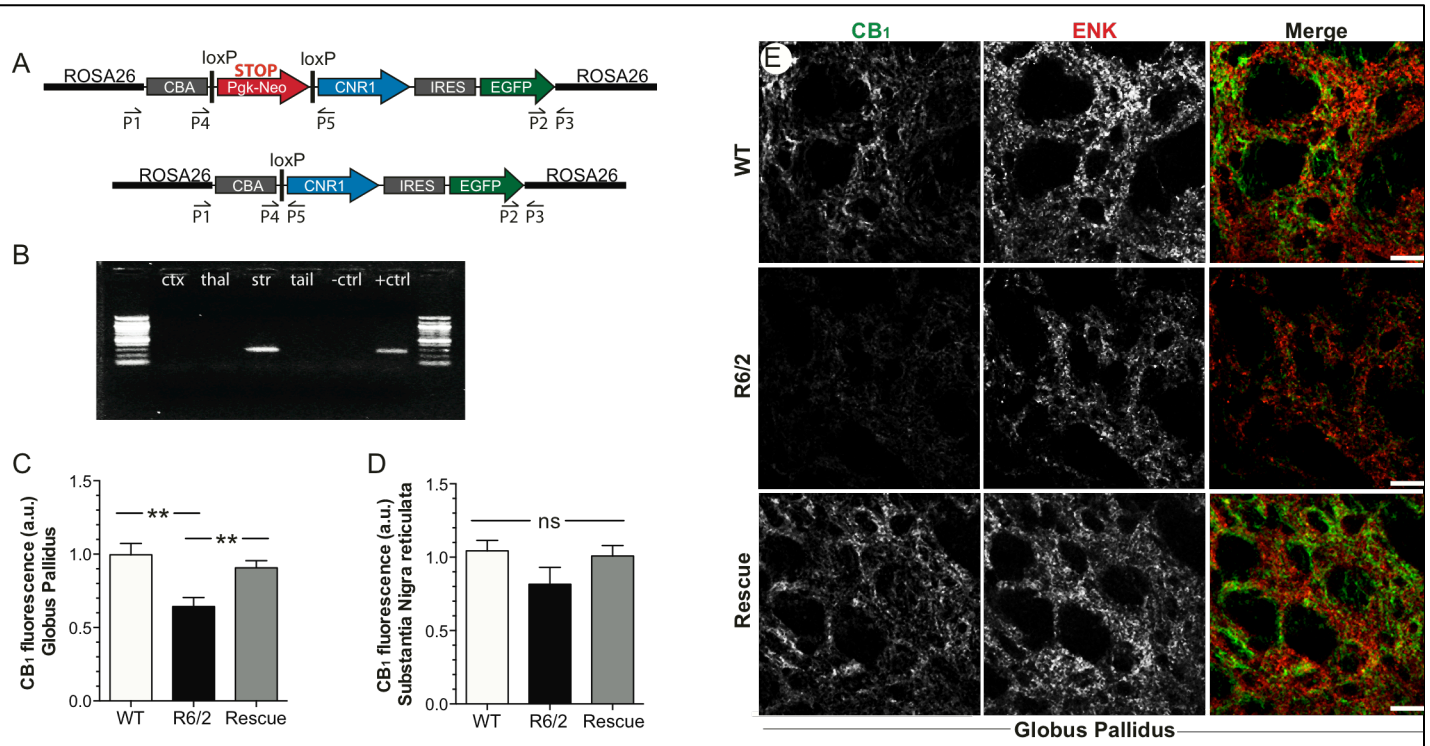


**Figure 2.2: Genetic $CB_{1(MSN)}$ rescue restores $CB_1$ receptor expression in R6/2 mice.**
(A): An fs$CB_1$ insert was generated and targeted to *Rosa26,* carrying *CNR1-IRES-EGFP* under a *CBA* promoter with a flox-stop containing *Pgk-neo*. (B): PCR was performed with primers flanking the pgk-neo sequence, such that the presence of a band would indicate that Pgk-neo has been removed and the insert has been activated. Pgk-neo excision by Cre was specific for striatal tissue, and was not observed in tail, cortex, or thalamus. (C-D): Semi-quantitative IHC was used to verify that R6/2-$CB_{1(MSN)}$ rescue (n=8) resulted in restoration of $CB_1$ to WT (n=14) levels in the GP and SNr. Whereas 12-week R6/2 mice (n=11) have a clear loss of $CB_1$ from the GP, R6/2-$CB_{1(MSN)}$ rescue mice expressed WT-levels of $CB_1$. Notably, $CB_1$ loss is not observed in the SNr in 12-week R6/2 mice. (E): Representative images are shown from the globus pallidus of R6/2, WT, and R6/2-CB1(MSN) rescue mice. Images were acquired on a Leica confocal, using an oil-immersion 63X objective. Scale bars indicate 25µm. All error bars indicate S.E., and post-hoc analyses were carried out with Fisher's T test as indicated by **P<.05, **P<.01, ***P<.001.*

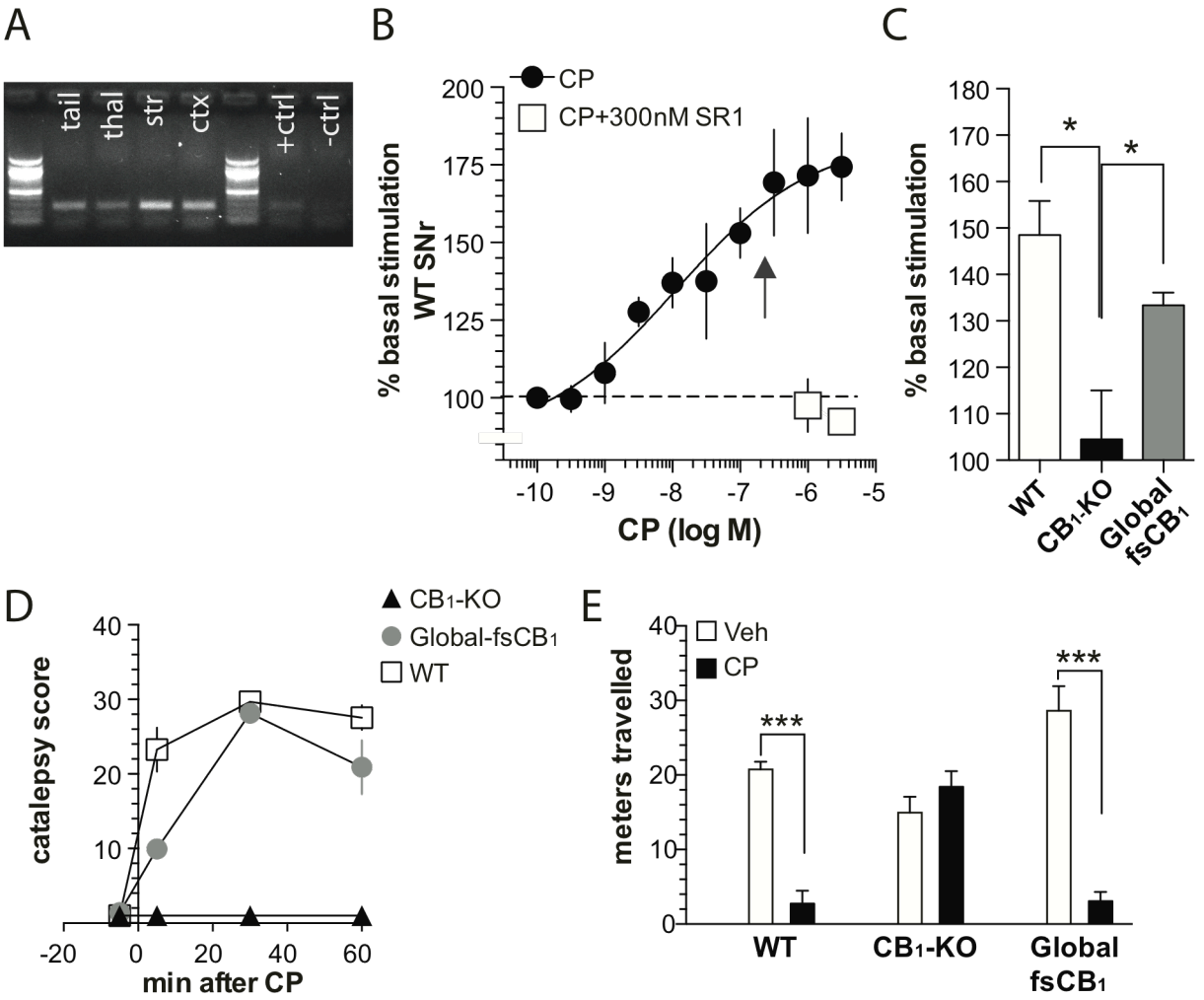


**Figure 2.3: Receptors expressed from fsCB$_1$ are functional.**
To test the functionality of fsCB$_1$-derived protein, we crossed *cnr1*$^{-/-}$ *Gpr88*$^{+/Cre}$ females with *cnr1*$^{-/-}$ *R26*$^{+/fsCB1}$ males, since *Gpr88* is expressed transiently in the ova and results in expression of Cre recombinase, and thus global excision of *Pgk-Neo* and global expression of fsCB$_1$ in adult mice. Thus, the resulting mice had no endogenous CB$_1$ protein, but expressed fsCB$_1$-derived CB$_1$ in all tissues (global-fsCB$_1$ mice). (A) PCR demonstrating *Pgk-Neo* excision in brain and peripheral tissue. (B) In dissected SNr tissue, GTP$\gamma$S binding was induced by CP55,940 in WT (n=4) and Global-fsCB$_1$ mice (n=5), but not in *cnr1*$^{-/-}$ mice (n=4). (C) After treatment with 0.3 mg/kg CP, and measured catalepsy in WT (n=6), *cnr1*$^{-/-}$ (n=7), and Global-fsCB$_1$ mice (n=7). The cataleptic response observed in WT mice was absent in *cnr1*$^{-/-}$ mice, and restored in Global fsCB$_1$ mice. (D) Similarly, CP55,940 induced hypolocomotion in WT mice, which was lost in *cnr1*$^{-/-}$ mice, and restored in global-fsCB$_1$ mice. Post-hoc comparisons were performed with Fisher's T-test, with **P*<.05, ***P*<.01, ****P*<.001. Error bars depict S.E.M.

receptors in freshly dissected homogenized SNr tissue from 5 WT mice (Figure 2.3B). Then, we dissected SNr tissue from WT, *cnr1*$^{-/-}$ or Global-fsCB$_1$ mice and performed GTPγS binding in triplicate, both with and without a CB$_1$ receptor agonist, CP55,940, at the EC$_{80}$ dose of 140nM (Figure 2.3C). Stimulation of GTPγS binding in response to CP55,940 (CP) was restored in Global-fsCB$_1$ mice nearly to WT levels compared to *cnr1*$^{-/-}$ mice (WT: 148.5±7.3%, *cnr1*$^{-/-}$ = 104.5±10.5%, Global-fsCB$_1$=133.4±2.7%; $F_{(2,10)}$=9.48, p=0.005). We tested the ability of Global-fsCB$_1$ mice to reproduce the motor response to cannabinoid agonists observed in WT mice. CP55,940-induced catalepsy (Figure 2.3D) was absent in *cnr1*$^{-/-}$ mice and rescued (genotype: $F_{(2,28)}$=111.3, P<.001; time: $F_{(3,28)}$=49.2, p<.001, interaction: $F_{(6,28)}$=15.1, p<.001) in Global-fsCB$_1$ mice (p<.001 at 5 and 30 min, p=.02 at 60 min). Similarly, global expression of fsCB$_1$-derived CB$_1$ receptors rescued (p<.001) CP55,940-induced hypolocomotion (interaction of genotype x treatment: $F_{(2,18)}$=29.58, p<.001, Figure 2E), which was absent in *cnr1*$^{-/-}$ mice. We conclude that fsCB$_1$-derived CB$_1$ protein both couples to G proteins and is capable of reproducing cannabinoid-induced behaviors.

### 2.2.3 The R6/2 motor phenotype is unchanged by genetic rescue of CB$_{1(MSN)}$ receptors.

Classical measures of motor function in R6/2 mice were tested for the effect of CB$_{1(MSN)}$ rescue. Rotarod performance (Figure 2.4A) showed a trend towards impairment at 4 wk of age in both R6/2 and R6/2-CB$_{1(MSN)}$ mice compared to WT mice and was clearly impaired at 8 wk ($F_{(2,8)}$=25.7, p<.001) and at 12 wk ($F_{(2,10)}$=285.7, p<.001) of age for both R6/2 and R6/2-CB$_{1(MSN)}$ mice. Locomotion was measured for 10 min in an open field chamber (Figure 2.4B), and both R6/2 and R6/2-CB$_{1(MSN)}$ rescue mice were hypolocomotive compared to WT mice beginning at 10 wk of age. At 4 and 6 wk, R6/2 mice performed fewer rearings (Figure 2.4C) than R6/2-CB$_{1(MSN)}$ mice and WT mice (pooled 4 and 6 wk: WT = 16.5±2.2, R6/2 = 5.8±1.2, R6/2-CB$_{1(MSN)}$ = 12.5±2.0), but after 8 wk R6/2-CB$_{1(MSN)}$ rescue mice were indistinguishable from R6/2 mice and both groups reared much less than WT mice (pooled 8, 10, and 12 wk: WT = 16.25±0.8, R6/2 = 2.8±1.4, R6/2-CB$_{1(MSN)}$ = 2.6±1.0). Phenotype was scored biweekly by blinded observers for nine factors on a 1-2 scale (see methods). Two-factor ANOVA showed an effect of genotype ($F_{(2,114)}$=81.6, p<.001), and of age ($F_{(4,114)}$=24.6, p<.001), and the

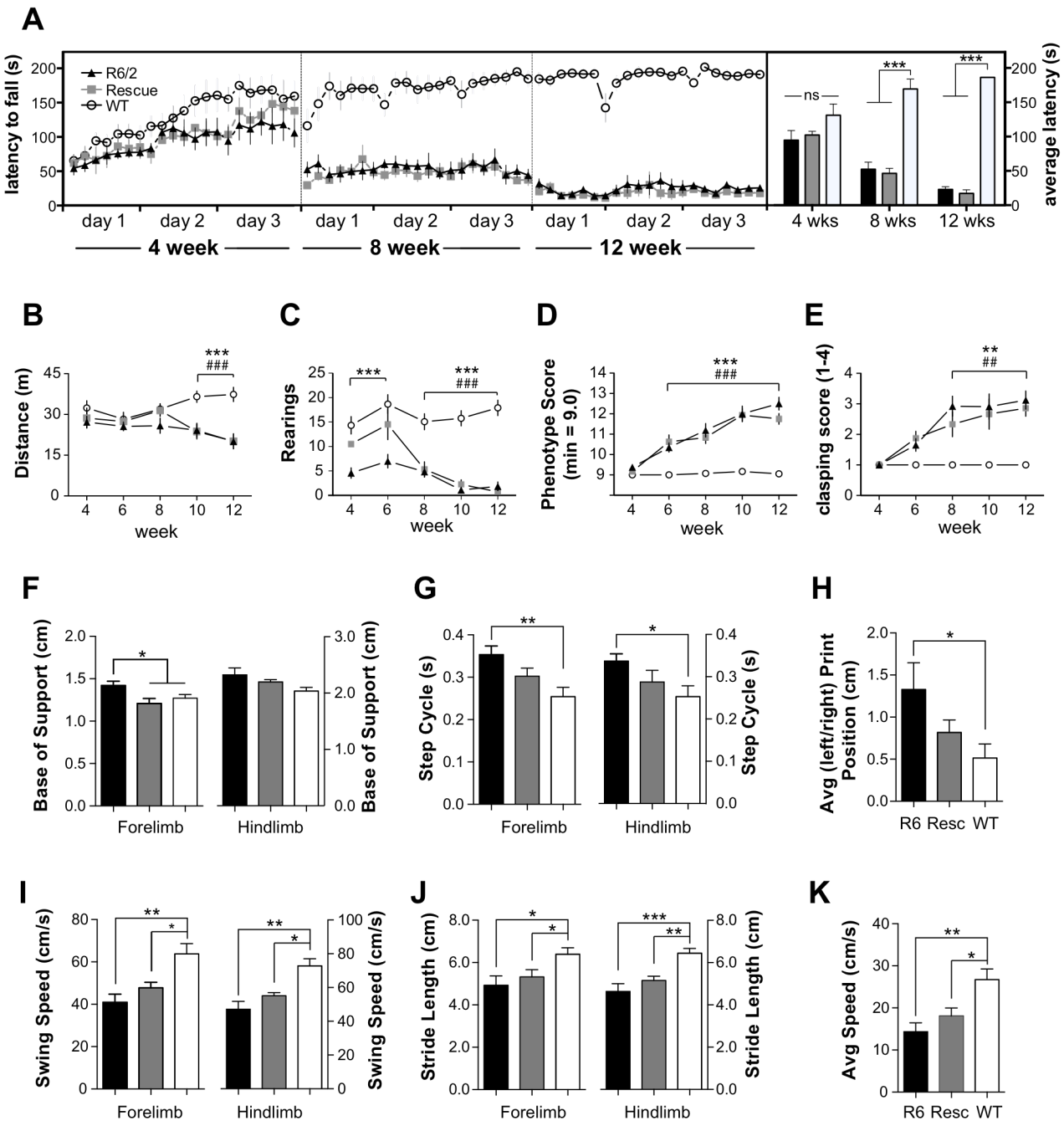


**Figure 2.4: $CB_{1(MSN)}$ rescue is insufficient to rescue the R6/2 motor phenotype.**
For all graphs, R6/2 mice are shown in black, R6/2-$CB_{1(MSN)}$ rescue mice are shown in grey, and WT mice are shown in white. (A): Rotarod performance was measured at 4, 8, and 12 wk, reflecting presymptomatic, early, and late symptomatic stages. The R6/2 motor phenotype was clearly observed beginning at 8 wk, and no improvement was measured in R6/2-$CB_{1(MSN)}$ rescue mice (n=4-6, all groups). (B) In an open field chamber, locomotion was scored using Noldus Ethovision software, and rearing (C) was manually recorded over the first two minutes (WT, n=15; R6/2, n=13; R6/2-$CB_{1(MSN)}$, n=8). R6/2 animals were hypolocomotor beginning at 8 wk, whereas R6/2-$CB_{1(MSN)}$ rescue developed a hypolocomotor phenotype after 10 wk, and were indistinguishable from R6/2 mice at 10 and 12 wk. Rearing behavior was decreased in R6/2 mice at all timepoints, whereas, R6/2-$CB_{1(MSN)}$ rescue mice did not show a deficit until after 8 wk. (D): Manual scoring of the R6/2 motor phenotype along 9 measures (see methods) showed a clear phenotype measurable starting 6 wk of age, in both R6/2 and R6/2-$CB_{1(MSN)}$ rescue mice, and clasping behavior (E) also began at 6 wk of age in both R6/2 and R6/2-$CB_{1(MSN)}$ rescue mice. The Noldus Catwalk system was used to perform gait analysis at 10 wk of age. Minor improvement was seen in step cycle (G) and paw placement (H), but not in base of support (F), limb swing speed (I), stride length (J), or average speed (K). Error bars indicate S.E., and Fisher's T test was used for post-hoc analyses with *$P<0.05$, **$P<0.01$, and ***$P<0.001$. For (h-k), * denotes comparisons between WT and R6/2, and # denotes comparisons between WT and R6/2-$CB_{1(MSN)}$ rescue mice.

interaction between genotype and age was also significant ($F_{(8,114}$=6.4, P<.001), reflecting a progressive motor phenotype in R6/2 mice that was not improved in the R6/2-$CB_{1(MSN)}$ cohort (Figure 2.4D).

To definitively establish that no improvement in motor phenotype had resulted from $CB_{1(MSN)}$ rescue, we performed automated gait analysis using the Noldus Catwalk XT system (Wageningen, The Netherlands). R6/2-$CB_{1(MSN)}$ mice showed mild improvement in base of support ($F_{(2,14)}$=4.4, p=.03), step cycle ($F_{(2,14)}$=6.0, p=.01) and print position ($F_{(2,13)}$=6.8, p=.01) in R6/2-$CB_{1(MSN)}$ rescue mice compared with R6/2 mice (Figure 2.4F-G) but no improvement in swing speed (forelimbs: $F_{(2,14)}$=8.31, p<.01; hindlimbs: $F_{(2,14)}$=10.86, p<.01), stride length (forelimbs:$F_{(2,14)}$=4.7, p<.03; hindlimbs: $F_{(2,14)}$=11.4, p<.01), or crossing speed ($F_{(2,14)}$=8.1, p<.01) (Figure 2.4I-K). In summary, we conclude that no appreciable motor rescue resulted from $CB_{1(MSN)}$ in R6/2 mice.

**2.2.4 $CB_{1(MSN)}$ receptor rescue is sufficient to prevent striatal loss of axonal proteins in R6/2 mice.**

We hypothesized that the pattern of early loss of $CB_1$ followed by loss of other markers in MSN terminals indicates that $CB_1$ loss precedes loss of the terminals themselves. To test this hypothesis, we costained for markers of MSN terminals (Leu-enkephalin in GP, substance P in SNr) and either vGAT, Neuroligin 2, or synaptophysin. Levels of neuropeptides, synaptophysin, vGAT, and neuroligin 2 were unchanged in R6/2 or R6/2-$CB_{1(MSN)}$ rescue mice (Figure 2.5), compared with WT mice. Previous studies demonstrated striatal loss of synaptophysin in R6/2 mice (Cepeda et al., 2003), and $CB_{1(MSN)}$ rescue was sufficient to block the loss of synaptophysin in both the dorsolateral and dorsomedial striatum (DL-STR: $F_{(2,28)}$=4.7, p=.018); DM-STR: $F_{(2,29)}$=5.0, p=.013) (Figure 2.6A-C). Furthermore, when synaptophysin was plotted against $CB_1$ in all R6/2 mice (WT mice were excluded to prevent genotype-driven bias), there was a positive correlation ($r^2$=0.29,

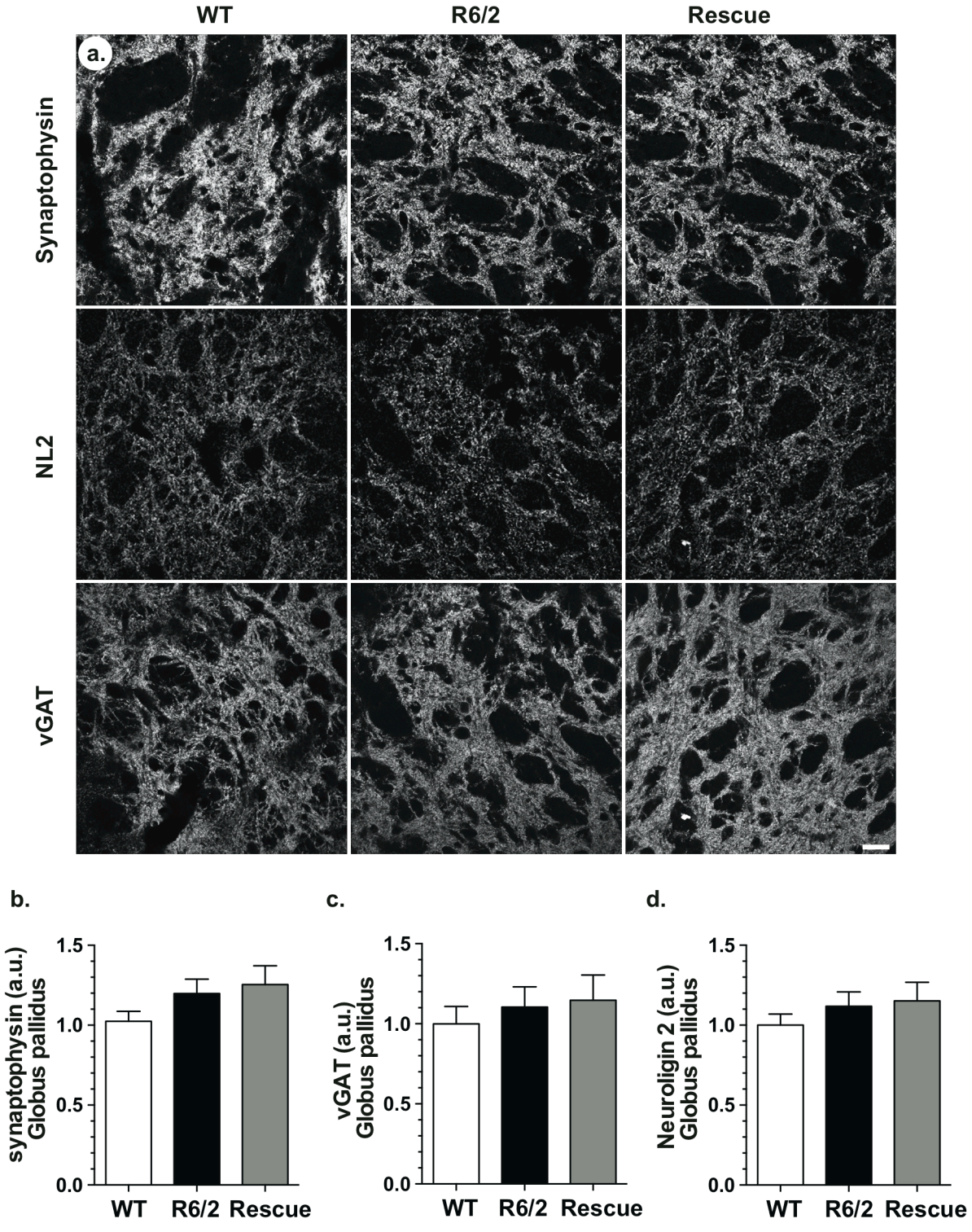


**Figure 2.5: No synaptic loss in the globus pallidus of R6/2 mice.**
(A) Representative images are shown for synaptophysin, neuroligin 2, and vGAT staining in the globus pallidus. (B-D) sqIHC was performed for each of the three synaptic markers, and no differences were observed between WT, R6/2, or R6/2-$CB_{1(MSN)}$ rescue. Analyses were carried out by one-way ANOVA, error bars depict SEM, and scale bar = 25μm.

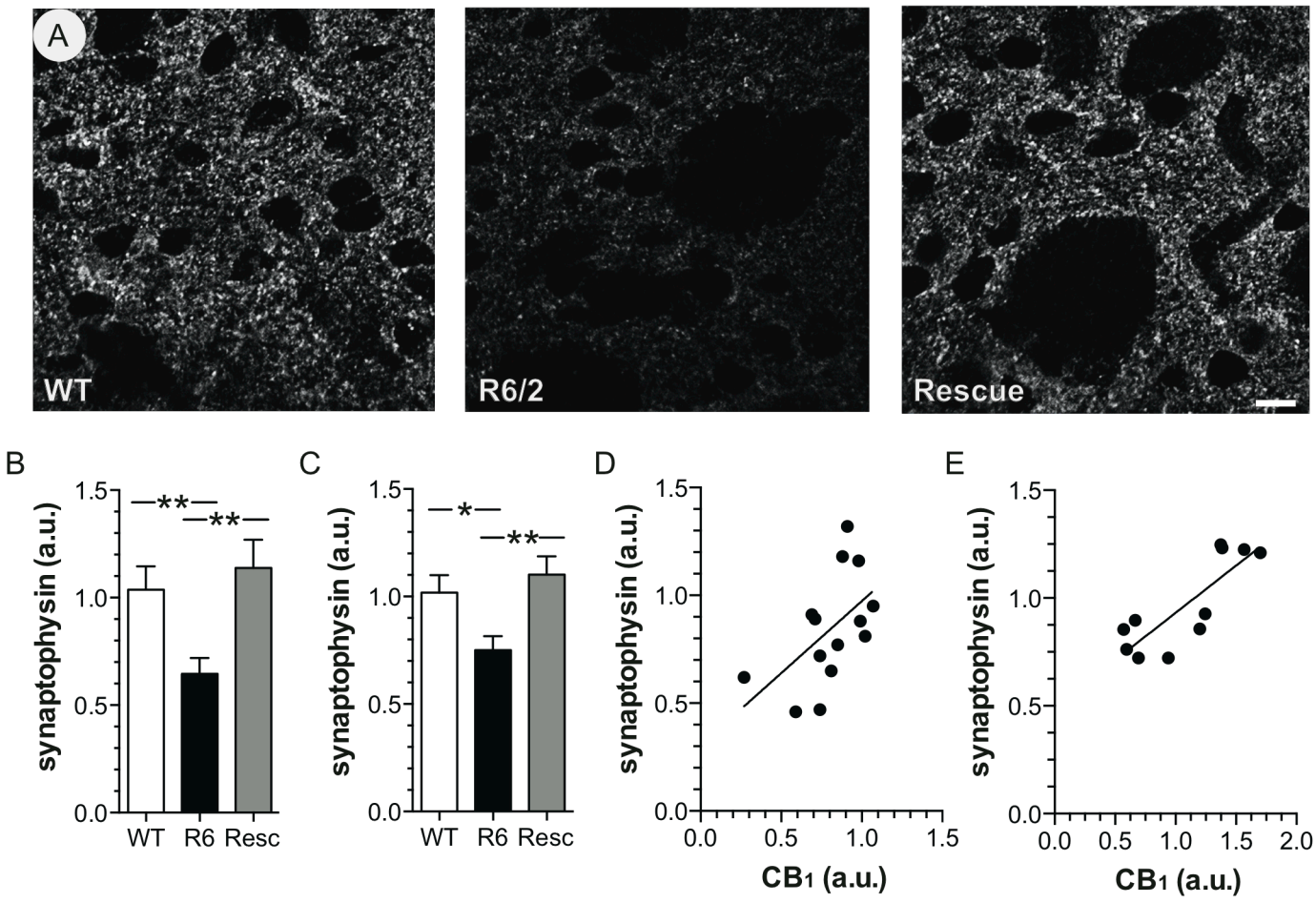


**Figure 2.6: Loss of striatal synaptophysin in R6/2 mice is rescued by genetic restoration of $CB_{1(MSN)}$.** (A) Representative images of dorsal medial striatal synaptophysin staining are shown with background subtraction. R6/2 sections showed both a decrease in overall intensity and fewer hyperintense foci. Both dorsal-medial (B) and dorsal-lateral striatum (C) showed decreased synaptophysin immunostaining in R6/2 mice, which were restored to WT levels in R6/2-$CB_{1(MSN)}$ rescue mice. (d) Within-subject plots of synaptophysin staining against $CB_1$ staining in the globus pallidus show a positive linear correlation between $CB_1$ and synaptophysin intensities in 12-week-old R6/2 mice (D) and in 20-month-old HdhQ150 mice (E). Error bars depict S.E., and Fisher's T-Test was used for post-hoc analyses, with $*P<.05$, and $**P<.01$. Scale bar = 10 mm.

p=0.045, slope=0.67±0.30) between $CB_1$ and synaptophysin loss within individual mice (Figure 2.6D). To test this relationship in a different mouse model of HD, we measured striatal synaptophysin loss and pallidal $CB_1$ loss in $Hdh^{+/Q150}$ and $Hdh^{Q150/Q150}$ mice, a knock-in model of HD. As with the R6/2 cohort, WT controls were not included in the analysis, since this can create an artificial genotype-driven correlation. We found a similar linear correlation between $CB_1$ expression and synaptophysin in HdhQ150 mice ($r^2$=0.69, P=.002, slope=0.44±0.10), indicating that our findings in R6/2 mice can be generalized to other models of HD (Figure 2.6E).

To determine which synapses lose synaptophysin in R6/2 mice, we co-stained for either vesicular GABA transporter (vGAT) and Neuroligin-2, a post-synaptic marker of GABAergic synapses (Varoqueaux et al., 2004), or vesicular glutamate transporter 1 (vGlut1) and vesicular glutamate transporter 2 (vGlut2), markers of corticostriatal and thalamicostriatal synapses, respectively. We observed decreased immunostaining in both vGlut1 ($F_{(2,25)}$=5.45, p=.011) and vGlut2 ($F_{(2,25)}$=7.01, p=.004) in the DM-STR of R6/2 mice compared to WT (vGlut1: p=.004, vGlut2: p=.002), and restored to WT levels (Fig. 2.7A-B, E-F) in R6/2-$CB_{1(MSN)}$ rescue mice (vGlut1: p=.012; vGlut2: p=.005). In contrast vGAT and Neuroligin-2 immunostaining was unchanged in either R6/2 or R6/2-$CB_{1(MSN)}$ rescue mice (Figure 2.7C-D, G-H), compared with WT mice. We conclude that excitatory, but not inhibitory, presynaptic proteins, are lost in the striatum of R6/2 mice, and that genetic rescue of $CB_{1(MSN)}$ is sufficient to prevent this loss.

Because some antibodies performed poorly on IHC (PSD95), it was not possible to perform quantitative analysis with this method. Generally, strong staining for synaptic proteins results in clearly visible puncta under high magnification (63X), whereas weaker staining has a low signal to noise ratio which results in diffuse staining under high magnification, and is not appropriate for quantitative analysis. Measurement of PSD95 is necessary because it is a postsynaptic structural protein, unlike vGlut1 and vGlut2, which provide information about presynaptic vesicles. We performed immunoblotting for synaptophysin, PSD95, and neuroligin 2, to validate our IHC findings and to measure PSD95 (Figure 2.8A-D). In accordance with our IHC findings, we observed no change in neuroligin 2, compared with a loss of synaptophysin in R6/2 mice which was restored in R6/2-$CB_{1(MSN)}$ mice ($F_{(2,6)}$=25.37, p=0.001). Additionally, we observed a dramatic loss of PSD95 in R6/2 mice,

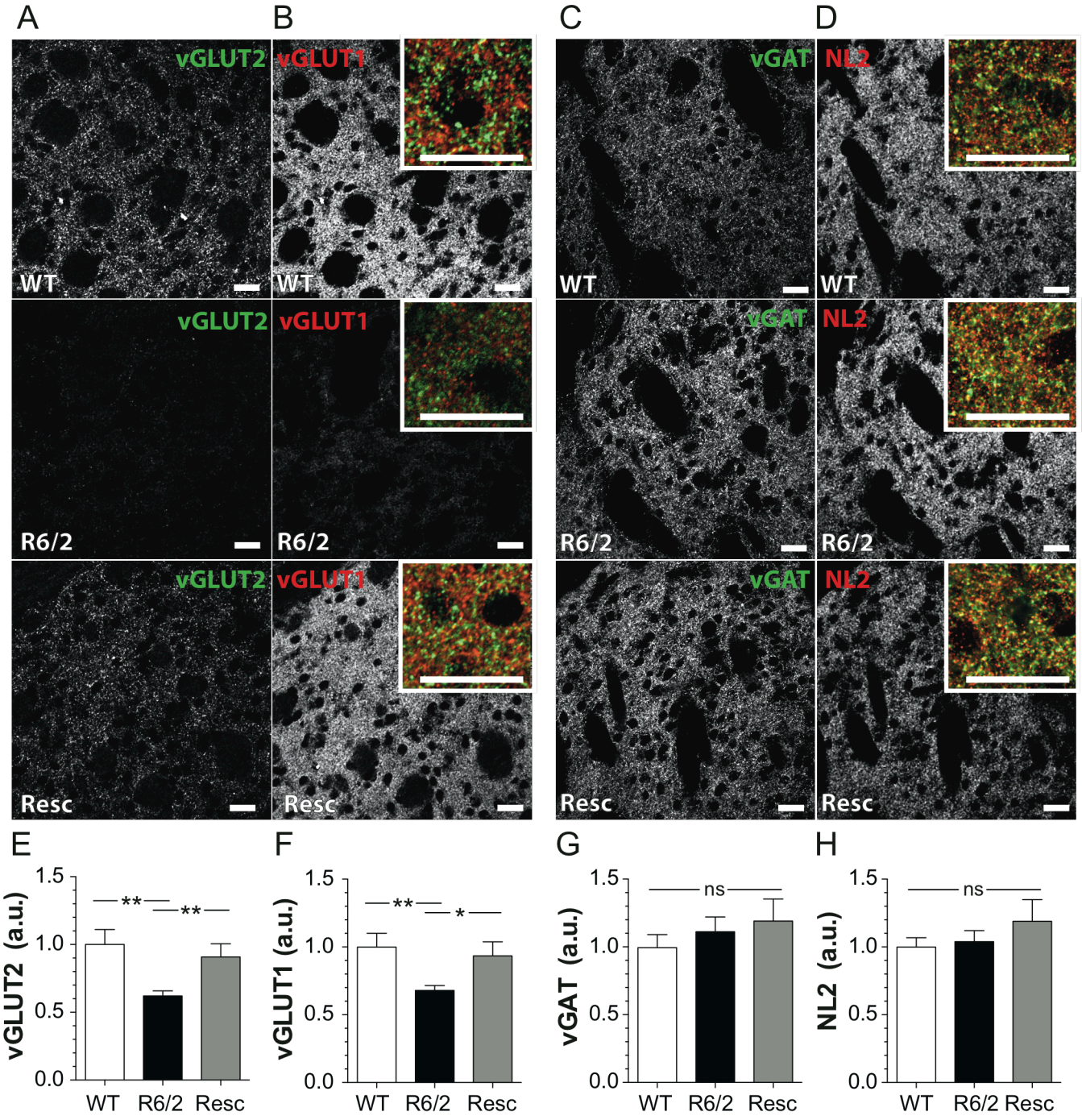


**Figure 2.7: Synaptic loss in R6/2 mice, and rescue in R6/2-$CB_{1(MSN)}$ rescue mice, is specific for excitatory striatal synapses.** To determine the specificity of synaptic loss, we costained for vGlut1 and vGlut2 (A-B, representative images, scale bar = 25 µm), or vGAT and NL2 (C-D, representative images, scale bar = 25 µm). There was a clear reduction in staining of both vGlut2 (E) and vGlut1 (F) in R6/2 mice, which was restored in R6/2-$CB_{1(MSN)}$ rescue mice. However, in the same mice, there was no reduction in staining of either vGAT or NL2 in either R6/2 or R6/2-$CB_{1(MSN)}$ rescue mice (G-H). All images were taken with a Leica confocal microscope, and are presented with the same settings. Insets represent a 4x digital zoom, with vGlut2 in green and vGlut1 in red (B) or with vGAT in green and NL2 in red (D). All scale bars depict 25 µm, and error bars show S.E. Post-hoc analyses were performed with Fisher's T Test, and are indicated by *$P<.05$, **$P<.01$.

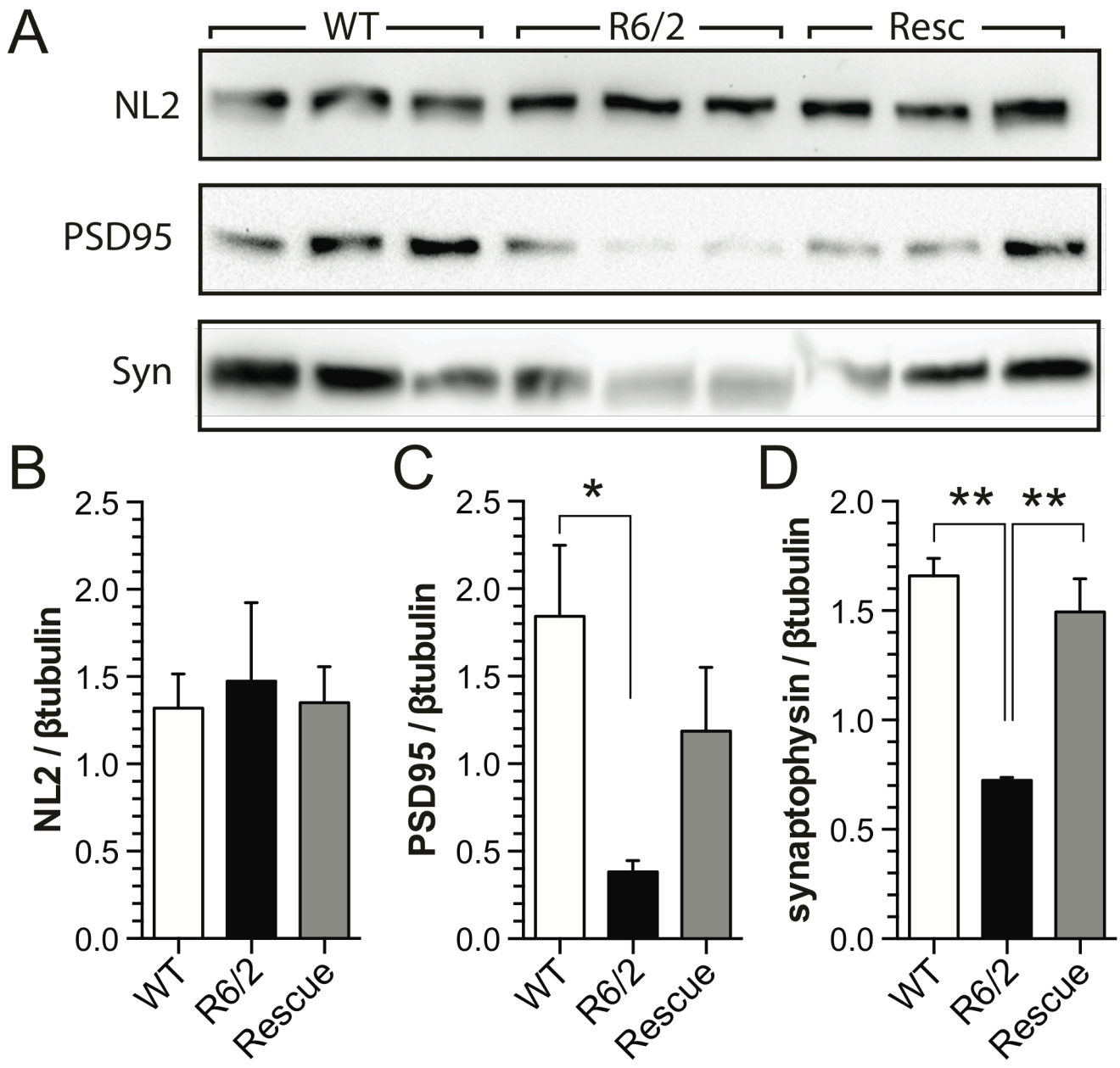


**Figure 2.8: Confirmation of IHC findings by immunoblotting.** (A) Representative immunoblots are shown for WT, R6/2, and R6/2-$CB_{1(MSN)}$ rescue mice (N=3 all groups). Each experiment was repeated 3 times and normalized to β-tubulin for quantitation. In confirmation of our earlier findings, there was no change in neuroligin 2 in R6/2 mice (B), but we measured a substantial loss of PSD95 in R6/2 mice compared to WT which was restored in R6/2-$CB_{1(MSN)}$ mice (C). Similarly, synaptophysin was lost in R6/2 mice and restored in R6/2-$CB_{1(MSN)}$ mice (D). Error bars show S.E and post-hoc analyses were performed with Fisher's T Test and are indicated by *$P<0.05$ and **$P<0.05$

but this loss was improved in R6/2-$CB_{1(MSN)}$ mice $F_{(2,6)}$=5.32, p=0.05). We conclude that R6/2 mice feature a loss of pre- and postsynaptic protein from excitatory striatal afferents, and that this loss is restored in response to genetic rescue of $CB_{1(MSN)}$.

**2.2.5 $CB_{1(MSN)}$ receptor rescue is sufficient to prevent loss of dendritic spines on striatal MSNs.**

To measure anatomical correlates of altered synaptic protein levels, we performed Golgi staining in 12 week old R6/2, R6/2-$CB_{1(MSN),}$ and WT mice. Prior studies have demonstrated reductions in spine density in 3rd and 4th order dendrites on MSNs by Golgi stain (Klapstein et al., 2001; Spires et al., 2004). We confirm these findings and extended them to demonstrate that this loss does not occur in R6/2-$CB_{1(MSN)}$ mice (Figure 2.9). Specifically, we measured an effect of branch order ($F_{(3,39)}$=81.61, p<0.001), of genotype ($F_{(2,13)}$=5.79, p=0.016, and an interaction effect ($F_{(6,39)}$=2.58, p=0.033), indicating a specific loss of spine density on higher order dendrites in R6/2 mice, but not in R6/2-$CB_{1(MSN)}$ mice. We conclude that the loss of $CB_1$ on MSNs controls the subsequent loss of dendritic spines.

**2.3 Discussion**

Here we describe a genetic restoration of functional $CB_{1(MSN)}$ receptors, which are lost early in the progressive phenotype of both R6/2 mice and HD patients. Unexpectedly, the rescue of $CB_1$ expressed on MSN terminals was able to prevent the loss of excitatory input to MSNs, one synapse removed from our intervention. Specifically, $CB_{1(MSN)}$ rescue spared excitatory synaptic proteins (synaptophysin, vGlut1, vGlut2) which were lost in R6/2 mice, whereas inhibitory synaptic proteins were unaffected. These data are consistent with reports that both GluR1 and PSD95, but not gephryn, are lost in the striatum of R6/1 mice (Nithianantharajah et al., 2008), and that PSD95 is lost in R6/2 mice (Luthi-Carter et al., 2003). Additionally, genetic rescue of $CB_{1(MSN)}$ expression spared both the density of dendritic spines and sEPSC frequency in MSNs, both of which are reduced in R6/2 mice.

Despite this reversal of synaptopathy among striatal inputs, the R6/2-$CB_{1(MSN)}$ mice did not show improvement in motor phenotype among a broad array of measures. Importantly, reduced sEPSCs are only one of many electrophysiological disturbances which have been described in the striatum of R6/2 mice (reviewed in Raymond et al., 2011), including reduced connectivity between MSNs (Cepeda et al., 2013), abnormally

increased MSN responses to input from fast-spiking (FS) interneurons (Cepeda et al., 2013), and impaired dopamine-dependent long-term potentiation (LTP) (Kung et al., 2007). Our data emphasize that multiple circuits are impaired in HD and combine to produce a behavioral phenotype, and suggest that localized interventions are unlikely to result in substantial changes in motor impairment. We conclude that although $CB_{1(MSN)}$ rescue spares the loss of excitatory striatal synapses in HD, striatal synaptic loss and motor deficits are dissociable features of the HD phenotype.

The mechanism by which $CB_{1(MSN)}$ controls striatal excitatory synapses is unclear. Because $CB_1$ signaling regulates presynaptic MSN GABA release, $CB_1$ signaling on MSN terminals may have an important role in balancing the output of direct- and indirect-pathway MSNs, and therefore the output of the basal ganglia. Altered basal ganglia output to thalamus and cortex may function as a feedback loop to alter cortical and thalamic input to the striatum. Another possibility is that $CB_1$ signaling is required for trophic support to MSN dendrites. $CB_1$ signaling can activate Erk1/2 and it is also required for the activation of Erk1/2 by dopamine (Corbillé et al., 2007). Indeed, mice lacking $CB_1$ in principal forebrain neurons or in GABAergic neurons failed to respond to dopamine release with Erk1/2 signaling, suggesting that $CB_{1(MSN)}$ might be required for this effect (Corbillé et al., 2007). In turn, dopamine depletion is known to cause loss of MSN spine density (Meredith et al., 1995), specifically for glutamatergic synapses (Day et al., 2006) – a similar pattern to what we observed in R6/2 mice. Therefore, it is possible that loss of $CB_{1(MSN)}$ impairs dopaminergic signaling, possibly by disinhibiting GABAergic control of dopamine neurons, resulting in decreased dopamine and resultant loss of excitatory synapses. A third possibility is that $CB_{1(MSN)}$ on MSN-MSN collaterals affects the inhibitory tone of MSN recurrent network activity. Developmental silencing of direct- or indirect-pathway MSNs has recently been shown to control the number of excitatory synapses onto MSNs, but to have no effect on the arborization of MSNs themselves (Kozorovitskiy et al., 2012). Although similar effects in adult brain have not yet been shown, it is possible that the mechanism by which MSN networks control excitatory input into the striatum is retained in adulthood, and that when $CB_{1(MSN)}$ is lost in R6/2 mice, this perturbs the balance of MSN recurrent network activity and causes loss of excitatory input.

Interest in targeting the eCB system in HD originally arose from the realization that $CB_{1(MSN)}$ are selectively lost in HD patients early in disease, and inspired the hypothesis that this loss constitutes a key pathogenic event. Implicit in this description is that reduced $CB_{1(MSN)}$ signaling is a common precursor to multiple pathologic cascades which culminate in behavioral impairment – our results do not support this hypothesis. Nevertheless, the finding that $CB_{1(MSN)}$ rescue is sufficient to prevent striatal synaptopathy demonstrates that $CB_{1(MSN)}$ signaling controls a subset of the anatomical and functional disturbances in HD mice, and that it is an important molecular component of healthy striatal function. Importantly, our data do not rule out the therapeutic use of cannabinoid agonists in HD, since other populations of $CB_1$ may be useful targets for controlling aberrant signaling, especially $CB_1$ on the corticostriatal synapse where $CB_1$ receptors are selectively spared (Chiodi et al., 2012). Because two independent groups found that knockout of $CB_1$ receptors in R6/2 mice worsened the motor phenotype (Mievis et al., 2011; 2010), we speculate that $CB_1$ receptors expressed on other (non-MSN) neuronal populations are responsible for this effect. In summary, our study has addressed a long-standing question in the field regarding the significance of the loss of $CB_{1(MSN)}$, but further work remains to be done to discover which other $CB_1$ receptor subpopulations might be targeted to improve the HD behavioral phenotype.

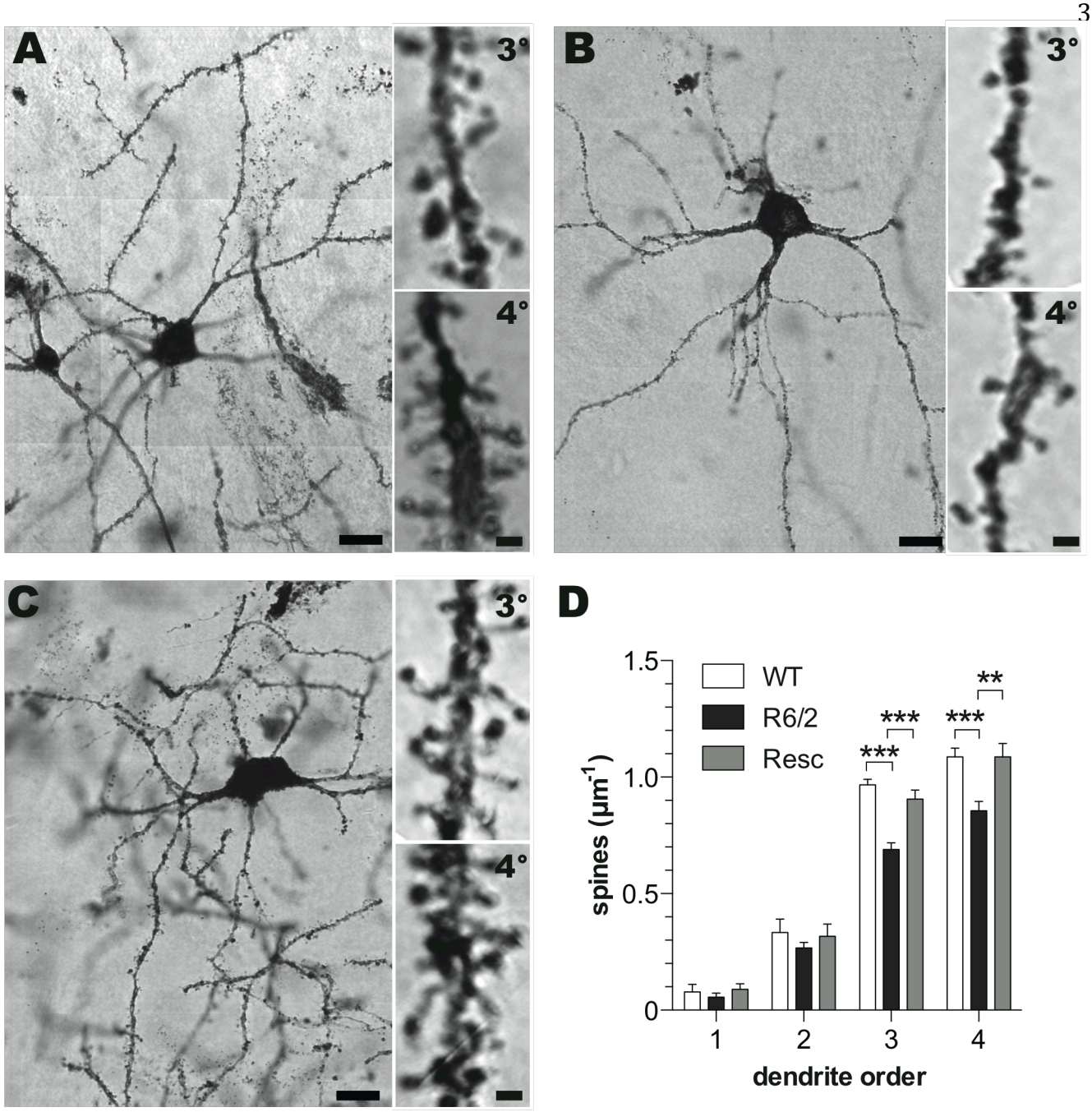


**Figure 2.9: Genetic rescue of $CB_{1(MSN)}$ is sufficient to prevent loss of dendritic spines in striatal MSNs.** Representative montage images are shown from Golgi staining performed on-slice in sections from WT (A), R6/2 (B), and R6/2-$CB_{1(MSN)}$ (C) mice. Inserts show high magnification extended focus images of 3$^{rd}$ and 4$^{th}$ order dendrites, for visualization of spine density. (D) Dendritic spines were counted in ImageJ from neurons with at least 4 orders of dendrites clearly visible, and for each neuron two dendrites per order were counted and averaged. Scale bars in main and inset images depict 10µm and 1µm, respectively. Error bars show S.E and post-hoc analyses were performed with Fisher's T Test and are indicated by *$P<0.05$, **$P<0.01$, and ***$P<0.001$.

**2.4 Materials and Methods**

***Mice:*** Mice were housed in a specific pathogen-free facility in accordance with the National Institutes of Health; the Institutional Animal Care and Use Committee at the University of Washington approved all experiments. Enrichment and *ad-libitum* access to food and water was provided and a 12-hr light/dark cycle was maintained in the facility. R6/2 and WT littermates were given a wet food mash in addition to dry pellets beginning at 10 wk of age. Both female and male R6/2, R6/2-$CB_{1(MSN)}$ rescue, and WT littermates were used in this study. The colony was maintained by breeding 6- to 8-week-old R6/2-*Gpr88*$^{+/Cre}$ males with *R26*$^{+/fsCB1}$ females, and all animals were on a 50/50 CBA, C57Bl/6 background. The average CAG repeat length of our colony is 114.1 ± 0.3 (n=10) and was determined by PCR from tail snips by Laragen, Inc [Culver City, CA, USA]. Genotyping was performed using the primers listed in Table 2, using kits as follows: $fsCB_1$, $CB_1$, and Pgk-Neo with Taq DNA Polymerase with ThermoPol Buffer (NE Biolabs, MA); *Gpr88*$^{Cre}$ with Phusion (NE Biolabs, MA); R6/2 with

***Generation of fsCB$_1$ mice:*** The open reading frame of mouse *cnr1* was inserted between a loxP-flanked Pgk-Neo gene and ires EGFP in a transfer plasmid. This flox'd *Pgk-Neo-cnr1-ires-EGFP* insert was then moved into a targeting vector that has the CBA promoter inserted at the transcription start site of the *Gt(Rosa26)*$^{Sor}$ locus and contains 7.7 kb of 5' flanking and 4.1 kb of 3' flanking *Gt(Rosa26)*$^{Sor}$ sequence and a PgK-DTa gene for negative selection. This construct was linearized and electroporated into G4 embryonic stem cells. Correct gene targeting was determined by Southern blot of DNA digested with *Nde1* using a probe that lies outside of the targeting vector. Correctly targeting ES cells were injected into the blastocyst of C57Bl/6 recipients and chimeric pups were bred with C57Bl/6 mice.

***[$^{35}$S]GTPγS Binding Assay:*** SNr tissue was rapidly dissected on ice and immediately homogenized in ice-cold 50 mM Tris-HCl (pH 7.4), 3 mM $MgCl_2$, and 1 mM EGTA. The homogenate was centrifuged at 45,000 x g for 10 min at 4°C, and then the pellet was homogenized in 50mM Tris-HCl, with 3 mM $MgCl_2$, 1 mM EGTA and 100 mM NaCl. The resulting membrane homogenate was pre-incubated with 3 mU/ml adenosine deaminase for 10 min at 30°C, to inactivate endogenous adenosine. Then, 10 mg of protein per reaction was incubated in reaction buffer containing 0.1% BSA, 30 μM GDP, 0.1 nM [$^{35}$S]GTPgS and 0.6 mU/ml adenosine deaminase,

with either 140 μM CP55,940 or vehicle, for 45 min at 30°C. The incubation was terminated by vacuum filtration through Whatman filters (GE Healthcare), followed by three washes with 3 ml ice-cold Tris-HCl, pH 7.4. Bound [$^{35}$S]GTPγS was quantified using a liquid scintillation counter in vials containing isolated [$^{35}$S]GTPγS-bound filter paper along with 4ml of Ecoscint scintillation fluid (National Diagnostics).

***Behavioral Studies:*** All behavioral tests were performed during the light phase of the light/dark cycle, between 9 am and 12 pm. All cages were cleaned with 70% ethanol between trials, and then dried with a paper towel. At 6 wk of age, mice were tested for hypothermia, hypolocomotion, catalepsy and analgesia, both before and after injection of 0.3 mg/kg CP55,940. Core body temperature was measured by anal probe. Hypolocomotion was measured in an open field chamber for 10 min starting 30 min after injection. Catalepsy was measured by placing the animals' front paws on a horizon bar approximately 3 cm high and recording the latency to remove the paws from the bar. An average of four trials was used per animal, and measurements were made both before and 30 min post-injection. Tail flick analgesia was measured by placing 1 cm of the tail in a 55$^{o}$C water bath (+/- 2$^{o}$C), and measuring the latency to tail withdrawal. Rotarod: After a 5-min training on the rotarod at 5 RPM, the mice were rested and then began 7 consecutive trials, separated by 30-min resting periods. The rotarod rotational speed used for the test trials began at 4 RPM and increased to 40 RPM, with an acceleration of 0.2 RPM per every 4 sec. Catwalk: At 10 weeks of age, animals were placed at one end of the Catwalk apparatus, with a vertically mounted camera beneath the catwalk. Five crossings were analyzed for each animal, and crossings where the animal stopped, reared, or turned around were excluded. Phenotype Assay: Phenotype was manually scored biweekly from 4-12 wk in an open-field chamber to generate a phenotype index (see methods) and to count rearings. Animals were placed in a 25 cm x 45 cm plexiglass cage for 2 min and were scored from 1-2 on 9 measures (tremor, body position, tail position, piloerection, exploration of all 4 corners, observed seizures, presence of hindlimb clasping, palpebral closure, and grooming), such that the possible scores ranged from 9-18, with increasing score indicating pathological phenotype. Open Field: Animals were placed in a 25 cm x 45 cm plexiglass cage and were allowed to explore for 10 min. Data were collected by vertically mounted video cameras and videos were analyzed in Noldus Ethovision 9.0 (Wageningen, The

Netherlands). Center-point tracking with dynamic- background subtraction was use to acquire the track for each animal. Elevated Plus: Mice were placed in the center of the maze, always facing the same arm, and were allowed to explore for 5 min. Live video tracking was performed using a vertically mounted camera connected to a computer running Ethovision 9.0, and the animal's position was determined using the center point of the animal, to control for sniffing or partial stretches which did not constitute full entry into an arm. Time spent in either the two closed or the two open arms was combined, and time spent in the center was not added to either measure.

***Immunohistochemistry and confocal microscopy****:* Mice were perfused with 20mL sterile PBS, followed by 10mL 4% paraformaldehyde. Brains were extracted, post-fixed overnight at 4C in 4% paraformaldehyde, then successively dehydrated in 15% sucrose and 30% sucrose for 24 hr each, and finally frozen. Coronal sections were cut on a freezing microtome to a thickness of 30μm, placed in cryoprotectant and stored at -20$^{o}$C. On the day of staining, slices were removed from cryoprotectant, washed 3x in PBS, and then incubated in blocking buffer (1% Triton X-100, 5% donkey serum in PBS) for 90 min at room temperature, and then transferred to primary staining solution (0.5% Triton X-100, 2.5% donkey serum in PBS) for 72 hr at 4$^{o}$C. Primary antibodies and dilutions used are listed in table 2. All primary antibodies were optimized by performing a dilution curve paired with quantitative analysis, and dilutions in the linear phase were chosen for further staining. After primary staining, sections were washed 8x in PBS-T for 5 min. Secondary staining was performed in 0.5% Triton X-100, 2.5% donkey serum in PBS, using Alexa secondary antibodies at a dilution of 1:500. After secondary staining, sections were washed 6 times in PBS-T for 10 min, once in PBS, and then mounted with Fluoromount (Sigma, St Louis MO) and sealed with nail polish. Images were collected on a Leica SL confocal microscope equipped with a 63x PL APO N.A. 1.40 oil immersion objective and with a 64 mW argon laser with lines at 457 and 488, a 10 mW helium-neon laser with a 543 nm line, and a 10 mW helium-neon laser with a 633 nm line. Optical sections were taken with the pinhole set at 1.0 AU, or 1.25 μm, with a resulting xy resolution of 0.163 μm and a z resolution of 0.290 μm. Noise reduction was achieved by averaging three scans for each image, after verification that this method did not result in any measurable bleaching (Alexa dyes).

Laser power was optimized to the brightest section for each stain, so that >99% of pixels were within the linear range, and 12-bit images were collected.

***Immunoblotting:*** Tissue was homogenized in ice-cold buffer (25mM HEPES pH 7.4, 1mM EDTA, 6mM $MgCl_2$, 1mM DTT, 1µg/ml Leupeptin, 1µg/ml Pepstatin A, 1µg/ml Aprotinin), and homogenates were sonicated for 10 seconds and stored at -20C. Protein concentration was determined by Bradford assay, and 30ug of protein per sample was loaded per lane in a Bio-Rad (Hercules, CA) gel. Gels were transferred onto nitrocellulose membrane at 200mA for 90 min, and then washed in TBST. Each primary staining was carried out at 4C overnight, followed by 3 5-minute washes, and a secondary staining at 1:1000 (goat anti-rabbit HRP) or 1:2000 (goat anti-mouse HRP) was carried out at room temperature for 1 hour. Imaging was performed using Supersignal Pico chemiluminescent substrate (Thermo-Fisher, xxx), and was followed by

***Semi-Quantitative Image Analysis and Statistics:*** All images were analyzed and quantified in ImageJ (National Institutes of Health), using custom written macros which were applied blindly to each batch of images. Each channel was split into an individual image and the mean intensity and standard deviation of each fluorophore in each image was measured. Background signal was removed by thresholding images to mean + standard deviation, corresponding to the top third brightest pixels in the Gaussian distribution. After thresholding, final measurements were made by taking the mean intensity of the (top-third) pixels which passed thresholding. Threshold values were validated by a human observer for each stain, to verify that pixels passing threshold corresponded to actual staining (threshold was not too low), and that actual staining was not being lost in thresholding (threshold was not too high). Statistical analysis and graphs were generated using GraphPad PRISM (San Diego, CA, USA). One-way ANOVAs were used for group comparisons and Fisher's T-test was used for post-hoc tests unless otherwise specified.

***Golgi Staining and analysis:*** Brains were cut in half at the midline and immediately placed in fixative (BioEnno, Irvine CA) for 5 hours. Fixative was changed once after 30 minutes. After fixation, brains were stored in 0.1M PB buffer for a maximum of 5 days at 4C. Brains were sliced to 100µm at RT on a vibratome (EMS, Hatfield PA) and striatal slices were collected. On-slice Golgi staining was performed using a SliceGolgi kit (BioEnno, Irvine CA). Staining was performed according to the kit protocol, and a 6 day Golgi impregnation

was used. Slices were mounted and allowed to dry for 24 hours, then dehydrated in 100% EtOH, and cleared in xylenes. Slides were coverslipped using a 1:1 mixture of xylenes and Permount, and were allowed to dry for 48 hours. Slides were imaged immediately after the drying period on a Marianas Live Cell Imaging Microscope (3i, Boulder, CO) equipped with an automated stage, using a 100X oil objective. Montage z-series images were collected and aligned together in SlideBook V5.5, and then exported as 16 bit TIF files. Counting of dendritic spines was performed in ImageJ (National Institutes of Health) using the multi-point selection tool with z-stacked montages, and x-y-z coordinates of each marked dendritic spine were recorded.

## 2.5 Tables

**Table 1:** Genotyping strategy.

| Name | Sequence | bands |
|---|---|---|
| *Pgk-Neo F (P4)* | ctc tgc taa cca tgt tca tgc c | Pgk-neo intact: no band<br>Pgk-neo excised, band ~300 bp |
| *Pgk-Neo R (P5)* | tctgcaaggccgtctaagat | |
| *fscnr1 – 1581 (P1)* | aaa gtc gct ctg agt tgt tat cag | WT: band ~600 bp<br>$R26^{+/fsCB1}$: band ~450 bp |
| *fscnr1 – 1575 (P2)* | gga gcg gga gaa atg gat atg | |
| *fscnr1 – 1583 (P3)* | tca ctg cat tct agt tgt ggt ttg | |
| *Gpr88-1569* | tggaggaacgaggagttccgc | WT: band ~200 bp<br>$Gpr88^{+/Cre}$: band ~300 bp |
| *Gpr88-1570* | agaaggaggcagtgcggcagg | |
| *cnr1 - F* | gctgt**c**tctggtcctcttaaa | $cnr1^{+/+}$: band ~400 bp<br>$cnr1^{-/-}$: band ~300 bp |

**Table 2:** Primers used.

| Stain | Thresholding | Antibody used |
|---|---|---|
| $CB_1$ (guinea pig) | Mean + SD | Gift from Ken Mackie |
| Leu-Enkephalin (rabbit) | Mean + SD | Millipore #AB5024 |
| Substance P (rabbit) | Mean + SD | Millipore #AB1566 |
| vGAT (mouse) | Mean + SD | Synaptic Systems #131011 |
| vGLUT1(mouse | Mean + SD | Synaptic Systems #135311 |
| vGlut2 (rabbit) | Mean + SD | Invitrogen #42-7900 |
| PSD95 (rabbit) | Mean + SD | Cell Signaling #3450S |
| Neuroligin 2 (rabbit) | Mean + SD | Synaptic Systems #129203 |

## 2.6 Acknowledgements

We are grateful to Dr. Yi Hsing Lin for technical assistance with the generation of the $fsCB_1$ mouse, and Dr. Gillian Bates, for the gift of HdhQ150 tissue. The CHDD Behavioral Core (Dr. Toby Cole and Dr. Sean Murphy, P30HD02274) provided both expertise and access to equipment used in the study, the KECK Microscopy Center (Dr. Greg Martin) for use of the Leica Laser Scanning Microscope, and the Digital Microscopy Center (Dr. Glen MacDonald) for the use of the Marianas Live Cell Imaging Microscope. Finally, we are grateful for helpful discussions with the UW Statistical Consult Service. This work was funded by NIH (RO1-DA026430) and CHDI (NS), T32-GM007108 (AN), F30-DA033747 (AN), and ARCS Seattle (AN).

**III. ABHD6 blockade controls PTZ-induced seizures and spontaneous seizures in HD models**

This section is adapted from a manuscript currently under review.

**3.1 Overview and Rationale**

In the brain, a major role of the eCB system is to control presynaptic neurotransmitter release. This system comprises the $CB_1$ and $CB_2$ receptors, and two main eCBs, anandamide and 2-AG. These lipids are produced and inactivated by distinct lipases and hydrolases. We recently demonstrated that the serine hydrolase ABHD6 is a *bona fide* member of the eCB signaling system that inactivates 2-AG, but not anandamide. Unlike other neurotransmitters which are synthesized and stored in synaptic vesicles for release, eCBs are produced on-demand in response to synaptic activity. In neurons, ABHD6 is located postsynaptically, at the site of 2-AG synthesis, where it fine-tunes the stimulated production of 2-AG and the resulting activation of presynaptic $CB_1$ cannabinoid receptors. Thus, ABHD6 inhibitors augment eCB availability at highly active synapses with spatiotemporal selectivity and restore synaptic homeostasis (Ahn et al., 2008; Blankman et al., 2007; Marrs et al., 2010). Furthermore, this enzyme represents a possible molecular hub that controls the 2-AG/$CB_1$ arm of eCB signaling and may control other arms of the lipid signaling network (Stella, 2012).

Epilepsy is a common condition that is refractory to current therapies in approximately 30% of patients (Kwan and Brodie, 2000), and is associated with pathologic cortical excitability. Currently available pharmacologic tools target voltage-gated ion channels to reduce neuronal excitability either directly or *via* modulation of synaptic transmission. However, effective treatment of epilepsy is limited by both lack of efficacy and the side effect profiles of current drugs, and there is a need for identifying new pharmacological strategies. Targeting neuromodulatory signaling systems, like eCB signaling, which control endogenous homeostatic mechanisms in a state-dependent manner, may provide greater efficacy and tolerability. Ample evidence shows that synthetic agonists at $CB_1$ receptors reduce glutamatergic synaptic activity and protect rodents against chemically-induced seizures (Chen et al., 2007; Lafourcade et al., 2007; Rudenko et al., 2012). Endocannabinoid (eCB) hydrolysis inhibitors retain the ability to reduce glutamatergic synaptic activity, but unlike $CB_1$ agonists which act at all synapses, these inhibitors only modulate $CB_1$ signaling at active synapses. Among eCB hydrolases, ABHD6 is unique because its postsynaptic location allows it to control 2-AG

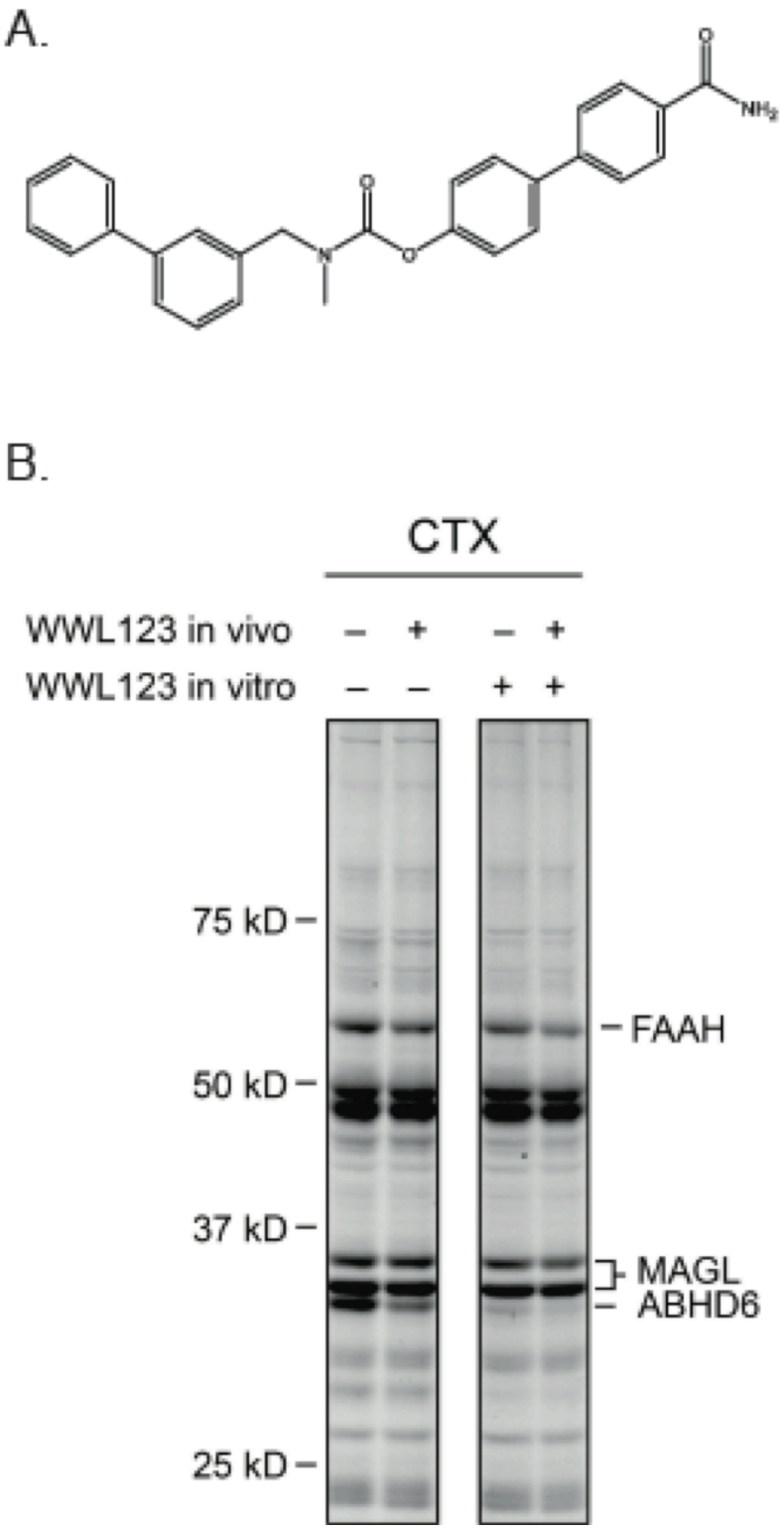


**Figure 3.1: WWL123 is a selective inhibitor of ABHD6.**
(A) The chemical structure of WWL123 is shown. (B) Four hours after i.p. administration of 10 mg/kg WWL123 (n=4) or vehicle (n=4), cortical homogenates were prepared and affinity based protein profiling was used to demonstrate selective inhibition of ABHD6 activity, but not MGL or FAAH activity. We conclude that WWL123 crosses the blood brain barrier, and selectively antagonizes ABHD6 at a dose of 10 mg/kg.

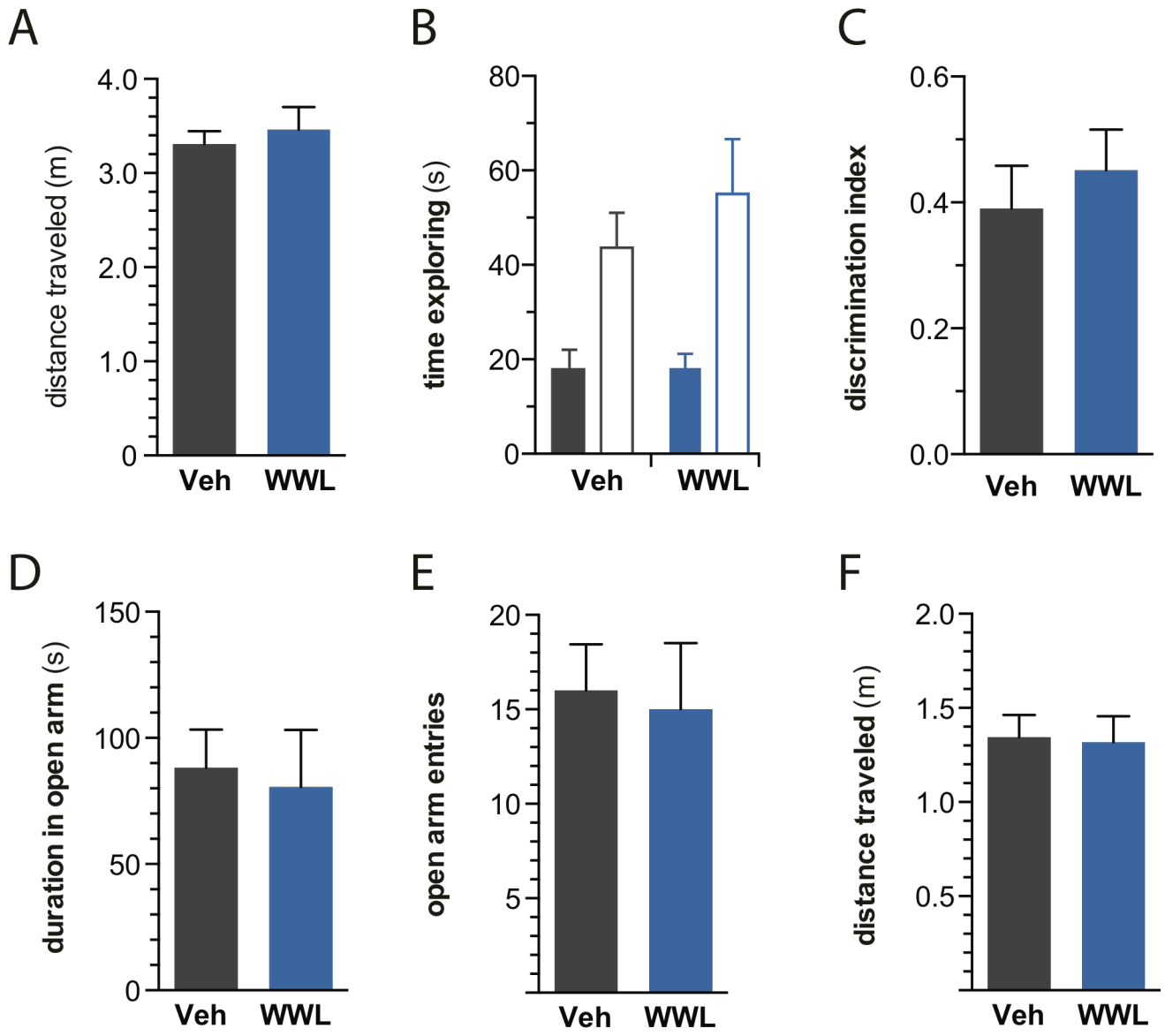


**Figure 3.2: WWL123 does not cause hypolocomotion or anxiety.**
To test whether WWL123 causes psychomotor impairment, we measured locomotion, memory, and anxiety-like behavior, because direct $CB_1$ agonists are known to cause hypolocomotion at high doses, and anxiety at low doses. (A) Four hours after vehicle (n=6) or 10mg/kg WWL (n=6), WT mice were placed in an open field chamber for 10 minutes, and movement was videorecorded and analyzed in ethovision.

Tracks were plotted for each vehicle-treated (B) or WWL123-treated (C) animal, in order to visually show locomotion around the open field chambers. Animals were placed in an elevated plus maze, and locomotion was videorecorded and analyzed in Ethovision. We found no difference in duration (D) or number of entries (E) in the open arms. Similar to what we observed in the open field assay, there was no difference in locomotion between vehicle or WWL123-treated mice on elevated plus maze (F). Error bars show SEM.

availability despite its low intrinsic activity compared to the primary brain 2-AG hydrolase, monoacylglycerol lipase (MGL), which is controls the bulk of 2-AG hydrolysis (Marrs et al., 2010). Therefore, whereas ABHD6 acts as a fine-tuning mechanism of controlling local 2-AG levels, other hydrolases control global eCB clearance in the brain.

We hypothesized that ABHD6 blockade by WWL123, a brain penetrant selective inhibitor, would protect against PTZ-induced seizures, without resulting in overt psychomotor effects. Chemically-induced seizure models represent a typical initial drug-screening platform and provide predictive power for the discovery of anti-epileptic drugs (White, 2003). However, this approach may miss compounds that could be effective against specific epilepsies, including therapy-resistant seizures, and have the drawback of inducing seizures in otherwise healthy mice (Bialer and White, 2010; Smith et al., 2007). Based on this notion, we sought to test the ability of ABHD6 blockade to control seizures in a genetic seizure model known to be associated with an impairment of eCB signaling. Specifically, R6/2 mice display both spontaneous and audiogenic seizures (Cepeda-Prado et al., 2012; Mangiarini et al., 1996) and reproduce the profound dysregulation of eCB signaling described in HD patients (Bisogno et al., 2008; Centonze et al., 2005). R6/2 mice reproduce the decreased 2-AG availability (Bisogno et al., 2008; Glass et al., 2000) and $CB_1$ receptor down-regulation in select neuronal populations (Dowie et al., 2009; Glass et al., 2000; 1993; Horne et al., 2012). Here too, we hypothesized that ABHD6 inhibition would prevent spontaneous seizures in R6/2 mice by augmenting 2-AG signaling.

## 3.2 Results

### 3.2.1 Pharmacokinetic profile and target engagement of WWL123 and SR141716.

To study the role of *in vivo* ABHD6 blockade in seizure incidence, we first validated our pharmacological approach. WWL123 is a carbamate compound that specifically inhibits the serine hydrolase ABHD6 (Figure 3.1) (Bachovchin et al., 2010). Four hours after dosing mice with vehicle or WWL123 (10 mg/kg, i.p.), we prepared homogenized cortical samples and used activity-based protein profiling (ABPP) to verify that WWL123 crosses the blood-brain-barrier and inactivates ABHD6 in the brain. Specifically, we found that this treatment reduces ABHD6 labeling by the FP-rhodamine probe, which labels serine hydrolases in an activity-dependent manner (Figure 3.1B). Importantly, WWL123 treatment did not affect the labeling of

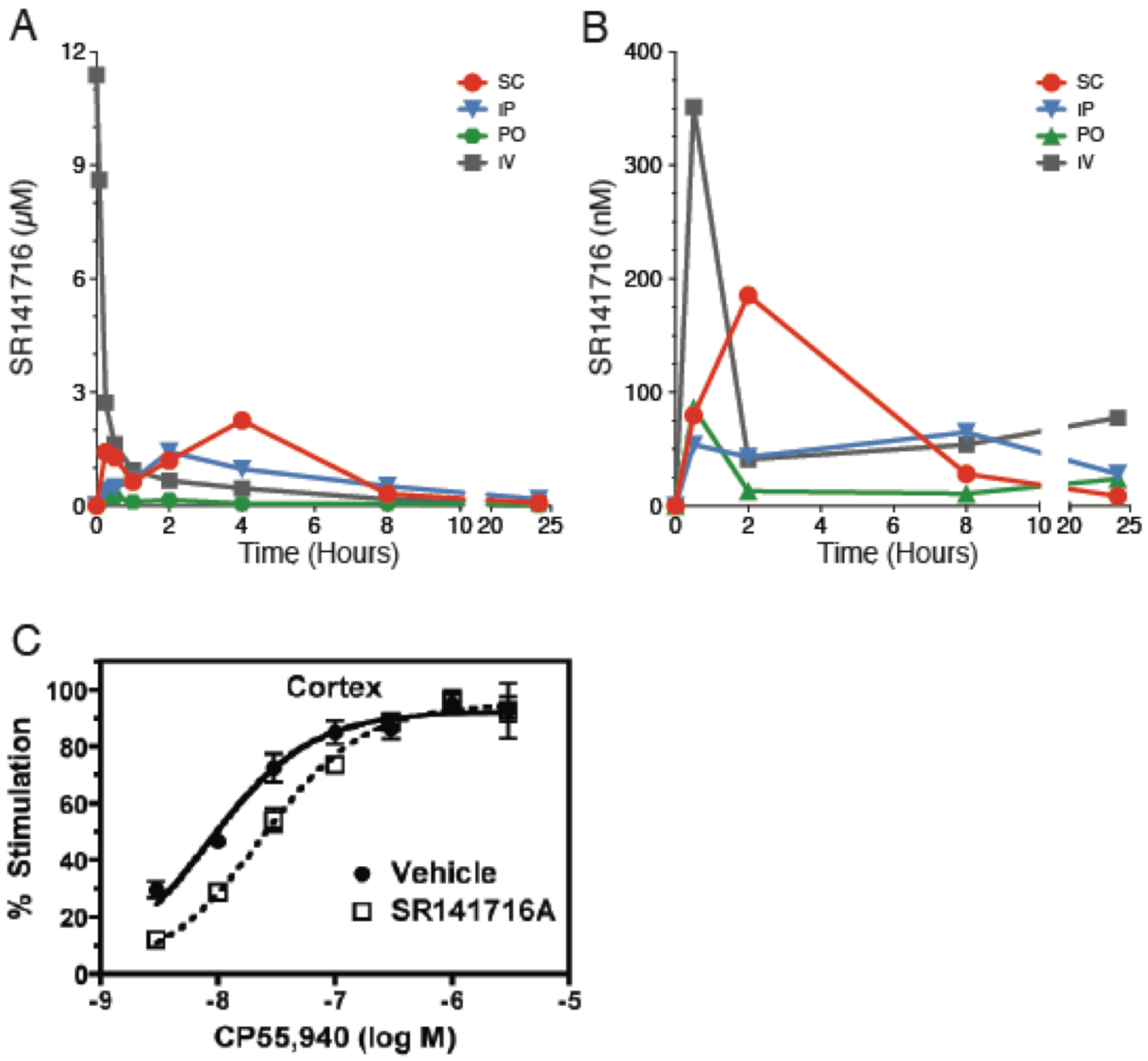


**Figure 3.3: Pharmakokinetics and functional validation of SR141716.**
(A) Blood levels of SR1 after i.v, i.p., p.o., or s.c. administration (4 mice per time point, per dosing regimen). Subcutaneous administration resulted in a biphasic rise in SR1 levels that peaked at 4 hours ($C_{max}$ = 2.25μM). (B) Brain levels of SR1 were highest for i.v. injection at 30 min ($C_{max}$ = 350nM), but s.c. administration resulted in similar levels ($C_{max}$ = 190nM) which were more broadly sustained. (C) Dose-response of GTPγS stimulation by CP55940 performed on homogenized cortical tissue demonstrated that 10mg/kg s.c. SR1 (n=5, both SR1 and vehicle) results in functional $CB_1$ antagonism in brain two hours after administration. Error bars show SEM.

other serine hydrolases, such as fatty acid amide hydrolase (FAAH) and monoacylglycerol lipase (MGL), further validating the selectivity of this inhibitor for ABHD6.

Similarly, we studied the pharmacokinetic profile of the $CB_1$ antagonist SR141716 (SR1), and found that subcutaneous (s.c.) injection results in sustained accumulation of the compound in brain tissue, resulting in the largest total drug exposure (6272 ng*hr/mL) compared to other routes of administration. Notably, s.c. SR1 reached a peak brain concentration of 180 ± 100 nM ($C_{max}$) 2 hours following s.c. injection and remained above 100 nM for several hours, providing a wide and reliable window for experimental manipulation (Figure 3.3A-B, Table 1). We confirmed the functional blockade of $CB_1$ signaling by harvesting cortical brain tissue from mice treated with this regimen and measuring $CB_1$ receptor activity by GTPγS assays (Figure 3.3C; vehicle, $EC_{50}$ = 8.9 ± 1.6 nM; SR1, $EC_{50}$ = 26.0 ± 2.8 nM; t=5.481, df = 8, p = 0.001). These results identify s.c. treatment with 10 mg/kg SR1 and i.p. treatment with 10 mg/kg WWL123 as optimal for $CB_1$ receptor antagonism and ABHD6 inhibition in mice, respectively.

**3.3.2 ABHD6 blockade controls PTZ-induced seizures.**

PTZ, a $GABA_A$ receptor antagonist, induces generalized seizures, and the efficacy of novel drug candidates in this model is predictive of their efficacy against similar seizures in humans (White, 2003). Mice pretreated with either vehicle or 10 mg/kg WWL123 were treated with 50 mg/kg PTZ, and then video recorded. PTZ induced seizures that progressed from hypoactivity (stage 1), to partial clonus (stage 2), to generalized clonus (stage 3), and culminated in global tonic-clonic (GTC) seizures (stage 4). Remarkably, pretreatment with WWL123 reduced seizure susceptibility (p = 0.002; Figure 3.4A), reduced the number of GTCs per mouse (1.36 ± 0.20 to 0.57 ± 0.17 (p = 0.006); Figure 3.4B), and also reduced the frequency of myoclonic seizures (11.84 ± 0.90 to 7.46 ± 0.90, p=0.003;Figure 3.4C).

To measure the electrographic changes between PTZ-treated mice and PTZ+WWL123 treated mice, we recorded electrocorticograms (ECoG) with bilateral epidural screw electrodes (see methods) in the following areas: primary somatosensory cortex (ECOG), cortical local field potential in layer V frontal cortex (LFP CTX, AP, LAT, Depth) and hippocampal local field potential in CA1 (LFP HIP, AP, LAT, Depth) with fine wire

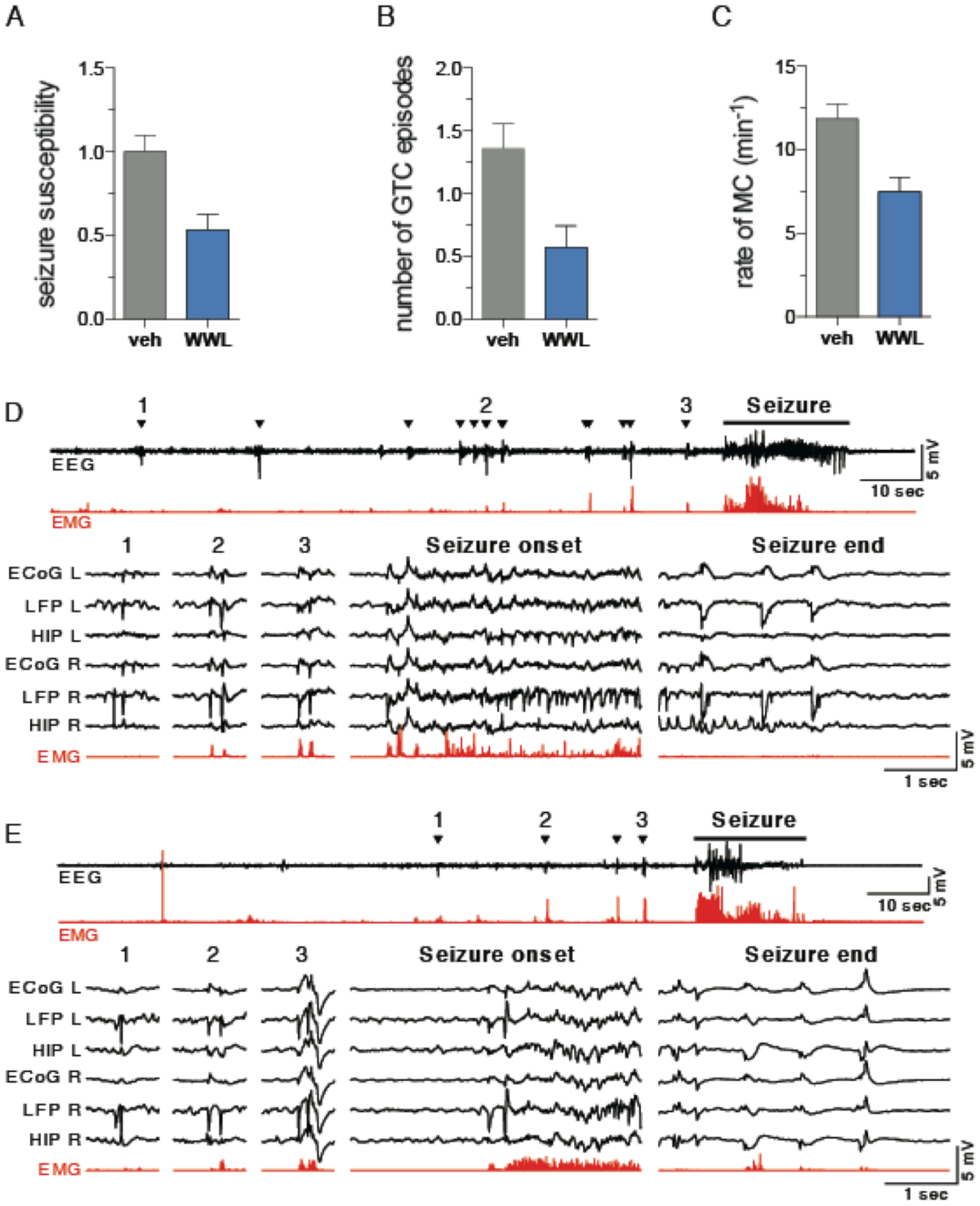


**Figure 3.4: ABHD6 blockade decreases PTZ-induced seizure incidence and severity.**
(A) Pretreatment with WWL123 completely blocked any seizure-associated mortality in response to PTZ. Mice pretreated with WWL123 (n=10) experienced (B) less severe PTZ-induced seizures (as calculated by the latencies to Stage 2-4), (C) fewer global tonic-clonic (GTC) seizures, and (D) fewer myoclonic (MC) seizures, compared to mice pretreated with vehicle (n=10). One week after surgical electrode implantation, mice were treated with (E) PTZ or (F) PTZ+WWL and EEG recordings were obtained. Condensed EEG (black) with corresponding EMG (red) is presented at the top, and 3 myoclonic seizures, along with the onset and end of the GTC seizures, are presented in greater detail below. Myoclonic seizures were accompanied by behavioral myoclonus (triangles). Fewer myoclonic seizures were observed in mice pretreated with WWL123. GTC seizures observed in mice receiving either PTZ or PTZ+WWL were similar in nature. Fisher's T-Test was used for post-hoc analyses with *$P<0.05$, **$P<0.01$, ***$P<0.001$. Error bars show SEM.

depth electrodes referenced to a screw electrode over the olfactory bulb. After recovery from surgery, the mice were administered PTZ, either with or without a 4 hour pretreatment with WWL123. Both mice receiving PTZ and mice receiving PTZ+WWL123 experienced a GTC episode (with behaviors corresponding to stage 4) within the first 10 min after PTZ administration, evolving in all channels simultaneously out of background EEG. Similarly, both mice experienced myoclonic seizures accompanied by behavioral myoclonus that preceded the GTC episode, however the mouse pretreated with WWL123 had fewer myoclonic seizures (Figure 3.4D-E). We conclude that WWL123 reduces the frequency and severity of PTZ-induced seizures and protects against seizure-related death. Video-EEG monitoring confirmed that electrographic features of PTZ-induced seizures were similar between treatments, and that no electrographic seizures without behavioral correlates were seen in either group. Therefore, to minimize the confounding effect of surgery, further studies were performed using behavioral observation.

### 3.3.3 $GABA_A$ inhibition, but not genetic deletion of $CB_1$ or $CB_2$, blocks anticonvulsive effects of WWL123.

We tested the effect of WWL123 in WT, *cnr1*$^{-/-}$, mice. *cnr1*$^{-/-}$ mice retained the protective effect of WWL123 in seizure susceptibility ($F_{(1,65)}$=13.09, p<0.001, Figure 2A), GTCs ($F_{(1,50)}$=13.72, p<0.001, Figure 2B), and MC ($F_{(1,48)}$=12.07, p=0.001, Figure 2C). There was no interaction between WWL123 and genotype, indicating that the effect of ABHD6 inhibition is unaffected by deletion of $CB_1$. The protective effect of ABHD6 blockade was also retained in *cnr2*$^{-/-}$ mice in seizure severity ($F_{(1,38)}$=15.72, p<0.001, Figure 2D), with no interaction between treatment and genotype. However, number of GTCs was not significantly affected by WWL123 in either genotype ($F_{(1,65)}$=1.45, p=0.236), but was increased in by $CB_2$ deletion ($F_{(1,38)}$=7.34, p<0.010, Figure 2E). MC was improved by WWL123 treatment ($F_{(1,36)}$=11.70, p=0.002, Figure 2F), with no effect of genotype and no interaction effect. We conclude that the protective effect of ABHD6 blockade is independent of $CB_1$ and $CB_2$ receptors.

Recent reports have described a direct interaction between 2-AG and the $GABA_A$ receptor {Sigel:2011hz}, therefore we sought to test whether $GABA_A$ receptors are required for the anticonvulsive effect of ABHD6 blockade, by co-treating with WWL123 and picrotoxin. We chose a dose of 1mg/kg picrotoxin, which is known

to result in hypolocomotion but is below the dose required to produce seizures (>3-5mg/kg). Animals were dosed with WWL123 or vehicle 4 hours prior to the experiment, and also with 1 mg/kg picrotoxin (i.p.) or vehicle 5 minutes prior to receiving PTZ. As expected, we observed a significant effect of WWL123 on severity ($F_{(1,62)} = 6.33$, p=0.015), GTCs ($F_{(1,62)} = 5.17$, p=0.026, and MCs ($F_{(1,62)} = 4.36$, p=0.041), but additionally there was an interaction between WWL123 and picrotoxin in severity ($F_{(1,62)} = 4.99$, p=0.029) and MCs ($F_{(1,62)} = 4.08$, p=0.048), and a trend in GTCs ($F_{(1,62)} = 2.00$, p=0.16), indicating that picrotoxin blocked the effect of WWL123.

### 3.3.4 R6/2 mice experience electrographic and behavioral seizures.

R6/2 mice are known to experience both spontaneous and audiogenic seizures (Cepeda-Prado et al., 2012; Mangiarini et al., 1996), yet neither quantitative nor qualitative analysis of spontaneous seizures or of the possible etiology of these seizures is available. To determine how electrographic features of seizures correlate with observed behaviors, we performed EEG recordings in tandem with video recording. ECoGs were recorded with screw electrodes placed bilaterally over frontal cortex, and LFPs were recorded with fine wire depth electrodes placed bilaterally superficial to CA1, referenced to a screw electrode over olfactory bulb. Animals were given 5-7 days to recover after surgeries, and were then monitored on two consecutive days for 6-hrs intervals. Spontaneous seizures were captured in this manner in three separate R6/2 mice and figure 3.5A shows a representative example of an EEG accompanying a spontaneous behavioral seizure. The electrographic and behavioral onsets of the seizure were closely time-locked with seizure behaviors, which persisted throughout the entire electrographic seizure and were followed by both a postictal suppression on the EEG and a behavioral pause (Figure 3.5B). Furthermore, similar behavioral findings were observed in mice with and without surgical procedures, indicating that surgeries did not change the nature of the seizures in R6/2 mice. To minimize the confounding effect of surgery on the frequency of spontaneous seizures, further studies were performed using behavioral observation (see discussion in methods).

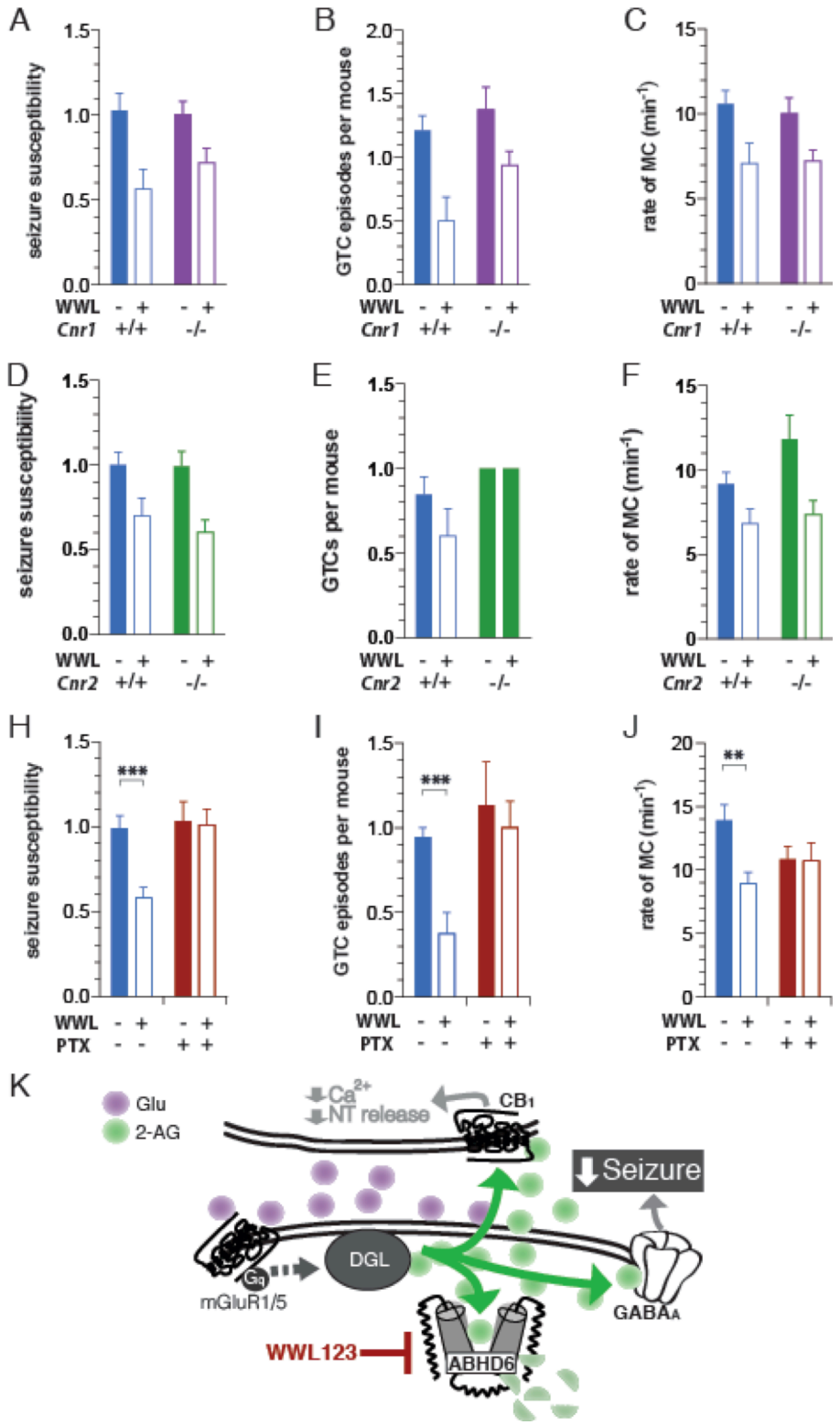


**Figure 3.5: The antiepileptic effect of ABHD6 inhibition is unaffected by genetic deletion of $CB_1$ or $CB_2$ receptors, but is blocked by $GABA_A$ antagonism.** WT (n=8) or *cnr1*$^{-/-}$(n=17) mice were treated with WWL123 or vehicle (WT: n=15, *cnr1*$^{-/-}$: n=18) and four hours later were injected with 50mg/kg PTZ i.p., and were video-recorded for 30 minutes and scored for seizure severity (A), GTCs per mouse (B), and MC (C). Similarly, WT (n=10) and *cnr2*$^{-/-}$(n=9) mice were treated with WWL123 or with vehicle (WT: n=13, *cnr2*$^{-/-}$n=10), and seizure behaviors were scored (D-F). To test the role of $GABA_A$ receptors, WT vehicle-treated (n=15) or WWL123 treated (n=15) mice were treated with 1mg/kg i.p. picrotoxin (PTX), or with vehicle (n=15, both groups) five minutes before receiving PTZ. Although by itself PTX did not exacerbate seizures, it blocked the effect of WWL on seizure susceptibility (H), GTCs (I), and MC (J). Error bars depict SEM, and Fisher's T-test is indicated as **P<0.05, **P<.01, ***P<.001*.

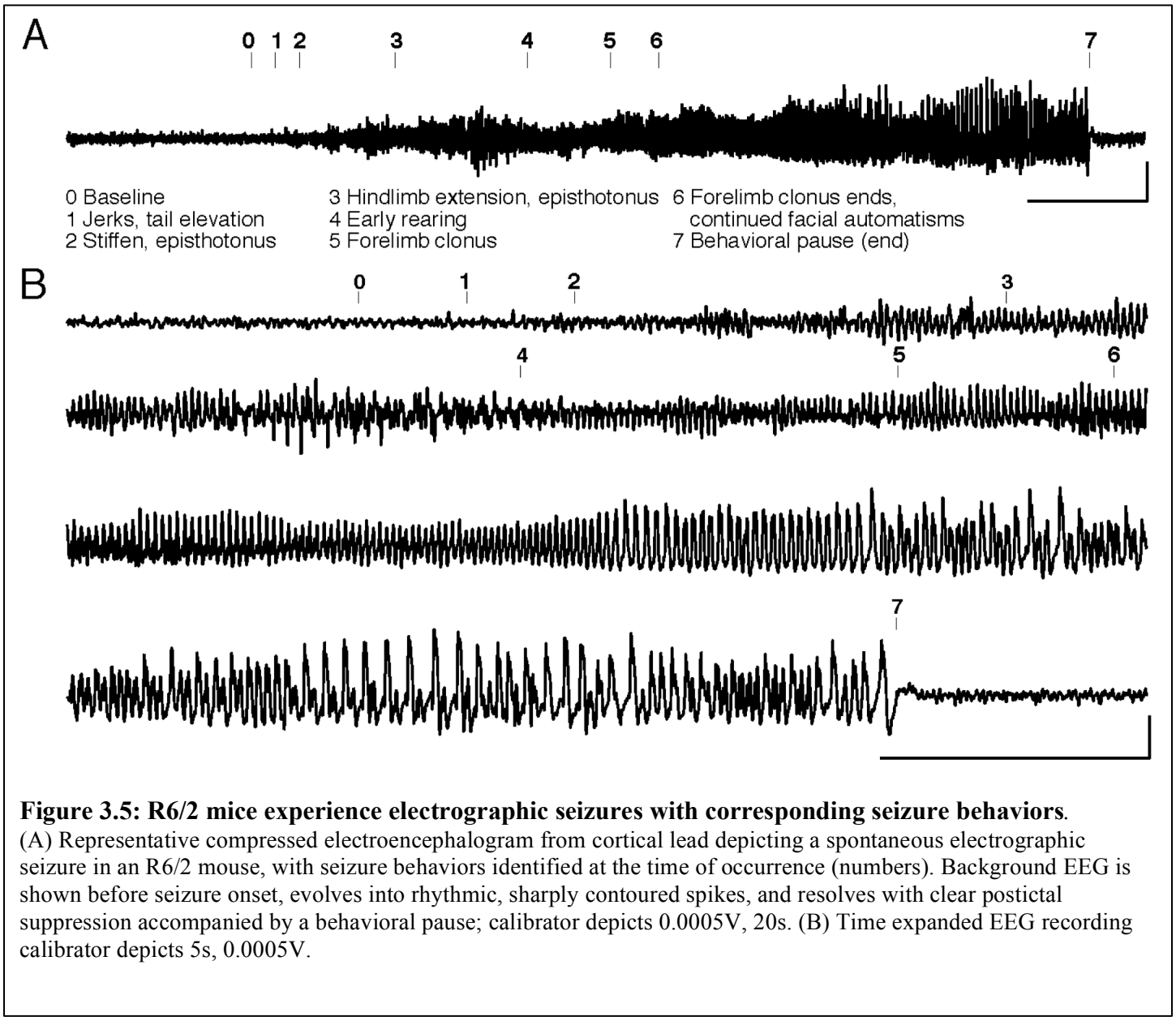


**Figure 3.5: R6/2 mice experience electrographic seizures with corresponding seizure behaviors**. (A) Representative compressed electroencephalogram from cortical lead depicting a spontaneous electrographic seizure in an R6/2 mouse, with seizure behaviors identified at the time of occurrence (numbers). Background EEG is shown before seizure onset, evolves into rhythmic, sharply contoured spikes, and resolves with clear postictal suppression accompanied by a behavioral pause; calibrator depicts 0.0005V, 20s. (B) Time expanded EEG recording calibrator depicts 5s, 0.0005V.

**3.3.5 Electrographic and histological abnormalities in R6/2 hippocampus.**

LFP recordings from hippocampi of R6/2 mice (Figure 4a-c, Supplementary Figure 4) revealed interictal epileptic discharges consisting of high amplitude (>3mV), sharply contoured complexes which transiently disrupted ongoing hippocampal activity (suppression), were associated with high frequency oscillations (fast ripples), two criteria for hippocampal epileptic discharge (Bragin et al., 1999). We reviewed EEG from a full observation session (6 hrs) which included a seizure, and unlike our findings in hippocampus, we did not find epileptic activity (sharply-contoured spikes which reached 3*SD over the rms noise) in cortical leads except in association with larger hippocampal spikes. Epileptic complexes were not seen in recordings of WT mice. Interictal spikes are associated with network hyperexcitability and are consistent with an increased risk of partial-onset seizures.

We stained for anatomical indices of synaptic excitability in hippocampal areas CA1, CA2, and CA3 and found increased vGlut1 (Figures 4c, 4f) expression in R6/2 mice compared to wild-type mice (CA1: p=0.02; CA2: p=<0.001; CA3 p=0.004), but vGAT expression remained unchanged (Figures 4d, 4f). The imbalance of these markers suggests increased excitability without a corresponding increase in inhibitory tone. While disturbances in the eCB system have been well described in the striatum and cortex of R6/2 mice, the eCB system hippocampus has not been described in detail. Surprisingly, we found a small increase in ABHD6 immunoreactivity in the CA1 (p=0.04) and CA2 (p=0.006) regions of R6/2 mice, whereas $CB_1$ was unchanged. This finding supports our initial strategy to test the utility of ABHD6 blockade in a seizure model featuring eCB dysfunction.

NPY inhibits excitatory neurotransmission (Colmers et al., 1988), by synapsing onto presynaptic mossy fiber (CA2/3) and Shaffer collateral (CA1) terminals, and exerts powerful anticonvulsant effects through Y5 receptors (Marsh et al., 1999; Vezzani et al., 1999; Woldbye et al., 1997). Deletion of *Npy* has been associated with temporal seizures (Baraban et al., 1997; Erickson et al., 1996) that can be blocked by both intraventricular administration of NPY (Woldbye et al., 1996) and NPY gene therapy (Noe et al., 2008). We measured NPY immunoreactivity in the hippocampus and found a profound reduction in R6/2 mice (p=0.004) (Figure 4e, 4i,

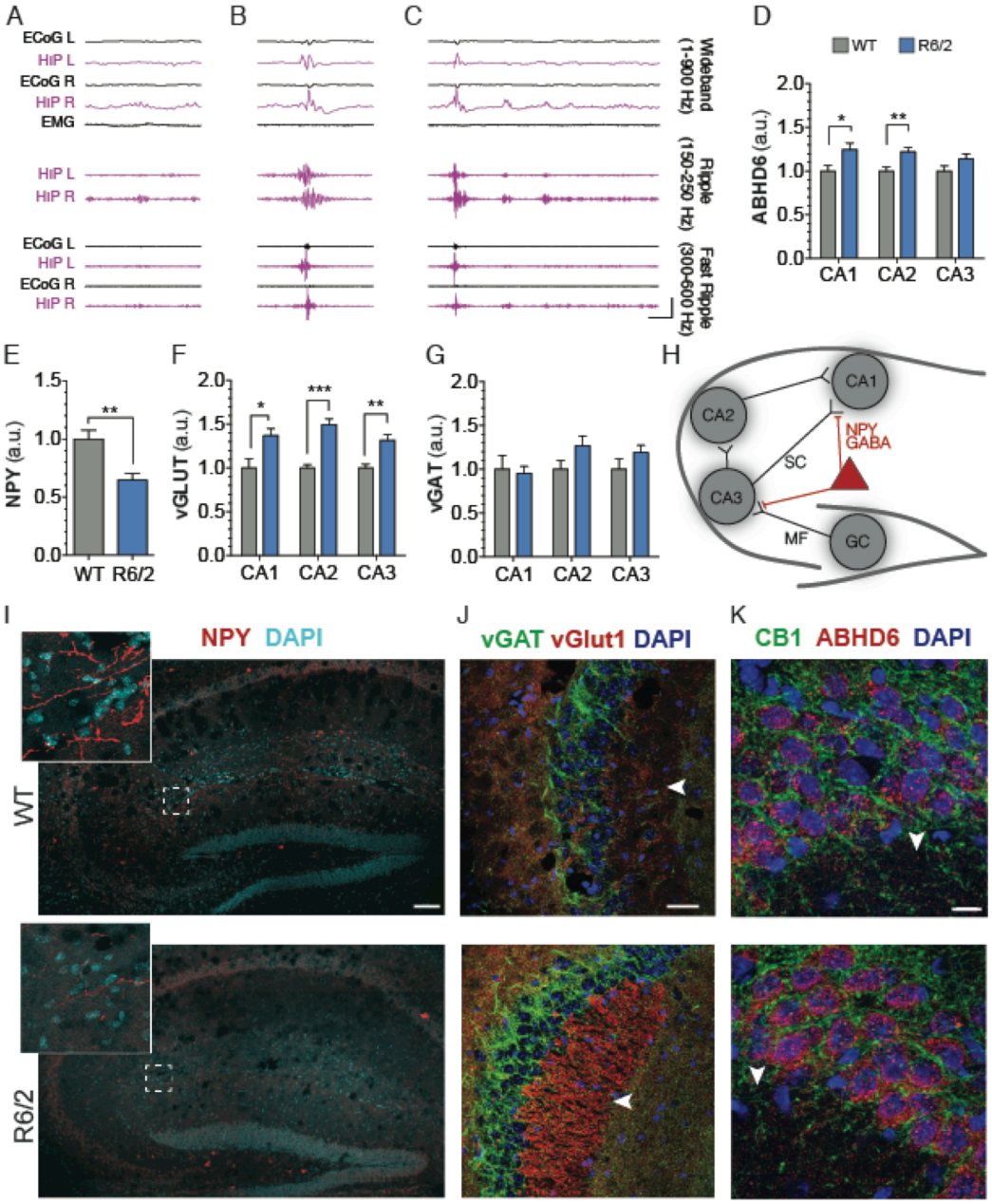


**Figure 4: Electrographic and histological abnormalities in the hippocampus of R6/2 mice.**
Representative example of hippocampal theta/gamma oscillations (A), and two representative examples of interictal discharges in R6/2 mice (B-C). Calibrator depicts 100ms, 5mV (wideband) or 0.5mV (ripple and fast ripple). Discharges in R6/2 mice exceeded 3mV in hippocampal leads (maximal voltage: B= 4.5mV, C= 5.0mV), a common criterion for epileptic discharge, and featured higher amplitude in ripple components (maximal peak-to-peak amplitude: A = 202μV; B = 587μV; C = 904 μV) as well as a fast ripple component not observed in theta/gamma (maximal peak-to-peak amplitude: B = 876μV, C= 847μV). (D) ABHD6 immunoreactivity is increased in CA1 and CA2 stratum pryamidale of R6/2 mice (n=7) compared to WT (n=5), without a concurrent change in $CB_1$ immunoreactivity (K, see also Supplementary Figure 6). Loss of NPY immunoreactivity is observed throughout the hippocampus in R6Q/2 mice (E). (F) Model depicting the NPY component of the hippocampal circuit. NPY interneurons provide presynaptic inhibition of excitatory inputs to CA1-3, and accordingly there was an increase in vGlut1 immunoreactivity (F) which was best observed in CA2, but also measureable in CA1 and CA3, and which was not accompanied by an increase in vGAT immunoreactivity (G). Measurements were made after thresholding to mean+SD (ABHD6, $CB_1$, vGlut1 and vGAT), or mean+2*SD (NPY), as determined by the percent of pixels for each stain which represented staining of target proteins. Representative montage images of NPY staining (I, scale bar = 100μm, see also Supplementary Figure 5) and confocal images of vGlut1/vGAT staining (J, scale bar = 50μm) and $CB_1$/ABHD6 (K, scale bar = 10μm) are presented. Error bars show SEM, and Fisher's T-test is indicated as *$P<0.05$, **$P<.01$, ***$P<.001$.

and Supplementary Figure 5). To our knowledge, this is the first report of hippocampal NPY loss in a genetic disease model featuring epilepsy, and is a candidate mechanism for epileptogenesis occurring in R6/2 mice.

**3.3.6 ABHD6 inhibitor blocks behavioral seizures in R6/2 mice in a CB1-independent manner.**

To test whether behavioral seizures exhibited by R6/2 mice are controlled by chronic pharmacological regulation of eCB signaling, we treated these mice with a daily injection of either vehicle, SR1 or WWL123 beginning at 4 weeks of age. We found that SR1 increased, and WWL123 blocked, the incidence of spontaneous behavioral seizures in R6/2 mice (Figures 5a-b; Vehicle=31%, SR1=80%, WWL123=0%; 2x3 contingency table analyzed by Fisher's Exact Test, p=0.023). There was no effect (Veh = 64.4 ± 7.5s; SR1 = 60.3 ± 20.1s, p=0.89) on duration of spontaneous seizures in response to chronic SR1 treatment (Veh = 64.4 ± 7.5s; SR1 = 60.3 ± 20.1s, p=0.89). These results indicate that ABHD6 inhibition is effective against spontaneous seizures in a genetic model of epilepsy and that no tolerance develops during chronic treatment with WWL123.

To assess the mechanism of antiepileptic action of ABHD6 blockade in R6/2 mice, we acutely treated 9-week-old drug-naïve mice with a single injection of vehicle, SR1, WWL123, or SR1+WWL123, and monitored the animals for six hrs with video recording (Figures 5c-d). Videos were scored for behavioral seizures of grade Racine 4-6. Similar to what we observed with chronic treatment, acute SR1 increased and acute WWL123 prevented behavioral seizures measured over 6 hours, however SR1 did not antagonize the effect of WWL123 (Vehicle=8%, SR1=63%, WWL123=0%, SR1+WWL123=0%; 2x4 contingency table analyzed by Fisher's Exact Test, p=0.006). Together with our result showing partial blockade of the antiepileptic effect of WWL123 by SR1 in PTZ-induced seizures, this result obtained in R6/2 suggest that the antiepileptic activity of ABHD6 inhibition in both a chemically-induced and a genetic seizure model operates through a $CB_1$-independent mechanism.

**3.3 Discussion**

ABHD6 is a newly identified member of the ECS system, responsible for degradation of 2-AG postsynaptically at the site of its synthesis in neurons. We show that ABHD6 blockade exerts a powerful antiepileptic effect in two models of epilepsy: PTZ-induced seizures and spontaneous seizures in R6/2 mice. Unexpectedly, we found

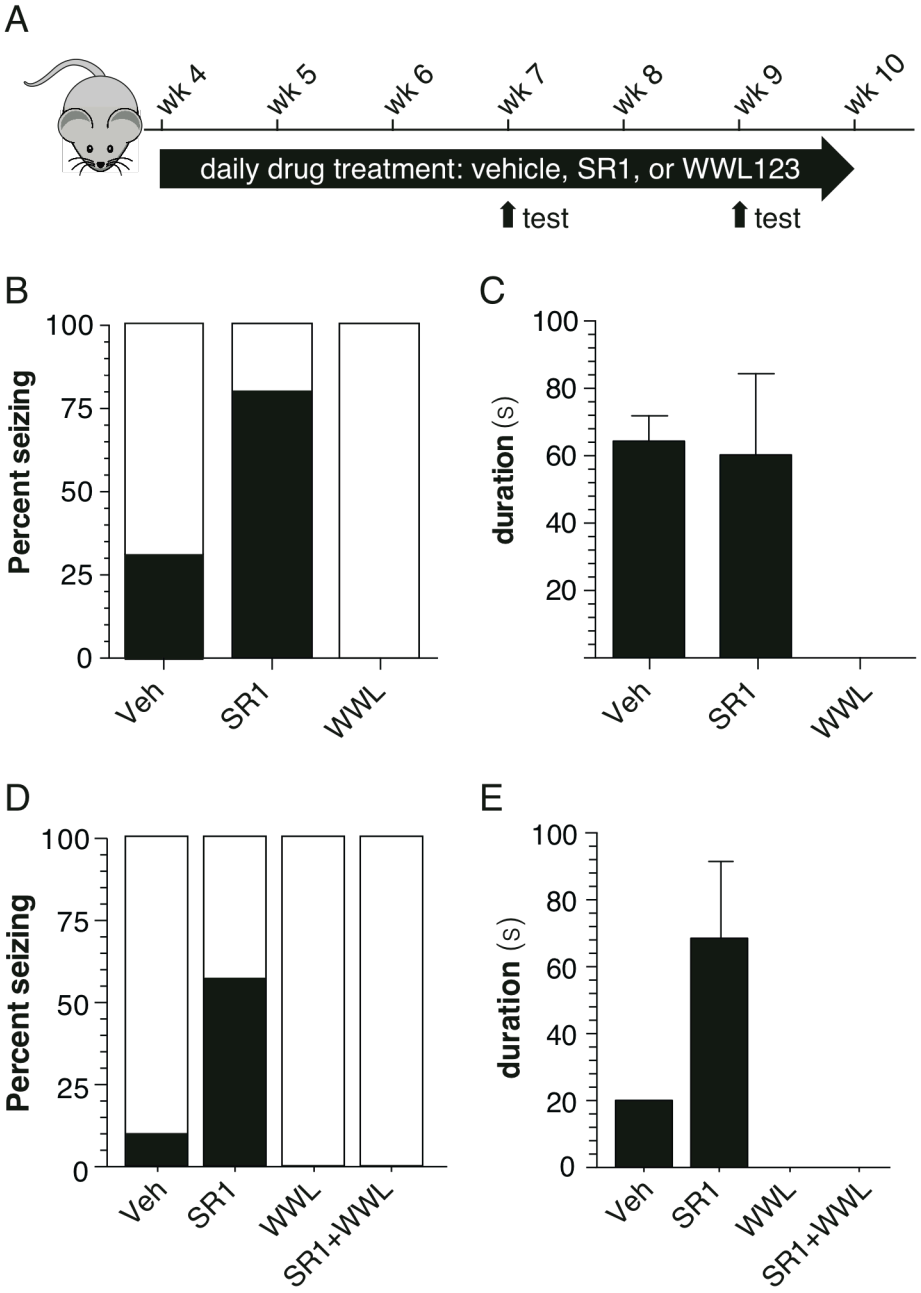


**Figure 5: ABHD6 blockade blocks spontaneous behavioral seizures in R6/2 mice in a $CB_1$-independent manner.**

(A) R6/2 mice were chronically treated with WWL123, SR141716, or vehicle from 4 weeks of age. 6 hour video-recorded seizure observations were performed after the daily drug treatment at 7 weeks and 9 weeks of age, and the data were pooled in order to obtain a more accurate estimate of seizure incidence using multiple observations. Seizure incidence was measured by scoring seizure behaviors corresponding to Racine 4-6 for i.p. vehicle (n=6), s.c. vehicle (n=6), 10mg/kg i.p. WWL123 (n=5), and 10mg/kg s.c. SR1 (n=5); the two vehicle groups did not differ from each other and were thus pooled for analysis. (B) SR1 treatment increased seizure incidence relative to vehicle treatment, and WWL123 treatment abolished seizures. (C) Seizure duration was unchanged between vehicle and SR1-treated mice under this chronic treatment regimen. In order to assess mechanism of action, drug-naïve R6/2 mice were treated acutely with vehicle (n=12), SR1 (n=8), WWL123 (n=8), or SR1+WWL123 (n=8), and seizure incidence was scored the same way as with the chronic cohort, but during a single six-hour observation. (D) Acute SR1 treatment increased seizure incidence relative to acute vehicle treatment, and acute WWL123 treatment abolished all seizures. (E) Seizure duration could not be statistically assessed for this cohort (Veh=20s; SR1=51±34s). Error bars show SEM.

that $CB_1$ antagonism resulted in only partial attenuation of the antiepileptic activity of ABHD6 blockade in PTZ-induced seizures, and failed to block the antiepileptic activity due to ABDH6 blockade in R6/2 mice. These results suggest that ABHD6 blockade exerts antiepileptic effects by two (or more) independent mechanisms.

There are major drawbacks to currently available therapeutic approaches for the treatment of epilepsy, including tolerance to the efficacy of antiepileptic drugs, and increases likelihood of dose-related side-effects, both of which reduce clinical utility. When treating mice daily with WWL123 for 5 weeks, we did not observe tolerance to chronic ABHD6 blockade, in contrast to what is seen after chronic treatment with $CB_1$ receptor agonists and with MGL inhibitors (Blair et al., 2009; Schlosburg et al., 2010). Furthermore, we did not observe signs of psychomotor impairment typically associated with both $CB_1$ agonists and to a lesser degree MGL inhibitors. Lack of tolerance and the absence of any measurable off-target behavioral effects might be due to the spatiotemporal specificity of ABHD6 blockade for 2-AG signaling in highly active synapses. Together, these findings suggest that ABHD6 inhibitors might exhibit a favorable safety profile and be amenable to long-term use.

Among HD patients, individuals that carry more than 60 CAG repeats in the huntingtin gene begin exhibiting symptoms in their teens (or even younger as the number of repeats increases). This subset of patients are afflicted by juvenile HD, an early and more aggressive variant of the disease which uniquely features myoclonic seizures in 35-50% of patients (Andrew et al., 1993) (Byers et al., 1973) which are refractory to standard anti-epileptic medications (Osborne et al., 1982; Landau and Cannard, 2003; Gonzalez-Alegre and Afifi, 2006). Therefore epilepsy is emerging as a major co-morbidity and unmet medical need of patients with juvenile HD, and yet, little is known about the molecular mechanisms underlying seizure incidence in this patient population. R6/2 mice recapitulate several aspects of an early-onset, rapidly progressive juvenile HD phenotype, including both spontaneous seizures and early death (Bates and Woodman, 2009; Mangiarini et al., 1996). Here, we show that behavioral seizures in R6/2 mice correspond to electrographic seizures, and that ABHD6 blockade controls these seizures through a $CB_1$ independent mechanism. Our initial characterization of

the seizures exhibited by R6/2 mice suggests hippocampal involvement. Interictal discharges with amplitude, morphology, and frequency components characteristic of epileptic discharges were observed in hippocampal leads. Since the purpose of the current study was to explore the anticonvulsive and antiepileptic efficacy of ABHD6 inhibition, follow-up studies are required. We note that our recordings do not rule out an epileptic focus outside of the hippocampus, and that recordings with higher spatial and temporal resolution are required, although this approach is technically challenging due to the hypersensitivity to anesthesia displayed by R6/2 mice and the fact that they experience anesthesia-related death with long surgery times (see methods). Additional, longer duration recordings with quantitative analysis are required to fully characterize the epileptic phenotype of R6/2 mice.

We observed a striking loss of NPY throughout the hippocampus, which is known to result in temporal seizures (Baraban et al., 1997; Erickson et al., 1996) and in turn can be rescued by intraventricular injection of exogenous NPY (Woldbye et al., 1996). The loss of NPY in R6/2 mice is surprising, since seizure activity is associated roughly twofold increases in hippocampal NPY expression (Vezzani et al., 1994). NPY interneurons provide presynaptic inhibition at mossy fibers (CA2/3) and at Shaffer collaterals (CA1), both of which are excitatory. Therefore, it is especially relevant to note that we also observed increased expression of vGlut1, but not vGAT, in CA1, CA2, and CA3 stratum pyramidale. Mutant huntingtin results dysregulated gene expression in hundreds of genes, including $CB_1$, and therefore one possible explanation of our data is that mutant huntingtin causes decreased NPY expression, which results in a disinhibition of Shaffer collaterals and of mossy fibers, resulting in increased excitatory drive in the hippocampus that manifests as seizure activity.

ABHD6 inhibition selectively increases the local abundance of 2-AG at highly active excitatory synapses and tightly regulates excitatory transmission (Marrs et al., 2011; 2010; Straiker et al., 2009). A notable finding of our study is that ABHD6 inhibition maintains its therapeutic efficacy despite concurrent $CB_1$ receptor antagonism in certain instances, suggesting that ABHD6 regulates a second, $CB_1$-independent mechanism. One possibility is that ABHD6 controls the hydrolysis of a different molecular species or lipid that act on its own target. In this scenario, ABHD6 would act as enzymatic hub controlling both the 2-AG/CB1 arm of the ECS and

a novel lipid signaling arm, both of which control epileptic seizures. Another possibility is that augmenting 2-AG levels activates a target other than $CB_1$ receptors with its own pharmacological profile. It has been reported that 2-AG potentiates signaling through $GABA_A$ receptors in a process that selectively requires the β2 subunit, and is super-additive with diazepam, a known anticonvulsant (Sigel et al., 2011). In this model, ABHD6 blockade would increase 2-AG concentration at the site of synthesis, and this 2-AG would then act postsynaptically at $GABA_A$ receptors and presynaptically at $CB_1$ receptors. Both of these mechanisms would decrease activation of the postsynaptic cell and would act in combination. Lastly, it is possible that elevated 2-AG is acting at $CB_2$ receptors, possibly to reduce inflammation. However, we regard this possibility as less likely, since it would not explain protection in an acute seizure model like PTZ, or the ability of a single dose of ABHD6 inhibitor to block seizures in R6/2 mice. Furthermore, little to no CB2 receptors are expressed in healthy and R6/2 brain (Bouchard et al., 2012).

This study identifies the recently described 2-AG hydrolase ABHD6 as a potential therapeutic target for epilepsy. To characterize the utility of this therapeutic strategy and its mechanism of action, it is necessary to outline the types of seizures that are sensitive to ABHD6 blockade. It would be useful to determine if ABHD6 blockade controls seizures in other established models, including models of treatment-resistant seizures such Dravet mice (Cheah et al., 2012; Kalume et al., 2013), classical models such as maximal electroshock, and acquired epilepsies such as traumatic brain injury (TBI)-induced seizures (White, 2003). We conclude that ABHD6 blockade exerts potent antiepileptic activity through spatiotemporally precise potentiation of $CB_1$-mediated "on-demand protection against excitotoxicity" (Marsicano, 2003), as well as a second, unknown mechanism. Furthermore, ABHD6 blockade sidesteps traditional caveats to the pharmacological targeting of the eCB system, including tolerance and psychomotor impairment. Together, our evidence suggests that ABHD6 blockade represents a promising novel antiepileptic strategy that may be effective against a broader array of epilepsies and associated with few side effects.

**3.4 Methodology**

**Animals:** All animal procedures were approved by the Institutional Animal Care and Use Committee for the University of Washington. For PTZ experiments, we used male C57Bl/6 mice. R6/2 mice present significant

challenges for breeding, as all females and approximately half of males are sterile. Because these difficulties are compounded on a C57Bl/6 background, spontaneous behavioral seizure assays in R6/2 mice were performed on a mixed CBA-C57Bl/6 background in male and female littermates, and genders were balanced between cohorts. R6/2 (6-8 week old) males and wild type females (CBA-C57Bl/6) were bred to maintain the R6/2 colony (114 CAG repeats; sequenced at Laragen, Culver City, CA). Mice had *ad-libitum* access to food and water and were given additional wet food mash at 9 weeks of age. All R6/2 cages were provided with enrichment, and mice were not handled prior to experiments, other than to change cages or perform injections for chronic studies.

**Drugs and Antibodies:** SR141716 (SR1) was supplied by NIDA drug supply, WWL123 (WWL) was synthesized by the Cravatt Laboratory (Bachovchin et al., 2010), pharmasolve-n-methyl-2-pyrrolidone (Pharmasolve) was purchased from ISP Technologies (Columbia, MD), Cremophor RH40 and Lutrol F68 were purchased from BASF (Florham Park, NJ). Antibodies used for immunohistochemistry are listed in Supplementary Table 2.

**PTZ-induced seizures and monitoring:** We performed i.p. injections of 50 mg/kg pentylenetetrazole (PTZ; Sigma, MO, USA) and then immediately placed animals in a 10”x18”x18” chamber with video recording for 30 min (Zhang et al., 2010). Seizures were scored by two blinded observers according to a modified Racine scale designed specifically for PTZ-induced seizures in mice (Ferraro et al., 1999):

*Stage 1:* Hypoactivity culminating in behavioral arrest with contact between abdomen and the cage.

*Stage 2:* Partial clonus (PC) involving the face, head, or forelimbs.

*Stage 3:* Generalized clonus (GC) including all four limbs and tail, rearing, or falling.

*Stage 4:* Generalized Tonic-Clonic seizure (GTC)

Seizure severity was calculated from the latencies to Stage 2-4, as previously described (Ferraro et al., 1999). Severity scores are reported as a fraction of the average score for mice receiving only PTZ.

Score = $\sum$ ( (0.2*(latency to PC)) + (0.3*(latency to GC)) + (0.5*(latency to GTC)) )

Myoclonic seizures (MC) and GTCs were also counted independently, because the seizure severity score does not take into account the number of seizures. GTCs are reported as total number observed over 30 min after

injection with PTZ. Because GTCs temporarily suppressed MCs, we counted MCs prior to GTC and reported them as MC/min, or in the case of animals that did not experience GTCs, we reported the rate of MCs over the first 10 min of the observation, in order to be comparable to animals that experienced GTCs.

**Spontaneous Seizure Assays:** Wild type and R6/2 mice were treated with 10 mg/kg SR141716 (s.c.), 10 mg/kg WWL123 (i.p.), or vehicle (Pharmasolve:Cremophor RH40:1% Lutrol F68 [1:9:40]). Daily chronic treatment began at 4 weeks of age, one week after mice were weaned. Spontaneous seizure observations were conducted in 7-week-old (chronic) and 9-week-old (chronic and acute) R6/2 and wild type littermates. Mice were treated with SR141716, WWL123, or SR141716 + WWL123; SR141716 was administered 90 min beforehand, and WWL123 was administered 120 min beforehand. Following injection, mice were placed directly into a 10”x18”x18” plexiglass box and monitored for spontaneous behavioral seizures by video recording for 6 hours, then returned to their home cage. Behavioral seizures were scored from video recordings on the Racine scale (Racine, 1972) (1 = mouth and facial movement; 2 = head nodding; 3 = forelimb clonus; 4 = rearing with forelimb clonus; 5 = rearing and falling with forelimb clonus; 6 = tonic seizure followed by death). Videos were scored by two blinded observers who scored only behavioral seizures with Racine score of 4-6.

We noted a pronounced effect of the surgeries on the progressive phenotype of R6/2 mice. Specifically, only 54% of R6/2 mice survived ketamine/xylazine anesthesia, and overall, the genotype displayed hypersensitivity to anesthetics and required reduced dosing. For those that survived anesthesia, mice which did not have tremors or obvious motor impairment before the surgeries showed clear acceleration in phenotype after the surgeries with hunching, tremors, ataxia, and hypoactivity. In addition, the average survival of R6/2 mice was 1 week after surgery, which shortened their lifespan from the normal phenotype by at least 2 weeks. Spontaneous seizures were not observed in the 72 hour window after surgery, suggesting a temporary effect of anesthesia on seizure incidence. Since our aim was to study spontaneous seizures which most accurately model the seizures occurring in juvenile HD patients, EEG surgeries were deemed confounding for accurate interpretation of our results and subsequent data was gathered by monitoring and grading behaviors without concomitant EEG. It should be noted that our monitoring protocol does not provide information on smaller seizures (Racine 1-3), or on electrographic seizures not resulting in seizure behaviors. Behaviors corresponding

to Racine 1-3 were deliberately excluded because the authors felt that without concomitant EEG, which is not technically feasible due to the aggressive phenotype of the mice, scoring minor behaviors would lead to substantial error.

**Semi-Quantitative Immunohistochemistry:** Mice were euthanized 3 days after seizures and perfused with paraformaldehyde (4% in PBS), brains were extracted, post-fixed for 24 hrs, and cryoprotected in 15% sucrose (24 hrs) followed by 30% sucrose (48 hrs). Staining was performed as described in Horne *et al.* (Horne et al., 2012). Images were collected on a Leica SP1 Confocal Laser Scanning microscope with a 63x oil objective, and on an Olympus Fluoview-1000 Confocal microscope equipped with an automated stage and a 20x air or 63X oil objective. Images were analyzed using automated macros in a Fiji distribution of ImageJ (Schindelin et al., 2012). Thresholding was performed to remove background staining (threshold = mean+SD for all stains except NPY, threshold=mean+2*SD for NPY), and mean intensity of remaining pixels was calculated, a method we have previously validated (Horne et al., 2012).

**Surgeries and Electroencephalograph (EEG) measurements:** EEGs were performed as described by Oakley et al. (Oakley et al., 2009). Under ketamine/xylazine (130/8.8 mg/kg) anesthesia 6-8 week old mice were secured in a stereotactic headframe (David Kopf instruments) and using aseptic techniques a midline incision was made over the cranium before small burr holes were drilled for electrode placement bilaterally at 3 positions: LFP (Anterior-posterior +1.2mm; lateral ± 3mm), EcoG (A-P -0.7mm; lateral ± 2.25mm), and Hippocampal (A-P -2.02mm; lateral ± 1.25mm). Higher impedance stainless steel fine wire electrodes (.003 inches uncoated, .0055 inches coated; A-M systems) were used for hippocampal and LFP depth electrodes and targeted to stratum radiatum of CA1 and layer V respectively. Lower impedance stainless steel screws (Amazon Supply) were used for ECoG recordings. Reference electrodes were placed over the olfactory bulb and ground was either a fully bared stainless steel fine wire or screw placed over the midline cerebellum. All electrodes were secured to the head with dental cement and connected to electrode interface boards (Neuralynx) for recording purposes. Animals were allowed to recover for one week following surgery. On the day of recordings, implanted mice were housed in a plexiglass box and EEG recordings were collected using a RZ2D bioamp processor (Tucker Davis Technologies) sampled at either 6 or 1.5 kHz and further analysis was

conducted offline. Offline digital filtering was performed with Hamming-window based FIR filter for wide-band (1-900 Hz), ripple (150-250 Hz), and fast ripple (300-600 Hz). Seizures were identified by characteristic sharp, rhythmic patterns consisting of repeated epileptic discharges followed by suppression of background activities. Simultaneous video recording was used to associate seizure behaviors with EEG patterns.

**[35S]GTPγS Binding Assay:** Cortex was rapidly dissected on ice and snap-frozen. Frozen samples were thawed and homogenized in Tris-HCl, pH 7.4, with 2 mM $MgCl_2$ and 1 mM EGTA. The homogenate was centrifuged at 48,000 x g for 10 min at 4°C, the supernatant was discarded and the pellet homogenized in Tris-HCl, pH 7.4, with 2 mM $MgCl_2$, 0.2 mM EGTA and 100 mM NaCl (assay buffer) and centrifuged again as above. The resulting pellet was homogenized in assay buffer and the protein concentration was determined. The resulting membrane homogenate was pre-incubated with adenosine deaminase (3 mU/ml) for 10 min at 30°C, to inactivate endogenous adenosine. For the assay, membranes (10 μg total protein) were incubated in assay buffer containing 0.1% (w/v) bovine-serum albumen, 30 μM GDP, 0.1 nM [$^{35}$S]GTPgS and 0.6 mU/ml adenosine deaminase, with and without 0.01-3 μM CP55,940, for 2 hours at 30°C. The incubation was terminated by vacuum filtration through GF/B glass fiber filters, followed by three washes with 3 ml ice-cold Tris-HCl, pH 7.4. Bound radioactivity was determined by liquid scintillation spectrophotometry after extraction of the filters in scintillation fluid. CP55,940 concentration-effect curves were analyzed by non-linear regression analysis to determine $E_{max}$ and $EC_{50}$ values and were calculated using GraphPad/Prism software.

**Activity-based protein profiling (ABPP):** Male C57BL/6 mice were injected with 10 mg/kg WWL123 and 4 hours later their brains were dissected and flash frozen. Cortical and striatal membrane homogenates were prepared by Dounce homogenization in phosphate-buffered saline (PBS) pH 7.5, sonication, and centrifugation (100,000 g for 45 min at 4°C). The pellet was washed and resuspended in PBS, sonicated, and saved as the membrane homogenate. The total protein concentration of each homogenate was determined using the Bio-Rad Dc Protein Assay kit. Control membrane homogenates (50 μg in 50 μl PBS buffer) were pre-treated with 20 μM WWL123 or DMSO vehicle for 30 min at 25ºC followed by incubation with 2 μM FP-rhodamine for 1 hr at 25ºC (Patricelli et al., 2001). Reactions were quenched with 2x SDS/PAGE loading buffer (reducing), separated

by SDS/PAGE (10% acrylamide) and visualized in-gel with a FMBio IIe flatbed fluorescence scanner (Hitachi). Rhodamine fluorescence is shown in grey scale.

**Behavioral testing:** Male 25g C57Bl/6-CBA mice were used for behavioral testing. For open field experiments, animals were placed in a 10”x18”x18” chamber four hours after receiving either vehicle or 10mg/kg WWL123. Movement was videorecorded by cameras mounted above the cages, and after 10 minutes, animals were removed. For elevated plus maze, animals were placed in the center of the elevated plus maze, facing a closed arm, and videorecorded for 5 minutes by a camera mounted above the apparatus. All video recordings were analyzed in Noldus Ethovision (Wageningen, the Netherlands).

**Data Analysis:** Data were graphed using GraphPad PRISM 5 (CA, USA) and post-hoc tests were analyzed by Fisher’s T-Test. Contingency tables were analyzed in R (http://cran.r-project.org), using Fisher’s Exact test. Error bars depict standard error of the mean. EEG data were analyzed offline using Igor Pro 5.0 (Wavemetrics, OR, USA). Immunohistochemistry was analyzed using automated and unbiased macros written in the Fiji release of ImageJ (http://fiji.sc/Fiji).

## 3.5 Tables

**Table 3.1**: Pharmakokinetics of SR141716.

| PARAMETER | IV | PO | IP | SC |
|---|---|---|---|---|
| Dose (mg/kg) | 5 | 10 | 10 | 10 |
| Total Drug Exposure(0-24 hr; ng x hr/mL) | 3721 | 628 | 5724 | 6272 |
| Bioavailability (%) | 100 | 8 | 77 | 84 |
| $C_{max}$ (ng/mL) | 5277 | 114 | 665 | 1041 |
| $T_{max}$ (hrs) | 0.0 | 0.25 | 2 | 4 |
| Trough (8 hr) | 77 | 29 | 239 | 144 |
| $C_{max}/C_{min}$ | 69 | 4 | 3 | 7 |
| Brain AUC (0-24 hr; ng x hr/ml) | 756 | 196 | 528 | 525 |
| Brain Penetrance (%) | 20 | 31 | 9 | 8 |

**Table 3.2**: List of antibodies for sq-IHC, threshold, dilutions, and suppliers used.

| **Antibody** | **Threshold** | **Dilution** | **Supplier** |
|---|---|---|---|
| NPY | Mean + (2 × SD) | 1:2000 | Immunostar #22940 |
| vGAT | Mean + SD | 1:1000 | Synaptic Systems #131011 |
| vGLUT1 | Mean + SD | 1:500 | Synaptic Systems #135311 |
| GFAP | Mean + SD | 1:1000 | Millipore #AB5541 |
| Iba1 | Mean + SD | 1:1000 | Santa Cruz #sc-28530 |
| S100b | Mean + SD | 1:1000 | AbCam #ab52642 |
| $CB_1$ | Mean + SD | 1:1000 | Gift from Ken Mackie |
| ABHD6 | Mean + SD | 1:500 | Gift from Ken Mackie |

**3.6 Acknowledgements:**

This study was a collaborative effort between myself and Dr. Eric Horne, who is co-first author on the manuscript and contributed the data described in section 3.3.7. Also, Dr. John Oakley and Dr. Christine Cheah contributed data to sections 3.3.3, 3.3.5, and 3.3.6.

**IV: Conclusion and Future Directions**

In the first part of this thesis, I have described how genetic rescue of $CB_{1(MSN)}$ in R6/2 mice is sufficient to spare the loss of excitatory striatal synapses, but does not result in changes in motor phenotype. The dissociation between striatal synaptopathy and motor phenotype is unexpected, and raises several questions for further inquiry. A primary question is whether loss of $CB_{1(MSN)}$ is sufficient to cause loss of striatal excitatory synapses in healthy mice, or whether a convergence of $CB_{1(MSN)}$ loss and other elements of R6/2 pathology is required. A simple test would be to quantify excitatory synapses in *cnr1*$^{f/f}$ mice crossed to either an *Rgs4*$^{+/Cre}$ or *Gpr88*$^{+/Cre}$. If any of these experiments produce an excitatory striatal synaptopathy comparable to what is seen in R6/2 mice, then this would suggest that $CB_{1(MSN)}$ loss is sufficient to cause loss of excitatory synapses. However, if these manipulations fail to reproduce loss of excitatory synapses, a next question would be to investigate whether the process resulting in synaptic loss is cell-autonomous in MSNs, or whether it requires dysfunction of the corticostriatal synapse. Selective expression of mutant huntingtin under a *Gpr88*$^{+/Cre}$ or *Emx1*$^{+/Cre}$ would resolve this question.

Having established the precise conditions required for loss/rescue of excitatory synapses in the striatum, a broader goal would be to describe the mechanism by which this happens. As discussed earlier, the pattern of synaptic loss observed in R6/2 mice is strikingly similar to that in dopamine deficient mice. Additionally, *cnr1*$^{-/-}$ mice have been described to have impaired Erk1/2 signaling in response to dopamine, and this effect was reproduced in *cnr1*$^{f/f;\ \text{CaMKIIα-Cre}}$ mice and in *cnr1*$^{f/f;\ \text{Dlx5/6-Cre}}$ mice, suggesting it was being mediated by $CB_1$ loss on a principal neuronal population which is also GABAergic (Corbillé et al., 2007). It is reasonable to speculate that $CB_{1(MSN)}$ is responsible for these effects. Thus, a logical experiment would be to measure Erk1/2 signaling in *cnr1*$^{f/f;\ Gpr88\text{-}Cre}$ mice, or in the corresponding knock-in mice, *Rosa26*$^{+/fsCB1;\ Gpr88\text{-}Cre}$. Additionally, the possibility that loss of $CB_{1(MSN)}$ first in the indirect and later in the direct pathway causes a disinhibition of GABAergic interneurons in the SNr, where the pathways converge, resulting in increased inhibition of dopamine neurons and reduced dopamine release to the striatum. This could be measured in R6/2 mice by either cyclic voltammetry or by microdialysis, and could be investigated as a possible mechanism for rescue of excitatory synapses by repeating the testing in R6/2-$CB_{1(MSN)}$ rescue mice. Lastly, it would be important to

understand the changes in intracellular signaling that accompany $CB_{1(MSN)}$-mediated rescue of excitatory synapses. One way to do this would to collect MSNs by laser capture microscopy and perform gene expression arrays, and mine the data with an emphasis on transcription factors.

Two independent groups have reported that genetic deletion of $CB_1$ in R6/2 mice results in a more severe HD phenotype (Blázquez et al., 2010; Mievis et al., 2011), but the data presented here would suggest that $CB_{1(MSN)}$ loss is not responsible for this effect. Therefore, one might wonder which populations of $CB_1$ receptors are protective in R6/2 mice? In the opinion of the author, a logical hypothesis would be that precisely the receptor populations which are spared in R6/2 mice are the best candidates for worsening the phenotype if deleted, since the other receptor populations are already being lost in R6/2 mice. In particular, the corticostriatal synapse stands out as an attractive target, because it encodes much of the plasticity observed in the striatum and because it mediates many behaviors associated with cannabinoid agonists. A simple experiment would be to generate R6/2-*cnr1*$^{f/f;\ Gpr88\text{-}Cre}$ mice, and measure their progressive phenotype. The author's prediction would be that these mice fully replicate the aggravated and accelerated phenotype of R6/2-*cnr1*$^{-/-}$ mice.

The second study presented in this thesis describes inhibition of the novel 2-AG hydrolase ABHD6 as a strategy for controlling induced convulsions and spontaneous seizures in R6/2 mice. ABHD6 is an attractive target because its inhibition does not result in psychomotor effects, likely because ABHD6 has comparatively low 2-AG hydrolysis activity - however, its postsynaptic localization allows it to exert local control over the availability of 2-AG, despite its weak enzymatic activity. To build on the data presented in this thesis, this strategy should be tested in a model of treatment resistant seizures, like Dravet mice, since this is the primary unmet clinical need in the field. Specifically, three questions could be tested in Dravet mice – 1) whether ABHD6 inhibition can control thermally-induced seizures, which are a good model of the febrile seizures observed in DS patients; 2) whether ABHD6 inhibition controls spontaneous seizures, and 3) whether chronic ABHD6 inhibition can change the course of the disease. This last point is particularly tantalizing. Dravet mice face repeated febrile seizures early in life, and pass through a period of increased risk of seizure–related mortality (Kalume et al., 2013). After this period, the mice begin to experience spontaneous seizures, which persist for the remainder of life. One possibility is that excitotoxic damage accrued during repeated febrile

seizures in early life may result in neuronal damage and plasticity that culminates in spontaneous seizures. If this hypothesis is correct, one might predict that chronic treatment with an agent which protects against early seizures would, even if discontinued, exert beneficial effects on the trajectory of adult disease.

Another question worth exploring would be whether ABHD6 inhibition is useful in conjunction with other, currently approved antiepileptic drugs. In particular, because there is evidence for a direct interaction of 2-AG at the β2 subunit $GABA_A$ receptors (Baur et al., 2013; Sigel et al., 2011), where it acts to potentiate GABAergic signaling, it would be intriguing to perform an isobolic study with clobazam and a ABHD6 inhibitor. Benzodiazepines are able to powerfully control seizures and are currently used in DS patients, but are associated with tolerance, addictive potential, and cognitive side effects. If 2-AG and clobazam are superadditive, the on-demand synthesis of 2-AG only at active synapses could be leveraged to augment a subclinical dose of clobazam specifically at active synapses, possibly achieving seizure control with reduced side effects.

Finally, the molecular mechanism by which ABHD6 inhibition controls seizures has not been clearly established. The best method by which to do this would be to generate $GABA_A$β2-null mice and test the electrophysiological response to either WWL123 or directly-applied 2-AG in organotypic slices. If 2-AG mediates the antiepileptic effect of WWL123, then either 2-AG or WWL123 should result in increased GABAergic current through $GABA_A$ receptors in WT but not in $GABA_A$β2-null mice. Additionally, the effect of WWL123 should be occluded by addition of 2-AG. This would be a highly novel finding, because it would establish that cannabinoid signaling is also able to execute autocrine signaling, complementing is well-established (retrograde) paracrine signaling across the synapse.

**V. REFERENCES**

Ahn, K., McKinney, M.K., and Cravatt, B.F. (2008). Enzymatic pathways that regulate endocannabinoid signaling in the nervous system. Chem Rev *108*, 1687–1707.

Aso, E., Ozaita, A., Valdizán, E.M., Ledent, C., Pazos, A., Maldonado, R., and Valverde, O. (2008). BDNF impairment in the hippocampus is related to enhanced despair behavior in CB 1knockout mice. J Neurochem *105*, 565–572.

Bachovchin, D.A., Ji, T., Li, W., Simon, G.M., Blankman, J.L., Adibekian, A., Hoover, H., Niessen, S., and Cravatt, B.F. (2010). Superfamily-wide portrait of serine hydrolase inhibition achieved by library-versus-library screening. Proc Natl Acad Sci USA *107*, 20941–20946.

Baraban, S.C., Hollopeter, G., Erickson, J.C., Schwartzkroin, P.A., and Palmiter, R.D. (1997). Knock-out mice reveal a critical antiepileptic role for neuropeptide Y. J. Neurosci. *17*, 8927–8936.

Bates, G.P., and Woodman, B. (2009). Juvenile Huntington's disease and mouse models of Huntington's disease (Oxford University Press, NY, USA).

Baur, R., Kielar, M., Richter, L., Ernst, M., Ecker, G.F., and Sigel, E. (2013). Molecular analysis of the site for 2-arachidonylglycerol (2-AG) on the β 2subunit of GABA Areceptors. J Neurochem *126*, 29–36.

Benn, C.L., Sun, T., Sadri-Vakili, G., McFarland, K.N., DiRocco, D.P., Yohrling, G.J., Clark, T.W., Bouzou, B., and Cha, J.H.J. (2008). Huntingtin Modulates Transcription, Occupies Gene Promoters In Vivo, and Binds Directly to DNA in a Polyglutamine-Dependent Manner. Journal of Neuroscience *28*, 10720–10733.

Bialer, M., and White, H.S. (2010). Key factors in the discovery and development of new antiepileptic drugs. 1–15.

Bisogno, T., Martire, A., Petrosino, S., Popoli, P., and Di Marzo, V. (2008). Symptom-related changes of endocannabinoid and palmitoylethanolamide levels in brain areas of R6/2 mice, a transgenic model of Huntington's disease. Neurochemistry International *52*, 307–313.

Bjorkqvist, M., Wild, E.J., Thiele, J., Silvestroni, A., Andre, R., Lahiri, N., Raibon, E., Lee, R.V., Benn, C.L., Soulet, D., et al. (2008). A novel pathogenic pathway of immune activation detectable before clinical onset in Huntington's disease. Journal of Experimental Medicine *205*, 1869–1877.

Blair, R.E., Deshpande, L.S., Sombati, S., Elphick, M.R., Martin, B.R., and DeLorenzo, R.J. (2009). Prolonged exposure to WIN55,212-2 causes downregulation of the CB1 receptor and the development of tolerance to its anticonvulsant effects in the hippocampal neuronal culture model of acquired epilepsy. Neuropharmacology *57*, 208–218.

Blankman, J.L., Simon, G.M., and Cravatt, B.F. (2007). A Comprehensive Profile of Brain Enzymes that Hydrolyze the Endocannabinoid 2-Arachidonoylglycerol. Chemistry & Biology *14*, 1347–1356.

Blázquez, C., Chiarlone, A., Sagredo, O., Aguado, T., Pazos, M.R., Resel, E., Palazuelos, J., Julien, B., Salazar, M., Börner, C., et al. (2010). Loss of striatal type 1 cannabinoid receptors is a key pathogenic factor in Huntington's disease. Brain *134*, 119–136.

Bouchard, J., Truong, J., Bouchard, K., Dunkelberger, D., Desrayaud, S., Moussaoui, S., Tabrizi, S.J., Stella, N., and Muchowski, P.J. (2012). Cannabinoid receptor 2 signaling in peripheral immune cells modulates disease onset and severity in mouse models of Huntington's disease. Journal of Neuroscience *32*, 18259–18268.

Bragin, A., Engel, J., Wilson, C.L., Fried, I., and Mathern, G.W. (1999). Hippocampal and entorhinal cortex high-frequency oscillations (100--500 Hz) in human epileptic brain and in kainic acid--treated rats with chronic seizures. Epilepsia *40*, 127–137.

Brown, T.B., Bogush, A.I., and Ehrlich, M.E. (2008). Neocortical expression of mutant huntingtin is not required for alterations in striatal gene expression or motor dysfunction in a transgenic mouse. Hum Mol Genet *17*, 3095–3104.

Centonze, D., Rossi, S., Prosperetti, C., Tscherter, A., Bernardi, G., Maccarrone, M., and Calabresi, P. (2005). Abnormal Sensitivity to Cannabinoid Receptor Stimulation Might Contribute to Altered Gamma-Aminobutyric Acid Transmission in the Striatum of R6/2 Huntington's Disease Mice. Biol. Psychiatry *57*, 1583–1589.

Cepeda, C., Galvan, L., Holley, S.M., Rao, S.P., Andre, V.M., Botelho, E.P., Chen, J.Y., Watson, J.B., Deisseroth, K., and Levine, M.S. (2013). Multiple Sources of Striatal Inhibition Are Differentially Affected in Huntington's Disease Mouse Models. Journal of Neuroscience *33*, 7393–7406.

Cepeda, C., Hurst, R.S., Calvert, C.R., Hernández-Echeagaray, E., Nguyen, O.K., Jocoy, E., Christian, L.J., Ariano, M.A., and Levine, M.S. (2003). Transient and progressive electrophysiological alterations in the corticostriatal pathway in a mouse model of Huntington's disease. J. Neurosci. *23*, 961–969.

Cepeda-Prado, E., Popp, S., Khan, U., Stefanov, D., Rodriguez, J., Menalled, L.B., Dow-Edwards, D., Small, S.A., and Moreno, H. (2012). R6/2 Huntington's disease mice develop early and progressive abnormal brain metabolism and seizures. Journal of Neuroscience *32*, 6456–6467.

Cheah, C.S., Yu, F.H., Westenbroek, R.E., Kalume, F.K., Oakley, J.C., Potter, G.B., Rubenstein, J.L., and Catterall, W.A. (2012). Specific deletion of NaV1.1 sodium channels in inhibitory interneurons causes seizures and premature death in a mouse model of Dravet syndrome. Proc Natl Acad Sci USA *109*, 14646–14651.

Chen, K., Neu, A., Howard, A.L., Földy, C., Echegoyen, J., Hilgenberg, L., Smith, M., Mackie, K., and Soltesz, I. (2007). Prevention of Plasticity of Endocannabinoid Signaling Inhibits Persistent Limbic Hyperexcitability Caused by Developmental Seizures. Journal of Neuroscience *27*, 46–58.

Chen, K., Ratzliff, A., Hilgenberg, L., Gulyás, A., Freund, T.F., Smith, M., Dinh, T.P., Piomelli, D., Mackie, K., and Soltesz, I. (2003). Long-term plasticity of endocannabinoid signaling induced by developmental febrile seizures. Neuron *39*, 599–611.

Chiodi, V., Uchigashima, M., Beggiato, S., Ferrante, A., Armida, M., Martire, A., Potenza, R.L., Ferraro, L., Tanganelli, S., Watanabe, M., et al. (2012). Unbalance of CB1 receptors expressed in GABAergic and glutamatergic neurons in a transgenic mouse model of Huntington's disease. Neurobiology of Disease *45*, 983–991.

Citraro, R., Russo, E., Ngomba, R.T., Nicoletti, F., Scicchitano, F., Whalley, B.J., Calignano, A., and De Sarro, G. (2013). CB1 agonists, locally applied to the cortico-thalamic circuit of rats with genetic absence epilepsy, reduce epileptic manifestations. Epilepsy Research *106*, 74–82.

Clement, A.B., Hawkins, E.G., Lichtman, A.H., and Cravatt, B.F. (2003). Increased seizure susceptibility and proconvulsant activity of anandamide in mice lacking fatty acid amide hydrolase. J. Neurosci. *23*, 3916–3923.

Cloud, L.J., Rosenblatt, A., Margolis, R.L., Ross, C.A., Pillai, J.A., Corey-Bloom, J., Tully, H.M., Bird, T., Panegyres, P.K., Nichter, C.A., et al. (2012). Seizures in juvenile Huntington's disease: Frequency and characterization in a multicenter cohort. Mov Disord *27*, 1797–1800.

Colmers, W.F., Lukowiak, K., and Pittman, Q.J. (1988). Neuropeptide Y action in the rat hippocampal slice: site and mechanism of presynaptic inhibition. J. Neurosci. *8*, 3827–3837.

Corbillé, A.G., Valjent, E., Marsicano, G., Ledent, C., Lutz, B., Hervé, D., and Girault, J.A. (2007). Role of Cannabinoid Type 1 Receptors in Locomotor Activity and Striatal Signaling in Response to Psychostimulants. J. Neurosci. *27*, 6937–6947.

Cravatt, B.F., Giang, D.K., Mayfield, S.P., Boger, D.L., Lerner, R.A., and Gilula, N.B. (1996). Molecular characterization of an enzyme that degrades neuromodulatory fatty-acid amides. Nature *384*, 83–87.

Cravatt, B.F., Demarest, K., Patricelli, M.P., Bracey, M.H., Giang, D.K., Martin, B.R., and Lichtman, A.H. (2001). Supersensitivity to anandamide and enhanced endogenous cannabinoid signaling in mice lacking fatty acid amide hydrolase. Proceedings of the National Academy of Sciences *98*, 9371–9376.

Crawley, J.N., Corwin, R.L., Robinson, J.K., Felder, C.C., Devane, W.A., and Axelrod, J. (1993). Anandamide, an endogenous ligand of the cannabinoid receptor, induces hypomotility and hypothermia in vivo in rodents. Pharmacol Biochem Behav *46*, 967–972.

Day, M., Wang, Z., Ding, J., An, X., Ingham, C.A., Shering, A.F., Wokosin, D., Ilijic, E., Sun, Z., Sampson, A.R., et al. (2006). Selective elimination of glutamatergic synapses on striatopallidal neurons in Parkinson disease models. Nat Neurosci *9*, 251–259.

Denovan-Wright, E.M., and Robertson, H.A. (2000). Cannabinoid receptor messenger RNA levels decrease in a subset of neurons of the lateral striatum, cortex and hippocampus of transgenic Huntington's disease mice. Neuroscience *98*, 705–713.

Devane, W.A., Hanuš, L., Breuer, A., Pertwee, R.G., Stevenson, L.A., Griffin, G., Gibson, D., Mandelbaum, A., Etinger, A., and Mechoulam, R. (1992). Isolation and structure of a brain constituent that binds to the cannabinoid receptor. Science *258*, 1946–1949.

Di Marzo, V. (2011). Endocannabinoid signaling in the brain: biosynthetic mechanisms in the limelight. Nat Neurosci *14*, 9–15.

Di Marzo, V., Fontana, A., Cadas, H., Schinelli, S., Cimino, G., Schwartz, J.-C., and Piomelli, D. (1994). Formation and inactivation of endogenous cannabinoid anandamide in central neurons.

Dowie, M.J., Bradshaw, H.B., Howard, M.L., Nicholson, L.F.B., Faull, R.L.M., Hannan, A.J., and Glass, M. (2009). Altered CB1 receptor and endocannabinoid levels precede motor symptom onset in a transgenic mouse model of Huntington's disease. Neuroscience *163*, 456–465.

Dowie, M.J., Howard, M.L., Nicholson, L.F.B., Faull, R.L.M., Hannan, A.J., and Glass, M. (2010). Behavioural and molecular consequences of chronic cannabinoid treatment in Huntington's disease transgenic mice. Neuroscience *170*, 324–336.

Duff, K., Paulsen, J.S., Beglinger, L.J., Langbehn, D.R., and Stout, J.C. (2007). Psychiatric Symptoms in Huntington's Disease before Diagnosis: The Predict-HD Study. Biol. Psychiatry *62*, 1341–1346.

Echegoyen, J., Armstrong, C., Morgan, R.J., and Soltesz, I. (2009). Single application of a CB1 receptor antagonist rapidly following head injury prevents long-term hyperexcitability in a rat model. Epilepsy Research *85*, 123–127.

Elphick, M.R. (2012). The evolution and comparative neurobiology of endocannabinoid signalling.

Philosophical Transactions of the Royal Society B: Biological Sciences *367*, 3201–3215.

Erickson, J.C., Clegg, K.E., and Palmiter, R.D. (1996). Sensitivity to leptin and susceptibility to seizures of mice lacking neuropeptide Y. Nature *381*, 415–421.

Ferraro, T.N., Golden, G.T., Smith, G.G., St Jean, P., Schork, N.J., Mulholland, N., Ballas, C., Schill, J., Buono, R.J., and Berrettini, W.H. (1999). Mapping loci for pentylenetetrazol-induced seizure susceptibility in mice. Journal of Neuroscience *19*, 6733–6739.

Foroud, T., Gray, J., Ivashina, J., and Conneally, P.M. (1999). Differences in duration of Huntington's disease based on age at onset. Journal of Neurology, Neurosurgery & Psychiatry *66*, 52–56.

Franklin, A., and Stella, N. (2003). Arachidonylcyclopropylamide increases microglial cell migration through cannabinoid CB2 and abnormal-cannabidiol-sensitive receptors. Eur J Pharmacol *474*, 195–198.

Gambardella, A., Muglia, M., Labate, A., Magariello, A., Gabriele, A.L., Mazzei, R., Pirritano, D., Conforti, F.L., Patitucci, A., Valentino, P., et al. (2001). Juvenile Huntington's disease presenting as progressive myoclonic epilepsy. Neurology *57*, 708–711.

Gerdeman, G., and al, E. (2002). Postsynaptic endocannabinoid release is critical to long-term depression in the striatum. Nat Neurosci *5*, 446–451.

Glass, M., Dragunow, M., and Faull, R.L. (2000). The pattern of neurodegeneration in Huntington"s disease: a comparative study of cannabinoid, dopamine, adenosine and GABA(A) receptor alterations in the human basal ganglia in Huntington"s disease. Neuroscience *97*, 505–519.

Glass, M., Faull, R.L., and Dragunow, M. (1993). Loss of cannabinoid receptors in the substantia nigra in Huntington's disease. Neuroscience *56*, 523–527.

Gonzalez-Alegre, P., and Afifi, A.K. (2006). Clinical characteristics of childhood-onset (juvenile) Huntington disease: report of 12 patients and review of the literature. J. Child Neurol. *21*, 223–229.

Goto, S., and Hirano, A. (1990). Synaptophysin expression in the striatum in Huntington's disease. Acta Neuropathol. *80*, 88–91.

Gómez del Pulgar, T., Velasco, G., and Guzmán, M. (2000). The CB1 cannabinoid receptor is coupled to the activation of protein kinase B/Akt. Biochem. J. *347*, 369–373.

Guggenhuber, S., Monory, K., Lutz, B., and Klugmann, M. AAV Vector-Mediated Overexpression of CB1 Cannabinoid Receptor in Pyramidal Neurons of the Hippocampus Protects against Seizure-Induced Excitoxicity. PLoS ONE *5*, e15707EP–.

Hashimotodani, Y., Ohno-Shosaku, T., Tsubokawa, H., Ogata, H., Emoto, K., Maejima, T., Araishi, K., Shin, H.-S., and Kano, M. (2005). Phospholipase Cbeta serves as a coincidence detector through its Ca2+ dependency for triggering retrograde endocannabinoid signal. Neuron *45*, 257–268.

Hodges, A. (2006). Regional and cellular gene expression changes in human Huntington's disease brain. Hum Mol Genet *15*, 965–977.

Horne, E.A., Coy, J., Swinney, K., Fung, S., Cherry, A.E.T., Marrs, W.R., Naydenov, A.V., Lin, Y.H., Sun, X., Dirk Keene, C., et al. (2012). Downregulation of cannabinoid receptor 1 from neuropeptide Y interneurons in the basal ganglia of patients with Huntington's disease and mouse models. Eur J Neurosci *37*, n/a–n/a.

Huntington, G. (1967). ON chorea. Arch. Neurol. *17*, 332–333.

Idris, A.I., van 't Hof, R.J., Greig, I.R., Ridge, S.A., Baker, D., Ross, R.A., and Ralston, S.H. (2005). Regulation of bone mass, bone loss and osteoclast activity by cannabinoid receptors. Nat Med *11*, 774–779.

Kalume, F., Westenbroek, R.E., Cheah, C.S., Yu, F.H., Oakley, J.C., Scheuer, T., and Catterall, W.A. (2013). Sudden unexpected death in a mouse model of Dravet syndrome. J. Clin. Invest. *123*, 1798–1808.

Karsak, M. (2005). Cannabinoid receptor type 2 gene is associated with human osteoporosis. Hum Mol Genet *14*, 3389–3396.

Katona, I., and Freund, T.F. (2008). Endocannabinoid signaling as a synaptic circuit breaker in neurological disease. Nat Med *14*, 923–930.

Katona, I., Sperlágh, B., Sík, A., Käfalvi, A., Vizi, E.S., Mackie, K., and Freund, T.F. (1999). Presynaptically located CB1 cannabinoid receptors regulate GABA release from axon terminals of specific hippocampal interneurons. J. Neurosci. *19*, 4544–4558.

Kearn, C.S. (2005). Concurrent Stimulation of Cannabinoid CB1 and Dopamine D2 Receptors Enhances Heterodimer Formation: A Mechanism for Receptor Cross-Talk? Mol Pharmacol *67*, 1697–1704.

Klapstein, G.J., Fisher, R.S., Zanjani, H., Cepeda, C., Jokel, E.S., Chesselet, M.-F., and Levine, M.S. (2001). Electrophysiological and morphological changes in striatal spiny neurons in R6/2 Huntington's disease transgenic mice. Journal of Neurophysiology *86*, 2667–2677.

Kozorovitskiy, Y., Saunders, A., Johnson, C.A., Lowell, B.B., and Sabatini, B.L. (2012). Recurrent network activity drives striatal synaptogenesis. Nature 1–8.

Kreitzer, A. (2002). Retrograde signaling by endocannabinoids. Current Opinion in Neurobiology *12*, 324–330.

Kreitzer, A.C., and Malenka, R.C. (2007). Endocannabinoid-mediated rescue of striatal LTD and motor deficits in Parkinson's disease models. Nature *445*, 643–647.

Kung, V.W.S., Hassam, R., Morton, A.J., and Jones, S. (2007). Dopamine-dependent long term potentiation in the dorsal striatum is reduced in the R6/2 mouse model of Huntington's disease. Neuroscience *146*, 1571–1580.

Kwan, P., and Brodie, M.J. (2000). Early identification of refractory epilepsy. N Engl J Med *342*, 314–319.

Lafourcade, M., Elezgarai, I., Mato, S., Bakiri, Y., Grandes, P., and Manzoni, O.J. (2007). Molecular components and functions of the endocannabinoid system in mouse prefrontal cortex. PLoS ONE *2*, e709.

Landau, M.E., and Cannard, K.R. (2003). EEG characteristics in juvenile Huntingon's disease: a case report and review of the literature. Epileptic Disorders *5*, 145–148.

Lawrence, J.J. (2008). Cholinergic control of GABA release: emerging parallels between neocortex and hippocampus. Trends Neurosci *31*, 317–327.

Luthi-Carter, R., Apostol, B.L., Dunah, A.W., DeJohn, M.M., Farrell, L.A., Bates, G.P., Young, A.B., Standaert, D.G., Thompson, L.M., and Cha, J.-H.J. (2003). Complex alteration of NMDA receptors in transgenic Huntington's disease mouse brain: analysis of mRNA and protein expression, plasma membrane association, interacting proteins, and phosphorylation. Neurobiology of Disease *14*, 624–636.

Luthi-Carter, R., Hanson, S.A., Strand, A.D., Bergstrom, D.A., Chun, W., Peters, N.L., Woods, A.M., Chan,

E.Y., Kooperberg, C., Krainc, D., et al. (2002). Dysregulation of gene expression in the R6/2 model of polyglutamine disease: parallel changes in muscle and brain. Hum Mol Genet *11*, 1911–1926.

Lutz, B. (2004). On-demand activation of the endocannabinoid system in the control of neuronal excitability and epileptiform seizures. Biochemical Pharmacology *68*, 1691–1698.

Maccarrone, M., Rossi, S., Bari, M., De Chiara, V., Fezza, F., Musella, A., Gasperi, V., Prosperetti, C., Bernardi, G., Finazzi-Agrò, A., et al. (2008). Anandamide inhibits metabolism and physiological actions of 2-arachidonoylglycerol in the striatum. Nat Neurosci *11*, 152–159.

MacDonald, M.E., Ambrose, C.M., Duyao, M.P., Myers, R.H., Lin, C., Srinidhi, L., Barnes, G., Taylor, S.A., James, M., and Groot, N. (1993). A novel gene containing a trinucleotide repeat that is expanded and unstable on Huntington's disease chromosomes. Cell *72*, 971–983.

Mackie, K., Devane, W.A., and Hille, B. (1993). Anandamide, an endogenous cannabinoid, inhibits calcium currents as a partial agonist in N18 neuroblastoma cells. Mol Pharmacol *44*, 498–503.

Maejima, T., Ohno-Shosaku, T., and Kano, M. (2001). Endogenous cannabinoid as a retrograde messenger from depolarized postsynaptic neurons to presynaptic terminals. Neuroscience Research *40*, 205–210.

Mangiarini, L., Sathasivam, K., Seller, M., Cozens, B., Harper, A., Hetherington, C., Lawton, M., Trottier, Y., Lehrach, H., Davies, S.W., et al. (1996). Exon 1 of the HD gene with an expanded CAG repeat is sufficient to cause a progressive neurological phenotype in transgenic mice. Cell *87*, 493–506.

Marrs, W.R., Horne, E.A., Ortega-Gutierrez, S., Cisneros, J.A., Xu, C., Lin, Y.H., Muccioli, G.G., Lopez-Rodriguez, M.L., and Stella, N. (2011). Dual inhibition of alpha/beta-hydrolase domain 6 and fatty acid amide hydrolase increases endocannabinoid levels in neurons. Journal of Biological Chemistry *286*, 28723–28728.

Marrs, W.R., Blankman, J.L., Horne, E.A., Thomazeau, A., Lin, Y.H., Coy, J., Bodor, A.L., Muccioli, G.G., Hu, S.S.-J., Woodruff, G., et al. (2010). The serine hydrolase ABHD6 controls the accumulation and efficacy of 2-AG at cannabinoid receptors. Nat Neurosci *13*, 951–957.

Marsh, D.J., Baraban, S.C., Hollopeter, G., and Palmiter, R.D. (1999). Role of the Y5 neuropeptide Y receptor in limbic seizures. Proceedings of the National Academy of Sciences *96*, 13518–13523.

Marsicano, G. (2003). CB1 Cannabinoid Receptors and On-Demand Defense Against Excitotoxicity. Science *302*, 84–88.

Matsuda, L.A., Lolait, S.J., Brownstein, M.J., Young, A.C., and Bonner, T.I. (1990). Structure of a cannabinoid receptor and functional expression of the cloned cDNA. Nature *346*, 561–564.

Mccaw, E.A., Hu, H., Gomez, G.T., Hebb, A.L.O., Kelly, M.E.M., and Denovan-Wright, E.M. (2004). Structure, expression and regulation of the cannabinoid receptor gene (CB1) in Huntington's disease transgenic mice. Eur J Biochem *271*, 4909–4920.

Meredith, G.E., Ypma, P., and Zahm, D.S. (1995). Effects of dopamine depletion on the morphology of medium spiny neurons in the shell and core of the rat nucleus accumbens. J. Neurosci. *15*, 3808–3820.

Mievis, S., Blum, D., and Ledent, C. (2011). Worsening of Huntington disease phenotype in CB1 receptor knockout mice. Neurobiology of Disease *42*, 524–529.

Miller, A.M., and Stella, N. (2008). CB 2receptor-mediated migration of immune cells: it can go either way. British Journal of Pharmacology *153*, 299–308.

Milnerwood, A.J., Gladding, C.M., Pouladi, M.A., Kaufman, A.M., Hines, R.M., Boyd, J.D., Ko, R.W.Y., Vasuta, O.C., Graham, R.K., Hayden, M.R., et al. (2010). Early Increase in Extrasynaptic NMDA Receptor Signaling and Expression Contributes to Phenotype Onset in Huntington's Disease Mice. Neuron *65*, 178–190.

Naderi, N., Aziz Ahari, F., Shafaghi, B., Hosseini Najarkolaei, A., and Motamedi, F. (2008). Evaluation of interactions between cannabinoid compounds and diazepam in electroshock-induced seizure model in mice. J Neural Transm *115*, 1501–1511.

Naver, B., Stub, C., Møller, M., Fenger, K., Hansen, A.K., Hasholt, L., and Sørensen, S.A. (2003). Molecular and behavioral analysis of the R6/1 Huntington's disease transgenic mouse. Neuroscience *122*, 1049–1057.

Nithianantharajah, J., Barkus, C., Murphy, M., and Hannan, A.J. (2008). Gene–environment interactions modulating cognitive function and molecular correlates of synaptic plasticity in Huntington's disease transgenic mice. Neurobiology of Disease *29*, 490–504.

Noe, F., Pool, A.H., Nissinen, J., Gobbi, M., Bland, R., Rizzi, M., Balducci, C., Ferraguti, F., Sperk, G., During, M.J., et al. (2008). Neuropeptide Y gene therapy decreases chronic spontaneous seizures in a rat model of temporal lobe epilepsy. Brain *131*, 1506–1515.

Oakley, J.C., Kalume, F., Yu, F.H., Scheuer, T., and Catterall, W.A. (2009). Temperature- and age-dependent seizures in a mouse model of severe myoclonic epilepsy in infancy. Proc Natl Acad Sci USA *106*, 3994–3999.

Ofek, O., Karsak, M., Leclerc, N., Fogel, M., Frenkel, B., Wright, K., Tam, J., Attar-Namdar, M., Kram, V., Shohami, E., et al. (2006). Peripheral cannabinoid receptor, CB2, regulates bone mass. Proceedings of the National Academy of Sciences *103*, 696–701.

Offertáler, L., Mo, F.-M., Bátkai, S., Liu, J., Begg, M., Razdan, R.K., Martin, B.R., Bukoski, R.D., and Kunos, G. (2003). Selective ligands and cellular effectors of a G protein-coupled endothelial cannabinoid receptor. Mol Pharmacol *63*, 699–705.

Ohno-Shosaku, T., Maejima, T., and Kano, M. (2001). Endogenous cannabinoids mediate retrograde signals from depolarized postsynaptic neurons to presynaptic terminals. Neuron *29*, 729–738.

Okamoto, S.-I., Pouladi, M.A., Talantova, M., Yao, D., Xia, P., Ehrnhoefer, D.E., Zaidi, R., Clemente, A., Kaul, M., Graham, R.K., et al. (2009). Balance between synaptic versus extrasynaptic NMDA receptor activity influences inclusions and neurotoxicity of mutant huntingtin. Nat Med *15*, 1407–1413.

Palazuelos, J., Aguado, T., Pazos, M.R., Julien, B., Carrasco, C., Resel, E., Sagredo, O., Benito, C., Romero, J., Azcoitia, I., et al. (2009). Microglial CB2 cannabinoid receptors are neuroprotective in Huntington's disease excitotoxicity. Brain *132*, 3152–3164.

Pan, B., Wang, W., Zhong, P., Blankman, J.L., Cravatt, B.F., and Liu, Q.S. (2011). Alterations of Endocannabinoid Signaling, Synaptic Plasticity, Learning, and Memory in Monoacylglycerol Lipase Knock-out Mice. Journal of Neuroscience *31*, 13420–13430.

Patricelli, M.P., Giang, D.K., Stamp, L.M., and Burbaum, J.J. (2001). Direct visualization of serine hydrolase activities in complex proteomes using fluorescent active site-directed probes. Proteomics *1*, 1067–1071.

Pertwee, R.G., Howlett, A.C., Abood, M.E., Alexander, S.P.H., Di Marzo, V., Elphick, M.R., Greasley, P.J., Hansen, H.S., Kunos, G., Mackie, K., et al. (2010). International Union of Basic and Clinical Pharmacology. LXXIX. Cannabinoid Receptors and Their Ligands: Beyond CB1 and CB2. Pharmacological Reviews *62*, 588–631.

Pouladi, M.A., Stanek, L.M., Xie, Y., Franciosi, S., Southwell, A.L., Deng, Y., Butland, S., Zhang, W., Cheng, S.H., Shihabuddin, L.S., et al. (2012). Marked differences in neurochemistry and aggregates despite similar behavioural and neuropathological features of Huntington disease in the full-length BACHD and YAC128 mice. Hum Mol Genet *21*, 2219–2232.

Quintana, A., Sanz, E., Wang, W., Storey, G.P., Güler, A.D., Wanat, M.J., Roller, B.A., La Torre, A., Amieux, P.S., McKnight, G.S., et al. (2012). Lack of GPR88 enhances medium spiny neuron activity and alters motor- and cue-dependent behaviors. Nature Publishing Group *15*, 1547–1555.

Racine, R.J. (1972). Modification of seizure activity by electrical stimulation. II. Motor seizure. Electroencephalogr Clin Neurophysiol *32*, 281–294.

Raymond, L.A., Andre, V.M., Cepeda, C., Gladding, C.M., Milnerwood, A.J., and Levine, M.S. (2011). REVIEWPATHOPHYSIOLOGY OF HUNTINGTON'S DISEASE: TIME-DEPENDENT ALTERATIONS IN SYNAPTIC AND RECEPTOR FUNCTION. Nsc *198*, 252–273.

Regehr, W.G., Carey, M.R., and Best, A.R. (2009). Activity-Dependent Regulationof Synapses by Retrograde Messengers. Neuron *63*, 154–170.

Reiner, A., Albin, R.L., Anderson, K.D., D'Amato, C.J., Penney, J.B., and Young, A.B. (1988). Differential loss of striatal projection neurons in Huntington disease. Proceedings of the National Academy of Sciences *85*, 5733–5737.

Rosas, H.D., Hevelone, N.D., Zaleta, A.K., Greve, D.N., Salat, D.H., and Fischl, B. (2005). Regional cortical thinning in preclinical Huntington disease and its relationship to cognition. Neurology *65*, 745–747.

Rosas, H.D., Tuch, D.S., Hevelone, N.D., Zaleta, A.K., Vangel, M., Hersch, S.M., and Salat, D.H. (2006). Diffusion tensor imaging in presymptomatic and early Huntington's disease: Selective white matter pathology and its relationship to clinical measures. Mov Disord *21*, 1317–1325.

Ross, R.A. (2009). The enigmatic pharmacology of GPR55. Trends in Pharmacological Sciences *30*, 156–163.

Rudenko, V., Rafiuddin, A., Leheste, J.R., and Friedman, L.K. (2012). Inverse relationship of cannabimimetic (R+) WIN 55, 212 on behavior and seizure threshold during the juvenile period. Pharmacol Biochem Behav *100*, 474–484.

Sagredo, O., González, S., Aroyo, I., Pazos, M.R., Benito, C., Lastres-Becker, I., Romero, J.P., Tolón, R.M., Mechoulam, R., Brouillet, E., et al. (2009). Cannabinoid CB 2receptor agonists protect the striatum against malonate toxicity: Relevance for Huntington's disease. Glia *57*, 1154–1167.

Schindelin, J., Arganda-Carreras, I., Frise, E., Kaynig, V., Longair, M., Pietzsch, T., Preibisch, S., Rueden, C., Saalfeld, S., Schmid, B., et al. (2012). Fiji: an open-source platform for biological-image analysis. Nat Meth *9*, 676–682.

Schlosburg, J.E., Blankman, J.L., Long, J.Z., Nomura, D.K., Pan, B., Kinsey, S.G., Nguyen, P.T., Ramesh, D., Booker, L., Burston, J.J., et al. (2010). Chronic monoacylglycerol lipase blockade causes functional antagonism of the endocannabinoid system. Nat Neurosci *13*, 1113–1119.

Sharp, A.H., Loev, S.J., Schilling, G., Li, S.H., Li, X.J., Bao, J., Wagster, M.V., Kotzuk, J.A., Steiner, J.P., and Lo, A. (1995). Widespread expression of Huntington's disease gene (IT15) protein product. Neuron *14*, 1065–1074.

Shonesy, B.C., Wang, X., Rose, K.L., Ramikie, T.S., Cavener, V.S., Rentz, T., Baucum, A.J., Jalan-Sakrikar, N., Mackie, K., Winder, D.G., et al. (2013). CaMKII regulates diacylglycerol lipase-a and striatal endocannabinoid signaling. Nature Publishing Group *16*, 456–463.

Sigel, E., Baur, R., Rácz, I., Marazzi, J., Smart, T.G., Zimmer, A., and Gertsch, J. (2011). The major central endocannabinoid directly acts at GABA(A) receptors. Proc Natl Acad Sci USA *108*, 18150–18155.

Smith, M., Wilcox, K.S., and White, H.S. (2007). Discovery of antiepileptic drugs. Neurotherapeutics *4*, 12–17.

Spires, T.L., Grote, H.E., Garry, S., Cordery, P.M., Van Dellen, A., Blakemore, C., and Hannan, A.J. (2004). Dendritic spine pathology and deficits in experience‐dependent dendritic plasticity in R6/1 Huntington's disease transgenic mice. Eur J Neurosci *19*, 2799–2807.

Steindel, F., Lerner, R., Häring, M., Ruehle, S., Marsicano, G., Lutz, B., and Monory, K. (2013). Neuron-type specific cannabinoid-mediated G protein signalling in mouse hippocampus. J Neurochem *124*, 795–807.

Steiner, M.A., Wanisch, K., Monory, K., Marsicano, G., Borroni, E., Bächli, H., Holsboer, F., Lutz, B., and Wotjak, C.T. (2007). Impaired cannabinoid receptor type 1 signaling interferes with stress-coping behavior in mice. Pharmacogenomics J *8*, 196–208.

Stella, N., Schweitzer, P., and Piomelli, D. (1997). A second endogenous cannabinoid that modulates long-term potentiation. Nature *388*, 773–778.

Stella, N. (2012). Inflammation to Rebuild a Brain: Inflammation in the zebrafish brain stimulates neurogenesis and tissue regeneration. Science *338*, 1303.

Straiker, A., Hu, S.S.-J., Long, J.Z., Arnold, A., Wager-Miller, J., Cravatt, B.F., and Mackie, K. (2009). Monoacylglycerol Lipase Limits the Duration of Endocannabinoid-Mediated Depolarization-Induced Suppression of Excitation in Autaptic Hippocampal Neurons. Mol Pharmacol *76*, 1220–1227.

Varoqueaux, F., Jamain, S., and Brose, N. (2004). Neuroligin 2 is exclusively localized to inhibitory synapses. Eur. J. Cell Biol. *83*, 449–456.

Vezzani, A., Civenni, G., Rizzi, M., Monno, A., Messali, S., and Samanin, R. (1994). Enhanced neuropeptide Y release in the hippocampus is associated with chronic seizure susceptibility in kainic acid treated rats. Brain Res *660*, 138–143.

Vezzani, A., Sperk, G., and Colmers, W.F. (1999). Neuropeptide Y: emerging evidence for a functional role in seizure modulation. Trends Neurosci *22*, 25–30.

Wallace, M.J. (2003). The Endogenous Cannabinoid System Regulates Seizure Frequency and Duration in a Model of Temporal Lobe Epilepsy. Journal of Pharmacology and Experimental Therapeutics *307*, 129–137.

Wallace, M.J., Martin, B.R., and DeLorenzo, R.J. (2002). Evidence for a physiological role of endocannabinoids in the modulation of seizure threshold and severity. Eur J Pharmacol *452*, 295–301.

Walter, L., Franklin, A., Witting, A., Wade, C., Xie, Y., Kunos, G., Mackie, K., and Stella, N. (2003a). Nonpsychotropic cannabinoid receptors regulate microglial cell migration. Journal of Neuroscience *23*, 1398–1405.

Walter, L., Franklin, A., Witting, A., Wade, C., Xie, Y., Kunos, G., Mackie, K., and Stella, N. (2003b). Nonpsychotropic cannabinoid receptors regulate microglial cell migration. J. Neurosci. *23*, 1398–1405.

White, H.S. (2003). Preclinical development of antiepileptic drugs: past, present, and future directions. Epilepsia *44 Suppl 7*, 2–8.

Wilson, R.I., and Nicoll, R.A. (2001). Endogenous cannabinoids mediate retrograde signalling at hippocampal synapses. Nature *410*, 588–592.

Woldbye, D.P., Larsen, P.J., Mikkelsen, J.D., Klemp, K., Madsen, T.M., and Bolwig, T.G. (1997). Powerful inhibition of kainic acid seizures by neuropeptide Y via Y5-like receptors. Nat Med *3*, 761–764.

Woldbye, D.P., Madsen, T.M., Larsen, P.J., Mikkelsen, J.D., and Bolwig, T.G. (1996). Neuropeptide Y inhibits hippocampal seizures and wet dog shakes. Brain Res *737*, 162–168.

Woodman, B., Butler, R., Landles, C., Lupton, M.K., Tse, J., Hockly, E., Moffitt, H., Sathasivam, K., and Bates, G.P. (2007). The Hdh(Q150/Q150) knock-in mouse model of HD and the R6/2 exon 1 model develop comparable and widespread molecular phenotypes. Brain Research Bulletin *72*, 83–97.

Zhai, W., Jeong, H., Cui, L., Krainc, D., and Tjian, R. (2005). In Vitro Analysis of Huntingtin-Mediated Transcriptional Repression Reveals Multiple Transcription Factor Targets. Cell *123*, 1241–1253.

Zhang, X., Bertaso, F., Yoo, J.W., Baumgärtel, K., Clancy, S.M., Van Lee, Cienfuegos, C., Wilmot, C., Avis, J., Hunyh, T., et al. (2010). Deletion of the potassium channel Kv12.2 causes hippocampal hyperexcitability and epilepsy. Nature Publishing Group *13*, 1056–1058.

Zimmer, A., Zimmer, A.M., Hohmann, A.G., Herkenham, M., and Bonner, T.I. (1999). Increased mortality, hypoactivity, and hypoalgesia in cannabinoid CB1 receptor knockout mice. Proceedings of the National Academy of Sciences *96*, 5780–5785.

Zuccato, C., Valenza, M., and Cattaneo, E. (2010). Molecular Mechanisms and Potential Therapeutical Targets in Huntington's Disease. Physiological Reviews *90*, 905–981.

Zuccato, C., Ciammola, A., Rigamonti, D., Leavitt, B.R., Goffredo, D., Conti, L., MacDonald, M.E., Friedlander, R.M., Silani, V., and Hayden, M.R. (2001). Loss of huntingtin-mediated BDNF gene transcription in Huntington's disease. Science *293*, 493–498.

Zucker, B. (2004). Transcriptional dysregulation in striatal projection- and interneurons in a mouse model of Huntington's disease: neuronal selectivity and potential neuroprotective role of HAP1. Hum Mol Genet *14*, 179–189.

(2010). LOSS OF STRIATAL CB1 CANNABINOID RECEPTORS IS A

KEY PATHOGENIC FACTOR IN HUNTINGTON’S DISEASE

. 1–55.